Master's thesis

NTNU
Norwegian University of Science and Technology
Faculty of Natural Sciences
Department of Chemical Engineering

Isabel Pascual García

Preparation and characterization of pelletized Mn-based sulfur sorbents

Master's thesis in Chemical Engineering
Supervisor: Edd Anders Blekkan
Co-supervisor: Mehdi Mahmoodinia, Kumar Ranjan Rout
July 2021

NTNU
Norwegian University of
Science and Technology

Isabel Pascual García

Preparation and characterization of pelletized Mn-based sulfur sorbents

Master's thesis in Chemical Engineering
Supervisor: Edd Anders Blekkan
Co-supervisor: Mehdi Mahmoodinia, Kumar Ranjan Rout
July 2021

Norwegian University of Science and Technology
Faculty of Natural Sciences
Department of Chemical Engineering

NTNU
Norwegian University of
Science and Technology

Abstract

The global energy situation is changing slowly into new sustainable patterns of production and consumption. However, fossil fuels still lead the world energy outlook, covering more than 80% of the energy mix. Between other alternatives, **biomass gasification** and its derived energy forms such as biofuels, biogas, or low carbon hydrogen, will contribute to the energy transition, playing a major role in the next decades.

Biomass gasification-derived syngas presents a major challenge regarding cleaning and conditioning steps due to the undesired components such as tar, particulate matter, nitrogen or sulfur compounds. Conventional methods for sulfur removal are not efficient in terms of energy, mainly due to low operation temperatures and large investments. Therefore, **high-temperature desulfurization** with solid sorbents is considered one of the alternatives. Within this project, Mn-based/γ-Al_2O_3, Mo-promoted sorbents are being developed to achieve a chemical looping desulfurization with sorption-regeneration cycles.

The objective of this project is to **synthesize and characterize** a series of sorbents with different compositions (15% Mn and 2,5-10% Mo), in the form of **egg-shell pellets**. Three synthesis methods have been performed, namely using ethylene glycol as a hydrophobic solvent for both sequential and co-impregnation (EG-SQ and EG-Co) or glycerol as the precursor's solvent for co-impregnation (GL-Co).

GL-Co method presented the highest time **efficiency** results. Additionally, **XRF** analysis showed the highest loading with one impregnation can be achieved with this method. However, the preparation step needs to be further upgraded, due to the challenging handling of glycerol and deficient material properties in the final sorbents. On the other hand, both ethylene glycol methods showed a high standard in material properties. Time efficiency improved in EG-Co in comparison with EG-SQ. Despite being very similar for the three approaches, **XRD** patterns clearly displayed a higher formation of the mixed oxide **$MnMoO_4$** in both co-impregnation methods, which could entail an enhancement in the desulfurization efficiency, as $MnMoO_4$ was previously found to play a role in the promotion mechanism. Sorbent textural properties such as surface area and pore volume were studied by **N_2 physisorption**. Neither pore blockage nor large surface area decrease were reported. The egg-shell profile distribution was confirmed by **SEM/EDS** analysis, performing both line scans and elemental mapping. The egg-shell thickness was higher in ethylene glycol sequential impregnation (200µm) than co-impregnation (100µm). Besides, it also showed a dependency with impregnation time for the GL-Co approach.

Preface

This master's thesis was written at Norwegian University of Science and Technology as part of a five-month Erasmus Programme with Universidad Politécnica de Madrid, for the completion of the course TKP4901, Chemical Process Technology, Master's Thesis.

I would like to express my sincere gratitude to Professor Edd Anders Blekkan for giving me the opportunity to come to Trondheim in the first place, and for his valuable guidance during this project. My wholehearted gratitude also goes to Professor María González Miquel, my mentor in Spain, for bringing her knowledge and cooperation in both my master's and bachelor's thesis.

A special thank you to Estelle Marie M.Vanhaecke and Karin Wiggen for being always available, helpful and understanding, for giving me the necessary training to complete this project, and for keeping the laboratory in good and secure conditions for all of us.

I would also like express my gratitude to other members of the KinCat group who provided me with help and advice throughout the project. Thank you Petter Tingelstad for your fruitful feedback. Thank you, Post-Doc Katarzyna Swirk, Ph.D. candidates Óscar Iváñez, Dumitrita Spinu, Consolato Rosmini, Mónica Pazos Urrea and Kishore Rajendran. Together with the master students' group in which I have felt completely welcomed from the first day. Thank you to my friend Leo Gosbert for the endless hours of company and lab conversations, for supporting me through the bright and dark days and for always believing in my work.

Finally, I could never forget to thank my family for their unconditional support. I love you and owe you everything I have achieved so far.

Gracias de corazón.

Trondhiem, July 16th, 2021.

Isabel Pascual García.

Contents

List of tables

List of figures

Symbols

- $\boldsymbol{\lambda}$: characteristic wavelength.
- $\boldsymbol{Z}$: atomic number.
- $\boldsymbol{V_{PT}}$: total pore volume.
- $\boldsymbol{n}$: order of reflection.
- $\boldsymbol{d}$: distance between two lattice planes.
- $\boldsymbol{\theta}$: angle between the incident beam and the normal to the reflecting lattice plane.
- $\boldsymbol{L}$: dimension of the particle.
- $\boldsymbol{\beta}$: peak width.
- $\boldsymbol{V_m}$: adsorbate volume required for the formation of a monolayer.
- $\boldsymbol{P}$: gas pressure.
- $\boldsymbol{P_o}$: gas saturation pressure.
- $\boldsymbol{V}$: volume of gas adsorbed.
- $\boldsymbol{\gamma}$: surface tension.
- $\mathbf{V_L}$**:** molar volume of liquid adsorbate.
- $\boldsymbol{R}$: gas constant.
- $\boldsymbol{T}$**:** temperature in Kelvin.
- $\mathbf{r_m}$**:** mean pore radius.
- $\boldsymbol{Q}$**:** flow rate of the gas.
- $\boldsymbol{C_{H2S}}$: concentration of H_2S.
- $\boldsymbol{C_{in}}$: H_2S concentration in the inlet (ppm).
- $\boldsymbol{C_{out}}$: H_2S concentration in the outlet (ppm).
- $\boldsymbol{m_s}$: solid sorbent mass.
- $\boldsymbol{M_{H2S}}$: molecular weight of H_2S.

Abbreviations

- CLD: Chemical Looping Desulfurization.
- MSW: Municipal Solid Waste.
- IWI: Incipient Wetness Impregnation.
- WI: Wetness Impregnation.
- HT: High temperature.
- FT: Fischer-Tropsch.
- AGR: Acid Gas Removal.
- MEA: Methylethanolamine.
- DEA: Diethanolamine.
- MDEA: Methyl-Diethanolamine.
- XRF: X-Ray Fluorescence.
- PHA: Pulse Height Analyser.
- BET: Brunauer–Emmett–Teller.
- BJH: Barrett-Joyner-Halenda.
- XRD: X-Ray Diffraction.
- FWHM: Full Width at Half-Maximum.
- SEM: Scanning Electron Microscopy.
- TEM: Transmission Electron Microscopy.
- EDS: Energy-dispersive X-Ray Spectroscopy.
- ETD: Everhart Thornley Detector.
- SE: Secondary Electrons.
- BSE: Back Scattered Electrons.
- BC: Breakthrough Capacity.
- IC: Ion Current.
- IGCC: Integrated Gasification combined cycle.
- WGS: Water Gas Shift.
- PBtL: Power and Biomass to Liquid.
- EG-SQ: Ethylene Glycol Sequential Impregnation.
- EG-Co: Ethylene Glycol Co-Impregnation.
- GL-Co: Glycerol Co-Impregnation.
- MS: Mass Spectrometer.
- MFC: Mass Flow Controller.

1. Introduction

Energy production and consumption models have a major impact in our society. Thus, great effort in research and implementation has been done in the last years, in order to stop unsustainable patterns which contribute to climate change and threaten future generations life standards.

Despite of the effort, a sustainable world energy mix is far from being a reality. Energy consumption has increased drastically in the last century due to industrial development and population growth (Figure 1.1). Clearly, fossil fuels still dominate the mix with 84,3% of the energy consumption. In 2019, only 15.7% of the global primary energy came from low-carbon sources [1]. Furthermore, the energy sector is responsible for more than 70 % of the greenhouse gas emissions globally [2].

Apart from the urgency of the situation, it must be considered that around 13% of the world's population still has no access to modern electricity services [3]. In this way, sustainable energy could also be a driver of social progress, equity, economic growth and environmental sustainability throughout the world.

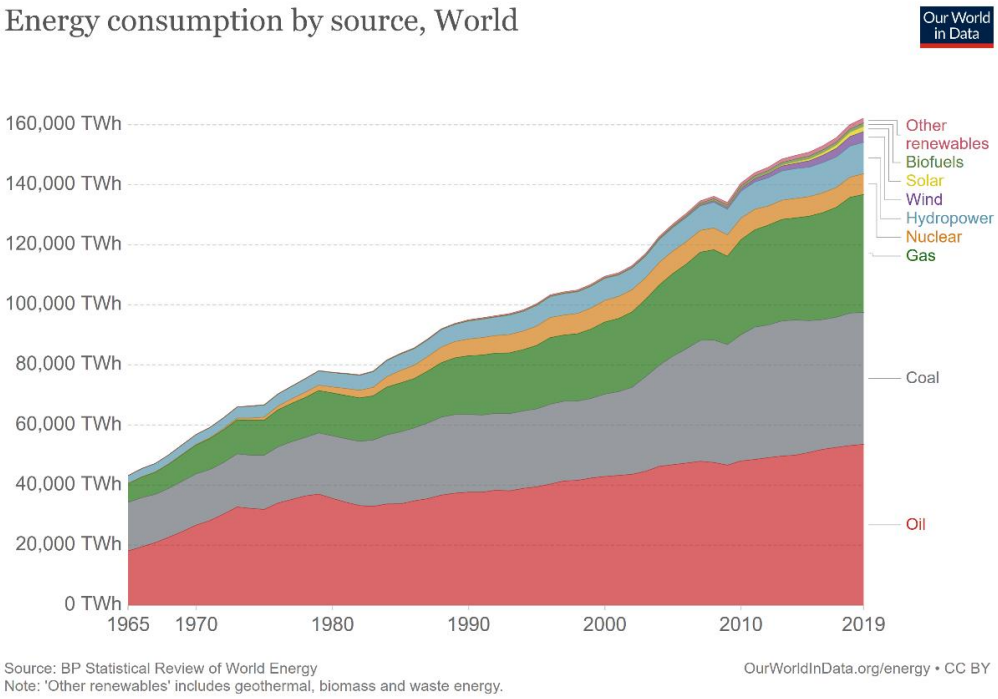

Figure 1.1 World energy mix 1965-2019 [1].

Within the world energy mix, solid biomass and its related energy forms such as biofuels, biogas or low carbon hydrogen will play an important role in the upcoming years [4]. The International Energy Agency reveals in its World Energy Outlook 2020 report that, in both stated policies and sustainable development scenarios, all biomass energy forms will need to rise much further (Figure 1.2).

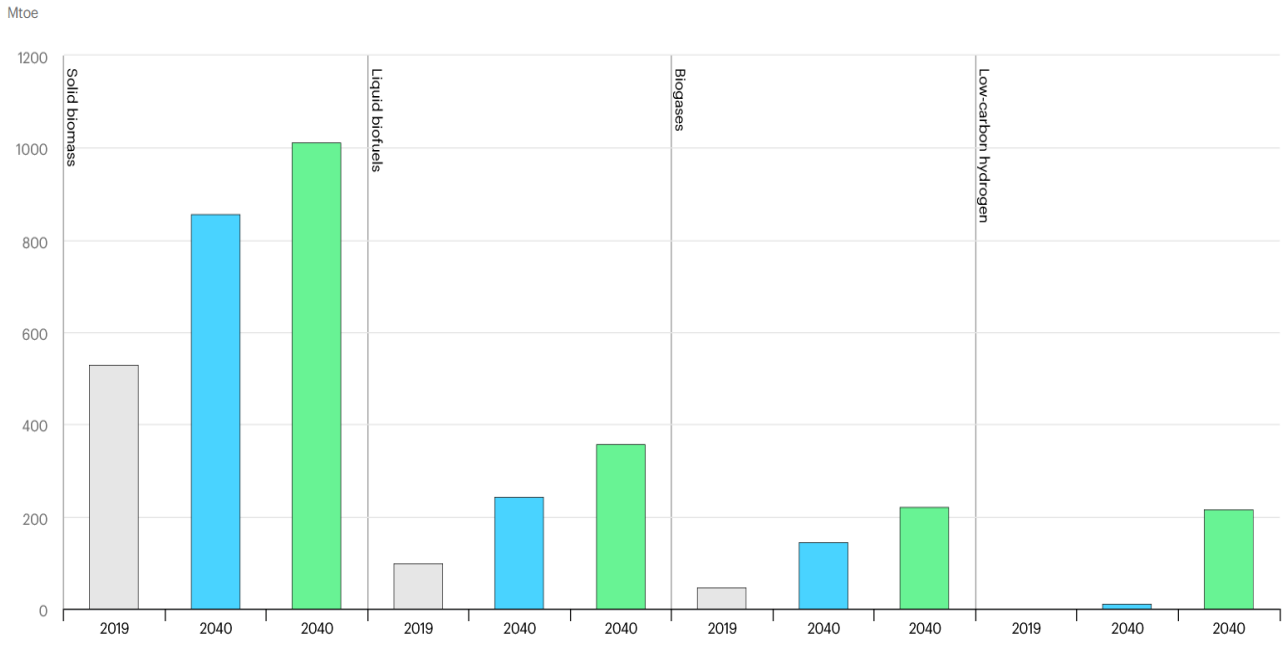

Figure 1.2 Global supply of low-carbon fuel by scenario: 2019-2040. Historical (grey), stated policies (blue), sustainable development (green) [4].

One of the paths for biomass utilization is gasification. Gasification of solid biomass produces synthesis gas, mainly a mix of H_2, CO, CO_2, CH_4, C_2H_4 and H_2O; useful for electricity production or downstream chemical applications. However, undesired species which can cause severe detrimental effects on industrial equipment and catalysts, are also present in the gas matrix. Sulfur compounds, important catalyst poisons, are one of these species. Currently, research is being made to develop a new energy efficient technology for sulfur removal, using a high temperature application, particularly with Mn-based/γ-Al_2O_3 solid sorbents [5].

This work is going to continue the research path of Mn-based/γ-Al_2O_3 solid sorbents for high temperature desulfurization, namely the CLD project (Chemical Looping Desulfurization). The focus will be in synthesis and characterization techniques.

1.1. Scope of the thesis

The scope of this master's thesis is described below, divided in three different sections:

1. **Synthesis** of pelletized egg-shell sulfur sorbents (Mn-based/γ-Al_2O_3, Mo-promoted) using different synthesis approaches. First, using a hydrophobic solvent to retard the penetration of the precursor/s solution, enabling the formation of an egg-shell pellet. Second, using a viscosifying agent, which entails slow diffusion and subsequent control of the egg-shell profile. The three approaches will be:
    - ✓ Hydrophobic solvent with sequential impregnation.
    - ✓ Hydrophobic solvent with co-impregnation.
    - ✓ Viscosifying agent with co-impregnation.

2. **Characterization** of synthesized sulfur sorbents applying a variety of techniques:
    - ✓ X-Rray fluorescence (XRF) to verify the metal loading of the samples.
    - ✓ X-Ray diffraction (XRD) to study the present crystallographic phases.
    - ✓ N_2 physisorption (BET) to study the textural properties of the sorbents.
    - ✓ Scanning electron microscopy (SEM) coupled with energy dispersive spectroscopy (EDS) to verify the egg-shell structure.

3. **Analysis** and further discussion of the following matters:
    - ✓ Metal loading.
    - ✓ Textural properties.
    - ✓ Crystallographic phases.
    - ✓ Time efficiency of the synthesis approaches.
    - ✓ Formation of the mixed oxide $MnMoO_4$.
    - ✓ Egg-shell profile distribution.

1.2. Structure of the thesis

This thesis is divided into six main sections:

1. **Introduction**

Offers an introduction to the project from a global perspective, and its scope.

2. **Theory**

Introduces some relevant theory about biomass, high-temperature desulfurization, sorbent preparation and characterization techniques.

3. **Experimental**

Presents the materials and methods used, as well as the procedures for each characterization technique.

4. **Results and discussion**

Presents the main results about sorbent preparation methods and characterization techniques, discussing the observed phenomena.

5. **Conclusion**

Presents the main findings and conclusion of the thesis.

6. **Further studies**

Gives some suggestion for future work within the project.

2. Theory

In this section, a deeper background regarding biomass conversion, gasification, sulfur removal technologies and chemical looping desulfurization will be covered. Together with an understanding of the sorbent preparation methods, egg-shell distribution, and the fundamentals behind the characterization techniques.

2.1. Biomass conversion

Biomass can be defined as biological matter from plants, animals, manure, or municipal solid waste (MSW). Plant biomass is divided into different categories: woody biomass (trees, bushes, scrubs), non-woody biomass (energy crops, grass, cereal straw), processed waste (cereal husks, bagasse, nutshells, sawmill waste, municipal waste) and processed fuels (plant oils, charcoal, biogas…) [6].

Biomass conversion has a wide range of possibilities. It can be transformed into valuable energy forms or chemical products via thermochemical, biochemical, or physical processes. Thus, biomass is regarded as one of the most promising alternatives to fossil fuels within the renewable energy transition. An overview of the feasible conversions is presented in Figure 2.1. Thermochemical processes include combustion, gasification and pyrolysis, which are going to be explained more in detail, with focus on gasification, as part of the scope of the project. Besides, biochemical and physical transformations such as fermentation, anaerobic digestion (methanisation) or extraction can also convert biomass into different biofuels [7].

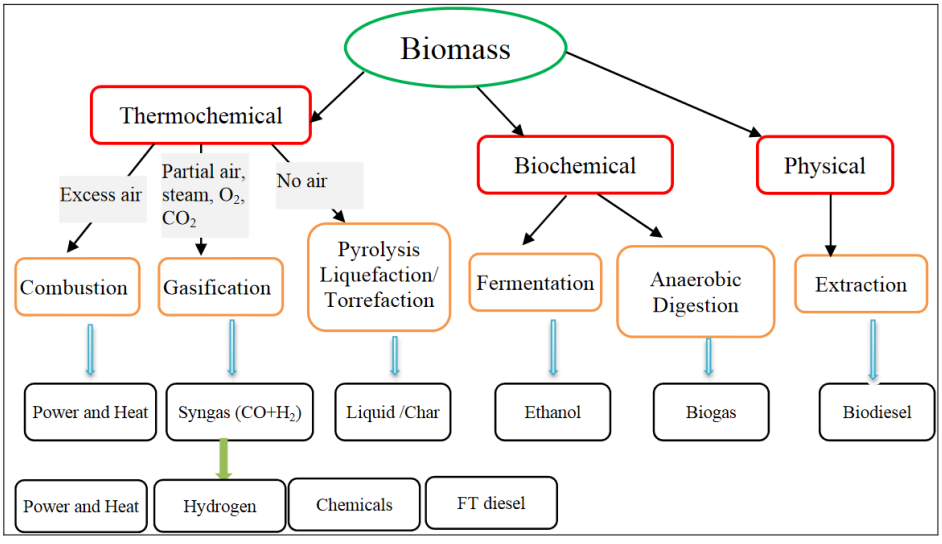

Figure 2.1 Biomass to energy conversion technologies [7].

2.1.1. Biochemical methods

Ethanol and biodiesel can be obtained through fermentation and transesterification, respectively, from food crops (sugar, amylaceous). This path is known as the first generation of biofuels, which brings an ethical debate as the feedstock is edible. However, the second generation avoids this controversy by introducing non-edible waste biomass (lignocellulosic), as the main source of energy. The third generation of biofuels is produced from cultivated aquatic feedstock as algae. From a sustainability point of view, the production of biofuels needs to be evaluated, preferably considering the integrated agro-industrial system. *Emergy* evaluation is a methodology used for that purpose, which calculates the energy balance of the system in terms of solar energy required, directly or indirectly, to create a specific product [8].

2.1.2. Thermochemical methods

Regarding thermochemical processes, **combustion** is the most widely extended method. The technology is well known, and approximately 90% of the energy from biomass is obtained from combustion processes. However, particulate matter, ashes, CO_2 emissions, air pollutants (NO_x, CO) and acid gases (SO_2, HCl, HF) remain an environmental concern in these types of plants. Hence, integration of carbon capture and storage technologies, pre/post-combustion treatments, and ash valorisation, can significantly improve the overall efficiency of the process [9, 10].

Pyrolysis is the process of heating biomass in the absence of oxygen at temperatures below 700ºC. Depending on the operation conditions, different product distributions can be obtained. Via slow or conventional pyrolysis (slow heating rates), solid char is the main product, which can be used for solid fuel production or soil amendment. On the contrary, fast pyrolysis (high heating rates) is intended to produce liquid bio-oil, for fuel production or other chemical-based applications. This bio-oil needs to be upgraded due to its oxygen content, high viscosity and water fractions. For that purpose, catalytic hydrodeoxygenation, steam reforming and hydrocracking are active research topics, in which progress is being made within the last years [9].

G**asification** is a partial oxidation process which uses a gasifying agent such as O_2, air, steam or CO_2 to obtain synthesis gas (mainly H_2 and CO) at temperatures between 700-1000 ºC. Syngas has many applications which range from chemicals such as methanol or ammonia (through WGS) to Fisher-Tropsch processes or heat and power applications (IGCC). Since these technologies are highly developed, they add value and interest to biomass gasification, contributing to both decrease fossil-fuel usage in chemical production and to finer process optimization [9, 11]. As an example of the latter, M. Hillestad et al. proposed a PBtL (Power and Biomass-to-Liquid) plant,

an improved concept of a Biomass-to-Liquid (BtL) plant, which introduces hydrogen production via electrolysis of high temperature steam and CO_2 recycling [12]. During gasification, several physical and chemical processes occur. Four steps take place depending on the temperature range: drying, pyrolysis, oxidation and reduction. A summary of the chemical reactions involved in the process is shown in Table 2.1.

Table 2.1 Chemical reactions and mechanisms in gasification of biomass [13].

Reaction name	Reaction	Endothermic/exothermic	Specific heating value	Temperature
Feedstock gasification				
	$C_xH_yO_z$ + heat → steam + biochar + gas + tar	Endothermic	–	–
Hydrocarbons reforming	$C_nH_m + 2_nH_2O \rightarrow (2n+m/2)H_2 + nCO_2$	Endothermic	–	–
Secondary Tar Cracking				
–	Tar + $H_2O \rightarrow H_2 + CO$	Endothermic	–	–
–	Tar + $H_2 \rightarrow$ light hydrocarbons + gases	Endothermic	–	–
–	Tar + $xH_2O \rightarrow yCO_2 + zH_2$	Endothermic	–	–
–	Tar → $CH_4 + H_2 + H_2O + C_nH_m$	Endothermic	–	–
Carbon oxidation				
Boudouard Reaction	$C + CO_2 \leftrightarrow 2CO$	Endothermic	162.4 kJ/kmol	> 700 °C
Water-Gas (Primary) Reaction	$C + H_2O \leftrightarrow CO + H_2$	Endothermic	131.3 kJ/kmol	> 700 °C
–	$C + 2H_2O \leftrightarrow CO_2 + 2H_2$	Endothermic	14.5 kJ/mol	–
Combustion of Char	$C + O_2 \leftrightarrow CO_2$	Exothermic	–	–
Methane Decomposition	$CH_4 + H_20 \leftrightarrow CO + 3H_2$	Endothermic	206.3 MJ/kmol	> 500 °C
–	$CH_4 + 2H_20 \leftrightarrow CO_2 + H_2$	–	–	–
Shift Reaction	$CO + H_20 \leftrightarrow CO_2 + H_2$	Exothermic	− 42.0 kJ/mol	300–600 °C
Steam Reforming Reaction	$C_nH_m + 2nH_2O \leftrightarrow (2n + (m/2))H_2 + nCO_2$	Exothermic	–	> 700 °C
Water-Gas Shift Reaction	$CO + H_2O \leftrightarrow CO_2 + H_2$	Exothermic	− 42.1 MJ/kmol	300–600 °C
Methane Forming				
Methanation Reaction	$CO + 3H_2 \leftrightarrow CH_4 + H_2O$	Exothermic	− 221.0 kJ/mol	300–600 °C
–	$CO_2 + 4H_2 \leftrightarrow CH_4 + 2H_2O$	Exothermic	− 223.0 kJ/mol	300–600 °C

Regarding gasification systems, there are mainly four different types of **gasifiers**: fixed bed (updraft and downdraft), fluidized bed (bubbling and circulating), entrained-flow gasifiers and plasma gasifiers**. Updraft fixed bed** gasifiers use a counter-current flow of biomass and gas, which allows high moisture feedstocks to dry quickly; however, it produces a large amount of tar. **Downdraft fixed bed** gasifiers use a concurrent flow which reduces the amount of tar, but lower energy efficiency and limited feedstock are two of its drawbacks. Both **bubbling and circulating fluidized bed** gasifiers have a comparable design except that, in the circulating configuration, a cyclone is installed for particle separation. Higher gas flow velocities are required compared to fixed bed configuration, but the heat and mass transfer is enhanced. **Entrained-flow** gasifiers operate in a concurrent flow of biomass and gasification agent. Even though the operating conditions require a large amount of heat and gasification agent, their feedstock flexibility is high, and they produce low amounts of tar. Finally, **plasma** gasifiers exhibit a new technology in which gasification is carried out at higher temperatures (3500–6500°C), where tar and ash are melted forming a slag outlet. Additionally, it can be a safe treatment for hazardous waste, but its economic feasibility stills uncertain [13]. In Figure 2.2 all the configurations are presented.

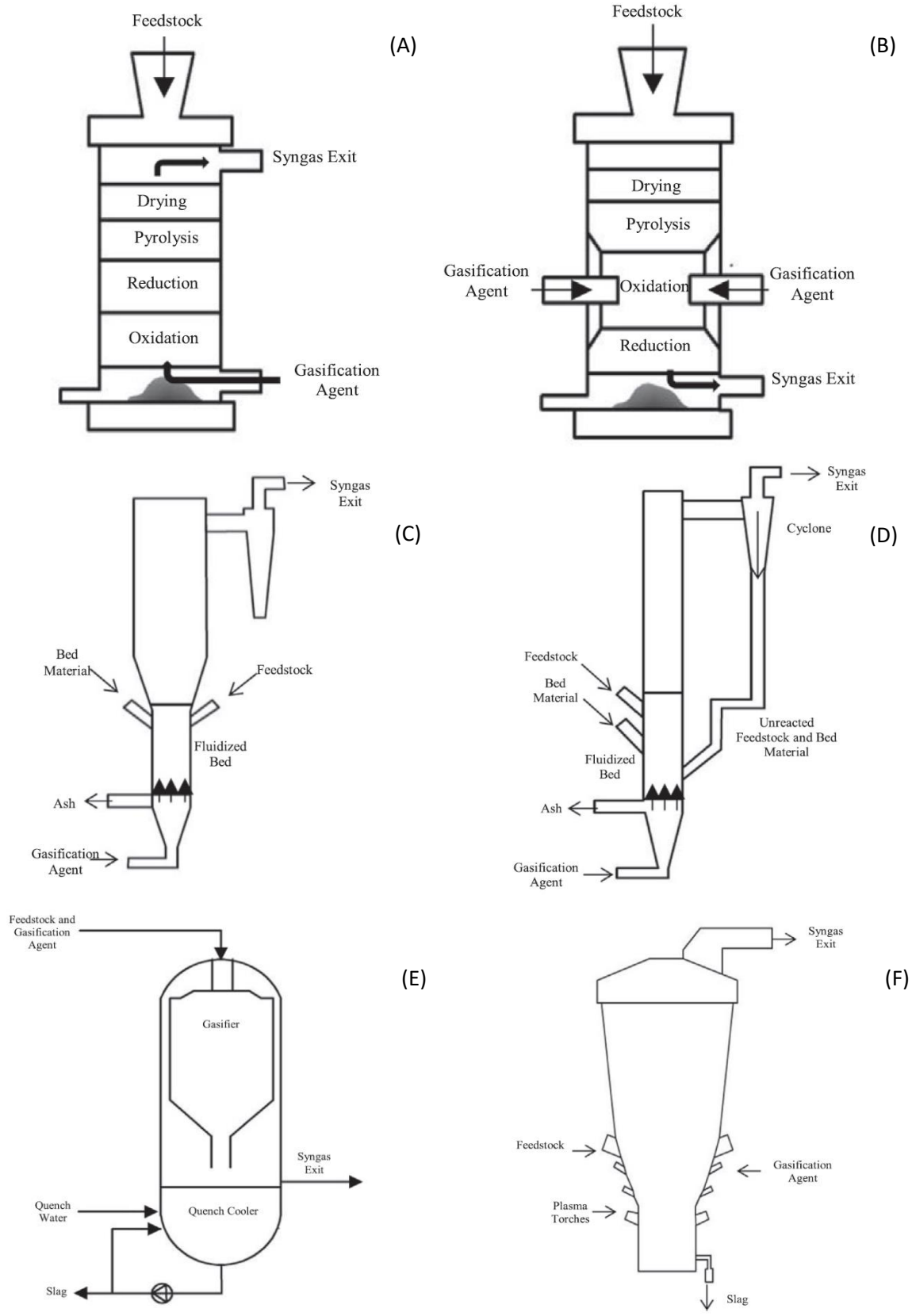

Figure 2.2 Reactor systems for biomass gasification (A): Updraft fixed bed gasifier, (B): Downdraft fixed bed gasifier, (C): Bubbling fluidized bed gasifier, (D): Circulating fluidized bed gasifier, (E): Entrained flow gasifier, (F): Plasma gasifier (adapted from Jamison Watson et al. [13]).

The composition of the raw syngas depends on the type of gasifier, as well as other parameters such as temperature, pressure, **gasifying agent**, residence time, and feedstock properties (ultimate and proximate analysis). For example, steam gasification produces more H_2 than O_2 or air gasification. Air is often employed due to its availability, but the product has a low heating value. Oxygen is also a good alternative, as it produces a medium heating value gas, and it can be mixed with steam to avoid the high cost of pure O_2 [9, 13].

Raw syngas has different **contaminants** or impurities such as sulfur, tar, particles, or nitrogen, along with the desired components. Its removal is critical not to exceed the permissible limits, which depend on the intended application (internal combustion engine, gas turbine, chemical synthesis, etc.) In Table 2.2 and Table 2.3, contaminant levels in raw syngas and permissible limits are summarized, respectively. For sulfur, nitrogen and tars, the limit is very low regarding chemical applications. Thus, syngas treatment is imperative to meet the requirements. [11].

Table 2.2 An example of contaminant levels in raw syngas [14, 11].

Compounds	Units	Amount
Hydrogen	Vol.%	30-45
Carbon monoxide	Vol.%	20-30
Carbon dioxide	Vol.%	15-25
Methane	Vol.%	8-12
C_{2+} hydrocarbons	Vol.%	1-3
Benzene	Vol.%	1
Nitrogen	Vol.%	1-3
Ammonia	ppm	500-1000
H_2S	ppm	50-120
Tar	g/m^3	0.5-1.5
Particles	g/m^3	10-20

Table 2.3 Permissible limits for contaminants in syngas regarding different applications [14, 11].

Contaminant	Application			
	IC engine	Gas turbine	Methanol synthesis	FT synthesis
Particulate	<50mg/m³ (PM10)	<30 mg/m³ (PM5)	<0.02 mg/m³	
Tars	<100mg/m³		<0.1 mg/m³	<0.01 µL/L
Sulfur		<20 µL/L	<1 mg/m³	<0.01 µL/L
Nitrogen		<50 µL/L	<0.1 mg/m³	<0.02 µL/L
Alkali		<0.024 µL/L		<0.01 µL/L
Halides		1 µL/L	<0.1 mg/m³	<0.01 µL/L

2.2. Sulfur removal technologies

In this section, some of the available sulfur removal technologies are reviewed. Sulfur content in biomass gasification is lower in comparison to coal gasification, however, for certain applications it needs to be further reduced [9].

Sulfur is converted into different compounds during gasification, such as H_2S or SO_2. Other forms of sulfur can also be present: carbon sulfide (CS_2), carbonyl sulfide (COS) or mercaptans (CH_3SH, CH_3CH_2SH). Sulfur species are considered one of the most harmful in terms of catalyst poisoning and subsequent deactivation, for example, for Fisher-Trops synthesis catalysts or tar reforming catalysts. The corrosive nature of H_2S can damage industrial facilities and cause environmental issues. Hence, sulfur content should be reduced to, for example, 20 ppmv in a gas turbine or 0.01 ppmv in FT synthesis. It must be pointed out that H_2S is a very toxic compound which can be mortal at the level of 400ppmv [15].

The conventional path regarding sulfur removal from syngas is **low-temperature** desulfurization, also known as acid gas removal (AGR). Using different solvents such as methanol (Rectisol process), polyethylene glycol (Selexol process) or amines (MEA, DEA, MDEA), through physical absorption or chemical reaction, acid gas is captured from the gas phase. Despite the maturity of these technologies, they still entail large investments. Furthermore, the cooling of raw syngas from around 850 ºC to less than 100 ºC and later reheating to 200-400 ºC of clean syngas for other processes, shows a clear energy inefficiency [15, 5].

For all the above mentioned, **high-temperature** (HT) desulfurization is a favorable approach to avoid energy loss. This method is based on the reaction of metal oxides with H_2S and H_2 at high temperatures, forming a metal sulfide, which can be regenerated to the previous oxide form. The released sulfur forms are brought to a sulfur recovery unit, to obtain either sulfuric acid or elemental sulfur. It was first proposed in 1976 by Westmoreland et al. [16].

HT desulfurization primarly depends on **adsorption**, both physical and chemical. Physical adsorption has low adsorption heat, relies on Van der Waals forces and can be a multilayer process. In contrast, chemical adsorption has high adsorption heat, involves a chemical bond between sorbent and adsorbate, and is a single layer process [17]. HT desulfurization has been studied for both in-situ (sorbent and feedstock together) and downstream (after gasification) capture. In situ sorbents include calcium-based materials, as limestone (CaCO3) and dolomite ($CaCO_3 \cdot MgCO_3$) [18]. Downstream applications can be classified into physical adsorption sorbents such as zeolites [19] and chemical adsorption sorbents, which are the scope of this project, and will be covered in the next section.

2.3. Chemical looping high-temperature desulfurization

As it has been advanced, in 1976, Westmoreland et al. reported that some **transition metal oxides** (iron, zinc, manganese, molybdenum, vanadium, etc.) had a good sulfur removal ability in the temperature range of 300-800 ºC [16]. The chemical reactions which take place can be divided into three stages: reduction, sulfidation and regeneration. Reduction and sulfidation take place together (reaction 1.), where metal oxides react with H_2S and H_2 forming metal sulfides and steam. Regeneration agents such as H_2O, SO_2 or O_2 can be used to convert sulfides back to oxides (reactions 2-4.) Reaction 5. illustrates a side reaction in which sulfates (for example, manganese sulfate) could be formed causing deactivation.

1. $M_xO_y(s) + xH_2S\ (g) + (y-x)H_2\ (g) \rightarrow xMS\ (s) + yH_2O\ (g)$
2. $MS(s) + H_2O\ (g) \rightarrow MO\ (s) + H_2S\ (g)$
3. $xMS\ (s) + \frac{y}{2}SO_2\ (g) \rightarrow M_xO_y(s) + \left(x + \frac{y}{2}\right)S\ (g)$
4. $xMS\ (s) + \frac{y}{2}O_2\ (g) \rightarrow M_xO_y(s) + xSO_2(g)$
5. $MS(s) + 2O_2\ (g) \rightarrow MnSO_4$

Given the nature of the process, these metal sorbents can be **regenerated**. As shown in Figure 2.3, the system can be turned into a closed cycle of sorption and regeneration: chemical looping HT desulfurization [5]. The selection criteria of a qualified HT desulfurization sorbent ranges from a high equilibrium constant, fast kinetics, high selectivity towards sulfur, resistance to H_2 reduction, to good mechanical properties and regeneration capabilities [20]. **Manganese** has been studied as the based sorbent material using different supports and promoters, giving promising results, mainly due to its thermal stability and high activity [21, 22, 23, 24].

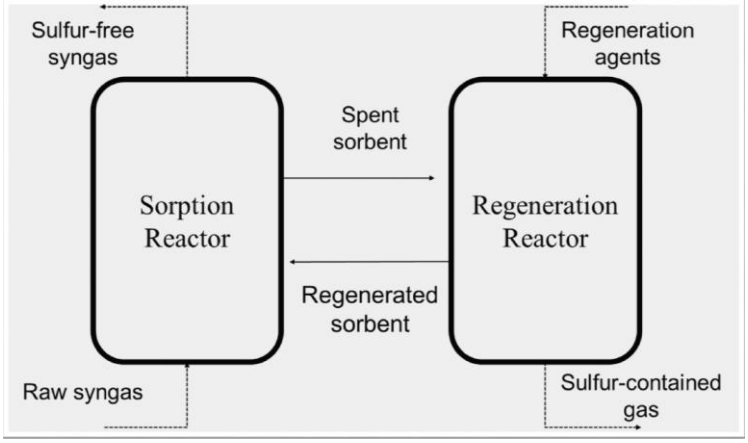

Figure 2.3 HT desulfurization cyclic sorption-regeneration process [14].

2.4. Sorbent preparation

Pelletized solid sorbents are supported metal oxides made and characterized in the same way as heterogeneous catalysts. The first step for its preparation is contacting the support with the precursor/s solution, this step is called **impregnation**. Then, in which is known as the **drying** step, the impregnated support is heated to a certain temperature under a gas flow and the solvent is evaporated, letting the precursor/s salt crystallize on the pores. Finally, a **calcination** step is carried out for the conversion of metal salts into metals or metal oxides. It consists in a heat treatment under air or nitrogen atmosphere, most commonly [25].

The impregnation step can be performed using two different approaches: Wetness Impregnation (WI) or Incipient Wetness Impregnation (IWI).

The **Wetness Impregnation** method can also be referred as "diffusional impregnation". It uses an excess volume of precursor solution. The distribution of the solute inside the pellet is governed by diffusion (Fick's law) and adsorption (equilibrium constant and adsorption capacity of the surface), as it can be seen in Figure 2.4(a). The balance between these two parameters regulates the final distribution of the precursor along the pellet.

For low concentrations and short-time impregnations, adsorption is strong, and the precursor will be mostly placed in the outside part of the pellet (egg-shell profile). On the contrary, if the concentration is high enough and a long-term impregnation is performed, diffusion is enhanced, and distribution will tend to be uniform [26]. These different precursors distributions will be covered in Section 2.5.

Porosity and pellet size also affect diffusional conditions. Porosity increases intra-pellet diffusion and, in regard to pellet size, characteristic diffusion time in a pellet is proportional to R^2 (being R the radius of the pellet) so, it will be significantly lower for small pellets. However, as stated by Ergun's equation, small pellets in a packed bed can cause a high pressure-drop. Thus, an optimal size should be found to avoid high pressure drop or poor diffusion [27].

The **Incipient Wetness Impregnation** method or "dry impregnation" involves the addition of a solution volume equal to the total pore volume of the support ($V = V_{PT}$). In this physical model, the capillary flow (Darcy's law) controls the impregnation process. Considering the pore radius sufficiently small, this flow is larger than the pressure of the entrapped air, which dissolves and escapes the pore (Figure 2.4(b)).

Apart from precursors concentration, contact time between support and solution, porosity or pellet size, other factors such as the drying regime, substances acting as competitors, or the viscosity term introduced by Darcy's law, can influence the final precursor distribution [26].

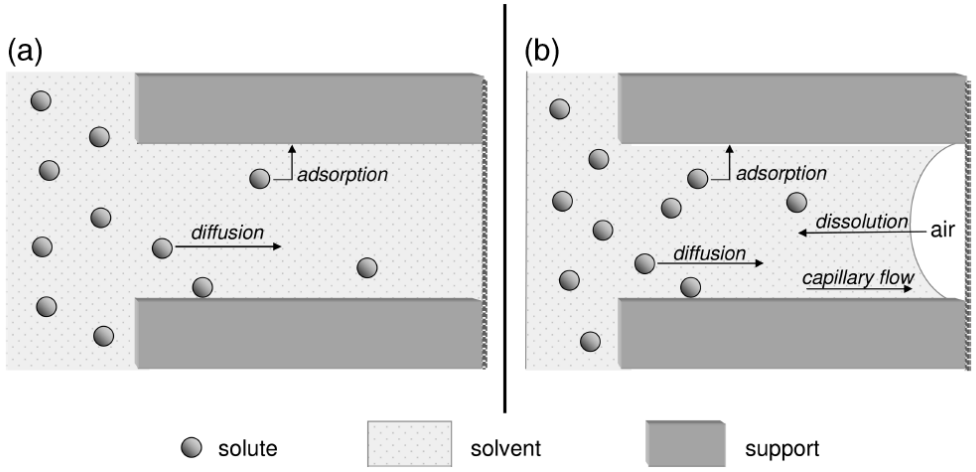

Figure 2.4 Physical models for (a) wet impregnation, (b) dry impregnation [26].

2.5. Egg-shell pellets

As it has been advanced in the previous section, regarding the singularity of each process, it may be of interest having different distributions of the active phase. Four main distribution profiles are shown in Figure 2.5. If the active phase is homogeneously distributed along the support, the profile is **uniform** while, if the active phase is located only in the outer part of the support, an **egg-shell** profile is attained. The **egg-white** profile includes the active phase in a region between the surface and the core, and the **egg-yolk** profile the active phase is in the inner-core of the support [28].

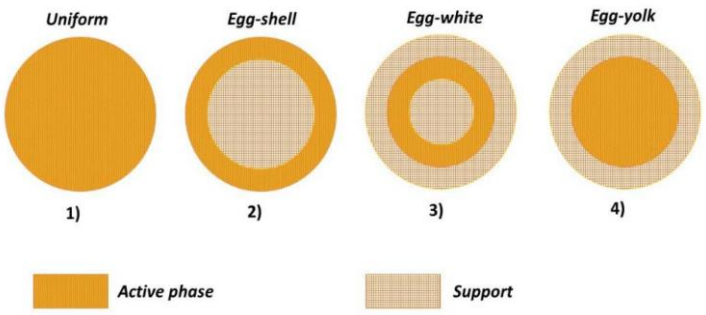

Figure 2.5 Distribution profiles for a spherical catalyst particle [28].

The **egg-shell distribution** can be of interest for different reasons. First, as catalysts are made of valuable metals, a uniform profile is often not desired. An example is the ethylene oxide synthesis, performed by Ag-based catalysts, that can be optimized using an egg-shell profile [29]. Besides, locating the active metals on the surface of the support is convenient for reactions such as Fisher–Tropsch synthesis, with internal mass transfer limitations affecting the conversion, or willing to improve yield for a desired product [30, 31]. Other examples are ammonia decomposition [32] or purification of exhaust gases [33].

Apart from the parameters discussed before (drying regime, concentration, impregnation time…), specific methods can be performed to achieve an egg-shell profile with a fixed egg-shell thickness. Before the impregnation step, the support can be soaked in a **hydrophobic solvent**, retarding the penetration of the precursor/s solution and enabling the formation of the desired profile. Jang et al. proposed octanol as a hydrophobic solvent to control metallic nickel inside alumina pellets, resulting in a higher conversion for steam methane reforming than the uniform profile and the commercial reference catalyst [34]. The hydrophobic nature of the solvent (which increases with the length of the carbon chain) and the hydroxyl group interaction with alumina made octanol a perfect candidate. Besides, for cobalt catalysts on silica supports, n-undecane has been employed as a hydrophobic solvent [35].

Another method is the usage of a **viscosifying agent** as solvent for the precursor/s solution. For example, glycerol can lead to a slow diffusion due to its high viscosity (954 cP at 25 ºC [36]) and it is used to control the egg-shell profile formation [32].

Overall, the **egg-shell thickness** plays an important role in the catalytic process. Its dimension can be controlled by the variation of already mentioned parameters such as impregnation time, concentration of precursor/s solution, porosity, or temperature [37]. Not every parameter has been deeply studied and, depending on the nature of the process, the effects can differ. To confirm that an egg-shell profile has been attained, SEM coupled with EDS can be used to obtain the concentration profile of the elements along the cross section. The concentration should be high in the outer part of the pellet and close to cero in the centre. Both procedure and results for this method are going to be later discussed.

2.6. Sorbent characterization

2.6.1. X-Ray Fluorescence

X-Ray fluorescence (**XRF**) technique can be used for qualitative and quantitative elemental analysis. By the irradiation of the sample with an X-Ray source, irradiated elements emit a characteristic fluorescence X-Ray radiation with a determined intensity, which is then evaluated by a detector.

The principle behind this technique is based on exciting inner shell electrons with high energy photons. As presented in Figure 2.6, these electrons are ejected from their position, leading to ionized atoms. Outer electron shells fill the vacant by the emission of a characteristic fluorescence radiation. Occasionally, instead of releasing energy by emitting a photon, the energy can be transferred to an outer electron called Auger electron, which is then ejected [38].

The wavelength of the characteristic X-ray radiation can be related to the atomic number by the Henry Mosley's law

$$\frac{1}{\lambda} = a \cdot (Z - b)^2 \qquad (2.1)$$

where λ is the characteristic wavelength, Z is the atomic number, and a and b are constants which depend on the series of the electrons (K, L, M).

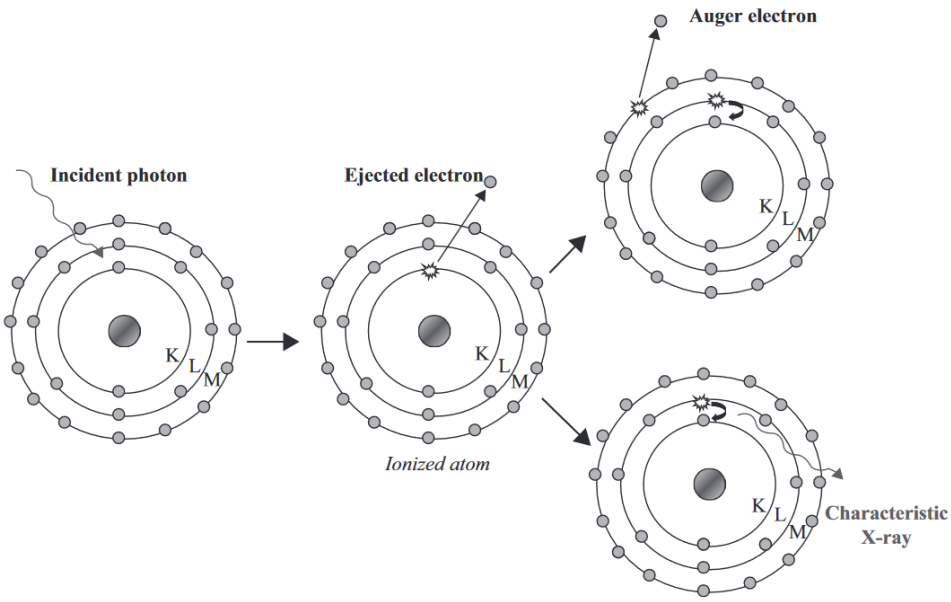

Figure 2.6 Atom ionization steps and X-ray characteristic emission [38].

The fluorescent yield is defined as the probability of electron transitions which lead to X-ray emission. It describes the effectiveness of the process in terms of the atomic number [39]. As it can be seen in Figure 2.7, X-ray spectrometry is poor for light elements. Additionally, fluorescent yield is limited for outer shell electrons. Common X-ray spectrometers have a range of 0.4-20 Å, which allows to measure elements from the K and L series.

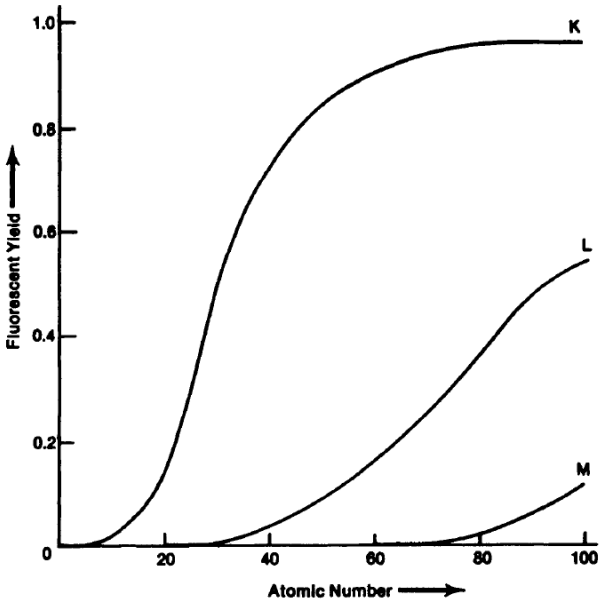

Figure 2.7 Fluorescent yield as a function of the atomic number [39].

2.6.2. X-Ray Diffraction

X-Ray Diffraction (**XRD**) technique is mainly used in catalyst characterization to identify the crystallographic phases present in the sample. It is a non-destructive technique with great potential. Given its penetrating power, it can also be used in specially designed *in situ* reactors. The principle of this technique is shown in Figure 2.8. X-ray photons are scattered by atoms in an ordered lattice, and a constructive interference is created between scattered X-rays that are in phase. Lattice spacings, which are characteristic of a given compound, can be calculated following Bragg's law:

$$n\lambda = 2d\sin\theta \qquad (2.2)$$

where λ is the wavelength of the X-rays, n is the order of reflection, which is an integer, d is the distance between two lattice planes, and θ is the angle between the incident beam and the normal to the reflecting lattice plane [40].

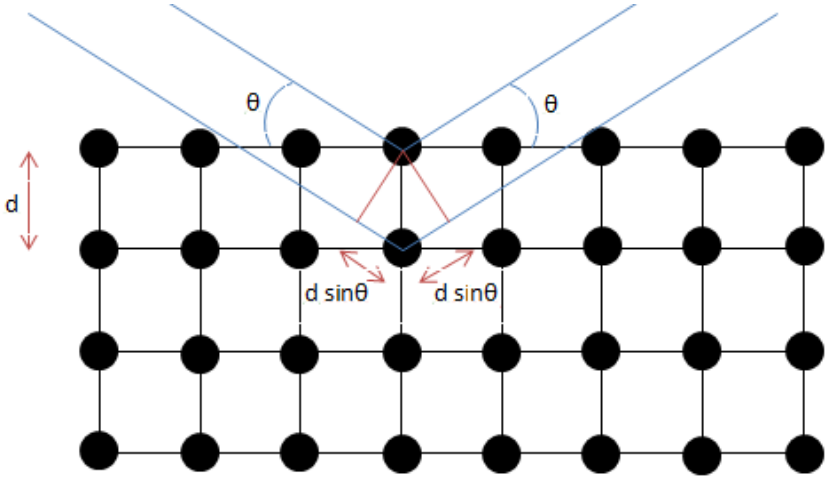

Figure 2.8 X-Ray Diffraction principle given by Bragg's law [41].

Diffraction peaks can be analysed comparing to standard reference patterns available in databases. X-Ray diffraction gives unequivocal information on sufficiently large particles, but its limitation comes when characterizing small or amorphous particles. There can be more present phases than the ones detected by XRD, and one must consider that the catalyst surface is invisible for standard XRD [42].

The width of the diffraction peaks has a relation with crystal size regarding Scherrer's equation (*2.3*). Diffraction peaks for perfect crystals are notably narrow, but broader peaks appear for lower crystallite size. Peak width is related to crystal size as follows:

$$L = \frac{k\lambda}{\beta \cos\theta} \qquad (2.3)$$

where L is a measure of the dimension of the particle, λ is the wavelength of the X-rays, k is a constant often taken as 1, β is the peak width and θ is the angle between the incident beam and the normal to the reflecting lattice plane. β can be determined systematically as the full width at half-maximum intensity (FWHM) of each peak.

Despite of the above, X-ray line broadening not always provides a reliable estimate of the particle size. Better procedures for determining particle size from XRD are based on line-profile analysis with Fourier transformation methods [42].

2.6.3. N_2 Physisorption

Physical adsorption with N_2 is used to characterize key **textural properties** of catalysts. For example, surface area, pore volume or pore size distribution. It is crucial to study these properties to understand the catalyst performance in a particular application. To run the experiment, liquid nitrogen is used as the adsorbate at a temperature of 77K. The amount adsorbed nitrogen is measured as a function of nitrogen pressure [40].

Brunauer-Emmet-Teller (**BET**) theory is used to explain multi-layer physical adsorption of gases onto solid surfaces. In the BET isotherm equation,

$$\frac{\mathrm{P}}{(\mathrm{P_o}-\mathrm{P})\cdot \mathrm{V}} = \frac{1}{\mathrm{V_m C}} + \frac{\mathrm{C}-1}{\mathrm{V_m C}}\frac{\mathrm{P}}{\mathrm{P_o}} \qquad (2.4)$$

V_m refers to the adsorbate volume required for the formation of a monolayer, P is the pressure of the gas, P_o is the saturation pressure of the gas at the temperature of the experiment, and V is the amount of gas adsorbed. According to this equation, the dependence of $\frac{P}{(P_o-P)\cdot V}$ on $\frac{P}{P_o}$ should be linear, with slope $s = \frac{C-1}{V_m C}$ and intercept $i = \frac{1}{V_m C}$. Therefore, V_m can be calculated as $V_m = \frac{1}{s+i}$.

The average area occupied by one adsorbed N_2 molecule is 0.162nm^2 [40]. Hence, the total BET surface area can be calculated from the monolayer coverage. Numerous experimental data follow the BET equation very accurately, mainly in the following range of relative pressures:

$$0.05 \leq \frac{P}{P_o} \leq 0.30 \qquad (2.5)$$

Depending on what type of material is being characterized, **BET isotherms** can adopt different shapes. For mesoporous materials (pore diameter between 2 and 50nm) such as alumina, isotherm type IV (Figure 2.9) is the most common. Point B represents the completion of the monolayer coverage and therefore, the beginning of multilayer adsorption. The hysteresis loop that appears between the adsorption and desorption curves is due to the capillary forces that need to be broken in the desorption step. This is only possible if performed at a lower relative pressure than the adsorption step.

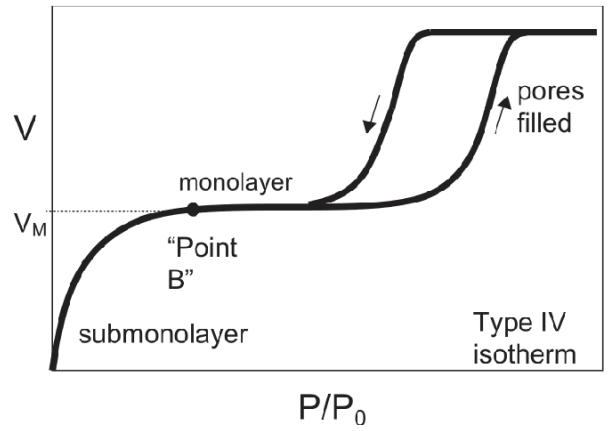

Figure 2.9 Type IV BET isotherm common in alumina supports [40].

The most common types of adsorption isotherms are illustrated in Figure 2.10. Type I corresponds to microporous solids like zeolites, type II is obtained with non-porous or microporous adsorbents, and type VI represents a stepwise multilayer adsorption on a uniform non-porous surface. Types III and V are the most uncommon, characterized by weak adsorbent-adsorbate interactions [43].

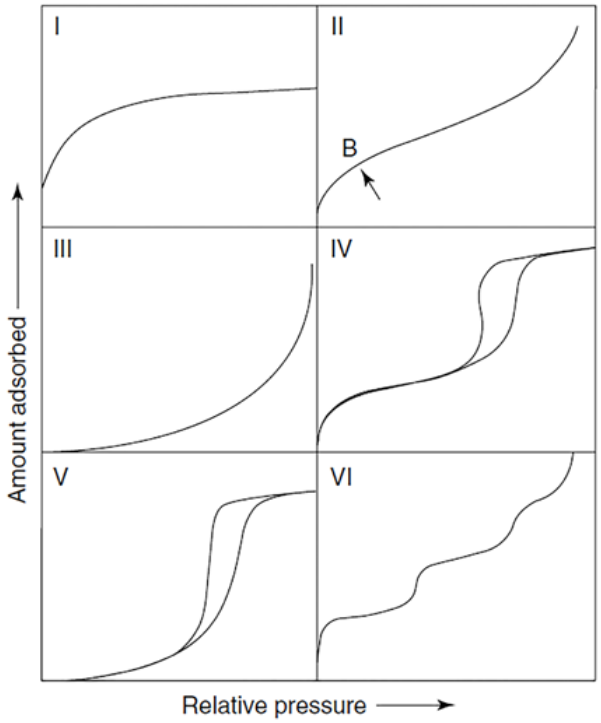

Figure 2.10 Different types of adsorption isotherms [43].

Pore size distribution in a catalytic particle defines its resistance with respect to internal heat and mass transfer. The Barrett-Joyner-Halenda (**BJH**) method, based on a variant of the Kelvin equation, is used to determine pore volume and pore size distribution. The equation which describes the method is the following

$$ln\left(\frac{P}{P_o}\right) = \frac{2\gamma V_L}{RTr_m} \quad (2.6)$$

Where γ is the surface tension of liquid adsorbate, V_L stands for the molar volume of liquid adsorbate, R is the gas constant, T is the temperature and r_m is the mean pore radius [44].

2.6.4. Scanning electron microscopy

Scanning electron microscopy (**SEM**) is an electron microscopy technique, among others such as TEM or STEM, mainly used to characterize the topography and composition of materials. It is carried out by scanning the surface of the material with a high-energy electron beam of around 100-400 keV. The interaction of the beam with the material causes the emission of secondary electrons (SE) or backscattered electrons (BSE), which are then collected by a detector and processed to build images [42]. Figure 2.11 shows the possible interactions between the electron beam and the material.

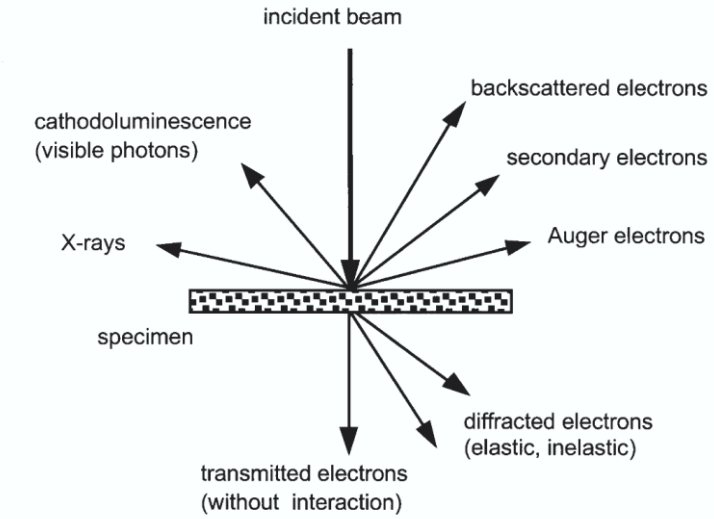

Figure 2.11 Interaction between the primary electron beam and the sample [45].

Secondary electrons carry low energies, in the range of 5-50 eV, and come from the surface of the material. On the contrary, backscattered electrons have higher energies and come from inner regions, providing information about the composition of the sample. SEM instruments operate in high vacuum to avoid undesired scattering, and normally have resolutions of about 5 nm. [42].

To perform elemental analysis in an electron microscope, the characteristic X-rays emitted need to be analysed. As energies of the atomic shells are clearly defined, it can be inferred that the energy of the X-ray photon belongs to a particular atom species. Thus, energy dispersive analysis of X-Rays can be carried out with a detector placed in the SEM chamber, usually referred to as energy dispersive X-Ray spectrometer (EDS) [46].

2.7. Sorbent performance

The performance of the sorbent can be evaluated in terms of capacity and stability during the sorption process. Sorbent **capacity** can be defined as the total mass of hydrogen sulfide removed per gram of sorbent. Besides, the breakthrough capacity (BC) is defined as the amount of sulfur removed by the sorbent before reaching the breakthrough, and can be calculated as follows:

$$\mathrm{BC}\left(\frac{\mathrm{g\ H_2S}}{\mathrm{g\ sorbent}}\right) = \frac{Q \cdot \int_0^t C_{in} - C_{out} \cdot M_{H2S}}{24{,}04 \cdot 10^9 \cdot m_s} \qquad (2.7)$$

where Q is the flow rate of the gas, C_{in} and C_{out} are the inlet and outlet concentration of H_2S in ppm, m_s is the mass of the solid sorbent and M_{H2S} is the molecular weight of H_2S. To obtain the concentration values, the ion current (IC) signal of the mass spectrometer should be transformed into concentration units (ppm), knowing that ion current linearly correlates to H_2S concentration according to:

$$IC = a \cdot C_{H_2S} + b \qquad (2.8)$$

where a and b are the slope and intercept of the IC signal linear function, respectively [14].

The robustness of a sorbent is also determined by its **stability**. The stability of a sorbent is related to the remaining capacity during time, and it can be evaluated by performing long term experiments with repeated sorption-regeneration cycles. As an example of these parameters, regarding the last study in this project, the promoted sorbent 15Mn8Mo was found to provide a 38% increase of the initial capacity and only 9.7% capacity loss after 10 sorption-regeneration cycles [5].

3. Experimental

3.1. Chemicals

Gamma-alumina (γ-Al_2O_3) LOT#1589-45-2 with purity 96% was used as the support material. Ethylene glycol (99,5% purity) was used as hydrophobic solvent and glycerol (99% purity) was used as the solvent for one of the approaches. Manganese nitrate ($Mn(NO_3)_2 \cdot 4H_2O$, 97% purity) was used as manganese precursor, and ammonium molybdate ($(NH_4)_6Mo_7O_{24} \cdot 4H_2O$, 99% purity) was used as molybdenum precursor. Both were purchased from Sigma Aldrich. Nitric acid with purity 65% was used to dissolve the precursors in one of the three approaches described in the next section.

3.2. Sorbent preparation

The main objective of this project is to compare different synthesis methods in terms of material parameters for ultimately, being able to study their role in the desulfurization efficiency. Three synthesis approaches were considered for sorbent preparation. Sorbents regarding the first and second approaches were synthesized using the Wetness Impregnation (WI) method, and sorbents from the third approach were synthesized using the Incipient Wetness Impregnation (IWI) method (See section 2.4).

1. Ethylene glycol (ethane-1,2-diol) was used as a hydrophobic solvent and a sequential impregnation of the support was applied (**EG-SQ**).
2. Ethylene glycol (ethane-1,2-diol) was used as a hydrophobic solvent and co-impregnation of the support was applied (**EG-Co**).
3. Glycerol (propane-1,2,3-triol) was used as precursor solvent and co-impregnation was also applied (**GL-Co**).

A graphical description of these three methods can be found in Figure 3.1, where the egg-shell formation is highlighted. The purple circle represents the synthesized egg-shell pellet with the desired concentration.

The choice of an egg-shell distribution profile relies on the fact that the sorption process is **diffusion-limited**, a concept which was previously introduced in Section 2.4. Thus, the reaction will take place mainly in the external surface of the catalyst and, creating an egg-shell distribution, the active phase can be optimized.

In the first and second approaches, immiscibility between ethylene glycol, pre-occupied inside the pellet, and the aqueous precursor solution is applied [34]. The hydrophobic solvent is introduced in the pellet before the impregnation step. Then, several impregnations can be carried out until the desired concentration of the sorbent is reached. It must be pointed out that these approaches are new methods within the CLD project, implying the synthesis procedure has been made from scratch for the completion of this master's thesis.

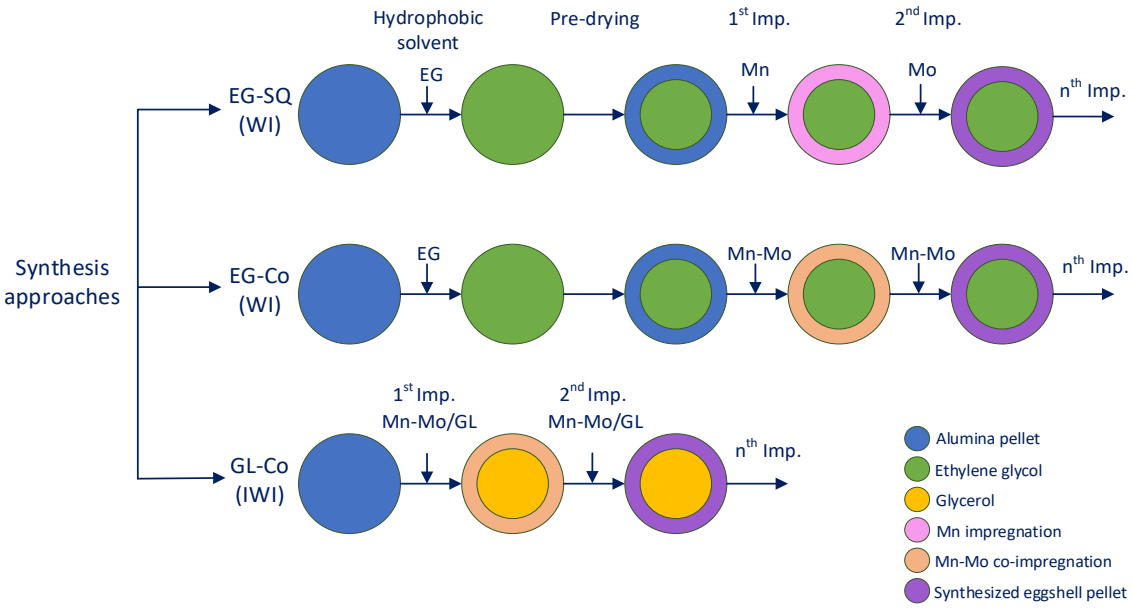

Figure 3.1 Synthesis approaches (own elaboration).

In Table 3.1 the synthesized sorbents are listed. They will also be referred as "target sorbents" throughout the report. The nominal Mn loading for all samples is 15 wt.%. This loading was chosen to both assure the clever usage of Mn as the active phase, and to allow the comparison with the previous study with powder sorbents [14]. The promoter (Mo) loading varies from 2,5 wt.% to 10 wt.%. The sorbent 15Mn8Mo (15 wt.% Mn and 8 wt.% Mo) was previously reported to enhance the desulfurization efficiency, and the formation of the complex $MnMoO_4$ was suggested to play a role in this effect [5]. This leads to the thought that, approaching to 1:1 molar ratio of both precursors, the formation of $MnMoO_4$ would be higher and the sorbent capacity would increase. Accordingly, a higher amount of Mo was chosen, and 15Mn10Mo sorbent was also synthesized. It can be observed that the number of impregnations in the second and third approaches is reduced comparing to the first one, thus improving the overall synthesis efficiency.

Table 3.1 Synthesized sorbents.

Method	Sorbent	Composition	Imp.1	Imp.2	Imp.3	Imp.4	Imp.5
EG-SQ (WI)	1	15Mn	Mn	Mn	-	-	-
	2	15Mn2,5Mo	Mn	Mn	Mo	Mo	-
	3	15Mn5Mo	Mn	Mn	Mo	Mo	-
	4	15Mn8Mo	Mn	Mn	Mo	Mo	Mo
	5	15Mn10Mo	Mn	Mn	Mo	Mo	Mo
EG-Co (WI)	6	15Mn2,5Mo	Mn-Mo	Mn-Mo	Mo	-	-
	7	15Mn5Mo	Mn-Mo	Mn-Mo	-	-	-
	8	15Mn8Mo	Mn-Mo	Mn-Mo	-	-	-
	9	15Mn10Mo	Mn-Mo	Mn-Mo	Mo	-	-
GL-Co (IWI)	10	15Mn8Mo	Mn-Mo	-	-	-	-

Pre-calcination of gamma-alumina was carried out at 500°C for 12 hours with a heating rate of 10°C/min, using a calcination set-up with flowing air at a flowrate of 70 mL/min.

For the first and second approaches, gamma-alumina was soaked into ethylene glycol for 30 minutes at 30°C using an ultrasonic bath. Afterwards, the excess of solvent was evacuated for 30 seconds using a Büchner funnel. Mn and/or Mo precursors were weight, dissolved in deionized water and impregnated for 20 minutes with continuous manual stirring, as shown in Figure 3.2. Again, the excess of precursor was evacuated for 5 seconds.

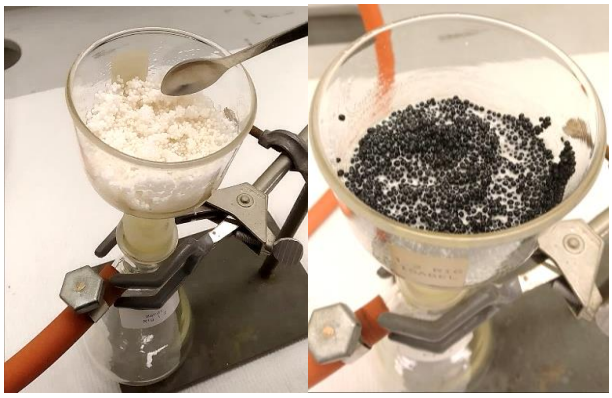

Figure 3.2 First impregnation (left) and second impregnation (right) of γ-Al_2O_3 in a Büchner funnel with continuous manual stirring.

For the **EG-SQ method**, impregnation was done either with Mn or Mo. This process was repeated until the desired concentration was reached (Figure 3.1). XRF characterization was carried out in between the impregnations to check the amount of metal loading and to consequently decide if another impregnation was needed.

For the **EG-Co method**, the same steps were followed. The difference relied on dissolving the precursors all together, performing a one-time impregnation. This involves the formation of a dense and stable precipitate of light red colour: $MnMoO_4$. Therefore, nitric acid was employed to dissolve it. This step was carried out with a magnetic stirrer at 80 ºC and 400 rpm for 20 min.

To add nitric acid systematically, the four existing ratios between precursors were analysed, choosing 10 g of Mn precursor as a reference. Then, the acid volume was extrapolated to the synthesis of the target sorbents. In Table 3.2, the experimental nitric acid volume used to dissolve the precursors is shown.

Table 3.2 Nitric acid volume for each sorbent composition.

Sorbent	Mn-prec (g)	Mo-prec (g)	Ratio	HNO_3 (mL)
15Mn2,5Mo	10,0	0,67	0,07	1,00
15Mn5Mo	10,0	1,34	0,13	2,00
15Mn8Mo	10,0	2,16	0,22	3,00
15Mn10Mo	10,0	2,69	0,27	3,50

Nitric acid addition should be gently and as small as possible, adding millilitres one by one with non-stop stirring until the precipitate is completely dissolved. If a high volume of acid is added to the solution, it can damage the final sorbent. Therefore, a trade between stirring and HNO_3 addition must be achieved.

As a **post-treatment**, for the first and second approaches, samples were dried in a high temperature furnace under air at 100°C (5°C/min) for 12 hours, and then calcined at 700°C (10°C/min) for 5 hours using a calcination setup with flowing air (70 mL/min). . In Figure 3.3, sorbents after drying and calcination steps can be seen, respectively.

Figure 3.3 Sorbents after drying (left) and after calcination (right).

In Figure 3.4, the target sorbents for EG-SQ method are shown. Qualitatively, as higher the promoter (Mo) concentration, the lighter is the final sorbent, turning from dark brown to grey. This was also reported quantitively by XRF characterization. (See Section 4.2.1)

Figure 3.4 Target sorbents from EG-SQ method increasing Mo concentration from left (15Mn) to right (15Mn10Mo).

In the **GL-Co method**, precursors were dissolved in glycerol alternatively to deionized water, accounting its high solubility for hydrated metal salts. The quantity of precursors and γ-Al_2O_3 was calculated regarding the sorbent amount and concentration required. The volume of glycerol necessary to fill the sorbent pores was estimated beforehand, performing a blank test with 1 g of pre-calcined alumina . The blank was left overnight to adsorb a volume of 0,6 mL/g γ-Al_2O_3. This data is consistent with the one reported in the literature [32].

To manage the formation of an egg-shell profile, the high viscosity of glycerol was used as the controlling step over the capillary pressures dominating the IWI or “dry impregnation”. This way, a fast suction of the active phase solution along the porous structure was avoided [32].

Given the challenge that glycerol handling involves, the preparation was reduced to sorbent 15Mn8Mo, with the aim of studying the egg-shell formation as a function of time.

Alumina pellets were soaked into the precursors/glycerol solution for 20, 40 and 60 minutes, respectively (Figure 3.5). After the soaking time, the excess of glycerol was evacuated using a Büchner funnel for approximately one minute.

Figure 3.5 Glycerol soaking of γ-Al_2O_3 pellets.

As a **post-treatment**, samples were dried in a high temperature furnace under air at 75°C (1°C/min) for 12 hours and at 260°C (1°C/min) for 4 hours, and then calcined at 700°C (10°C/min) for 5 hours using a calcination setup with flowing air (70mL/min). Due to the viscosity of glycerol, ensuring that no excess solvent is left before drying could be an arduous task but is of great relevance to perform a successful post-treatment.

3.3. Sorbent characterization

3.3.1. X-Ray Fluorescence

Rigaku Supermini200 Analyser for Wavelength Dispersive X-Ray Fluorescence (WDXRF) is used to determine the elemental composition of the sorbents. An outline of the XRF Spectrometer can be found in Figure 3.6. Primary X-Rays are created in an X-Ray tube by the traveling of electrons from the cathode to the anode. The X-Ray tube window material is Be (30-1000 µm).

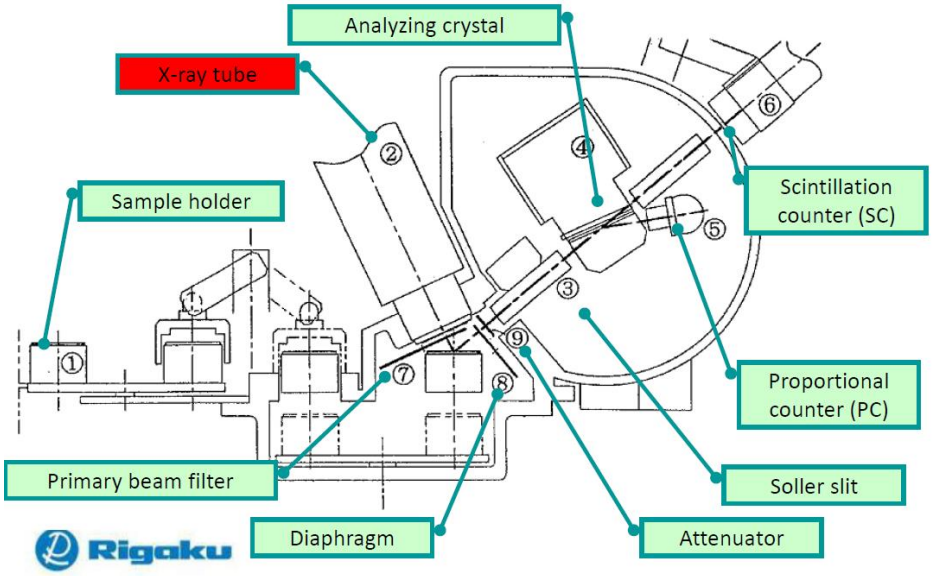

Figure 3.6 WDXRF spectrometer outline [47].

For sample preparation, the homogeneous mixture method is employed. A 3 g pellet is prepared mixing 2,8 g of boric acid (binder) and 200 mg of each sample. The mixture is crushed homogeneously by hand for 10 minutes using a mortar and then, pelletized with an iron pellet-form. The pellet-form is introduced into a hydraulic press at 10 tons for 10 minutes. The final step is to gently remove the pellet from the pellet-form and put it into a sample holder with polypropylene film of 6μm and a sample retainer. The pellet and the sample holder can be seen in Figure 3.7. Finally, the sample holder is introduced into Rigaku Supermini200 for analysis, specifying the exact weight of both binder and sample, to assure the mixing ratio calculation. Each time the instrument was used, a PHA standard calibration was carried out. To achieve reliable results, having a reproducible sample preparation method is of great importance, as well as avoiding contamination along the process.

Figure 3.7 XRF pellet taken out from the iron pellet-form (left) and sample holder (right).

3.3.2. X-Ray Diffraction

A **Bruker D8 DaVinci-1 X-ray Diffractometer** with CuKα radiation (Figure 3.8) was used to obtain the X-ray diffractograms in order to identify the present phases. The analysis was performed for 120 minutes with a 2θ angle and a scan range of 10-80 º. Variable divergence slit (V6) was chosen, which keeps a constant 6 mm of sample illuminated at all angles and provides a deeper penetration.

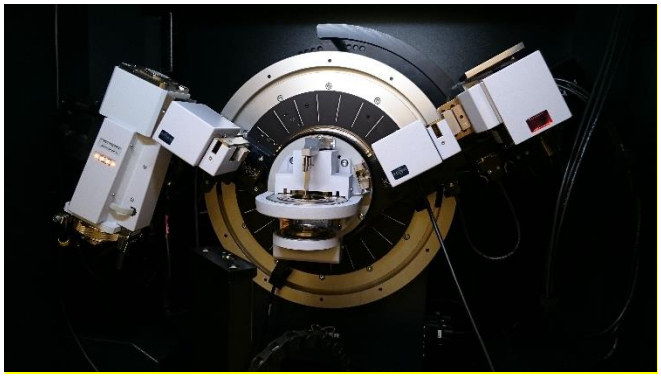

Figure 3.8 Bruker D8 DaVinci-1 X-ray Diffractometer [48].

For sample preparation, the sorbent pellets were crushed by hand with a mortar to obtain homogeneous powder. The powder was then placed into a sample holder and the surface was flatted with the help of a glass piece (Figure 3.9). The samples were placed in a queue rack and the responsible engineer put the samples from the queue rack for analysis. Afterwards, the software DIFFRAC.EVA, which has several databases available, was used for the XRD patterns analysis.

Figure 3.9 XRD samples ready for analysis. Darker brown corresponds to a higher concentration of precursor.

3.3.3. N_2 Physisorption

Nitrogen adsorption measurements were performed using a **Micrometrics TriStar II 3020 Surface Area and Porosity Analyzer**. First, the sample and sample tubes were weighed and placed in a VacPrep 061 degassing unit. They were left evacuating for one hour in the cooling station. Then, using a heating station adapter, they were moved to the heating station (200 ºC) for 12 hours.

The sample weight for analysis should be adjusted to aim for 30 m^2 in the sample tube. Knowing the expected surface area, about120 m^2/g in this case, an approximate weigh of 250 mg of sorbent was chosen for all the analysis. Three sample tubes can be prepared each time.

The sample is ready for analysis when the pressure in the degas unit is 100 mTorr or less. After degassing, samples were weighed again. A filling rod to reduce the stem free space volume, and an isothermal jacket for maintaining a constant temperature profile were placed to each sample tube before installing them into the instrument. Then, the cryogenic container for liquid nitrogen was filled and placed underneath the sample tubes. When the information is provided to the software, the analysis starts and runs for approximately 15 hours. After the analysis, the tubes are weighed again.

The adsorption/desorption isotherm was used to calculate the BET surface area, and the BJH method was used to determine the pore volume and pore-size distribution.

3.3.4. Scanning electron microscopy

Scanning electron microscopy and Energy dispersive X-ray spectroscopy analysis (SEM/EDS) were performed using a **SEM Apreo (**Figure 3.10**)** with the aim of confirming the egg-shell profile of the sorbents and the egg-shell thickness.

This instrument is located in a cleanroom which belongs to **NTNU NanoLab**. To get access to this space, a course and an on-line exam were previously completed. Cleanrooms are designed to reduce particles to a controlled level, for example, ISO5 classification means that the area has a controlled environment of less than 100 particles larger than 0.5 μm in any given cubic foot of air. Thus, appropriate personal protective equipment should be worn to enter the cleanroom in order to avoid contamination [49].

Figure 3.10 SEM Apreo instrument.

An outline of SEM Apreo can be found in Figure 3.11. The electron beam enters the chamber through the A-tube and irradiates the sample causing electrons to be emitted. Different detectors are installed: Everhart Thornley Detector (ETD) is a SE detector situated in the main chamber; Trinity 1 (T1) and Trinity 2 (T2) detectors are in-lens, and process BSE and SE, respectively. Additionally, three operational lens modes exist: Standard (lower magnification), OptiPlan (electrostatic field applied) and Immersion (electrostatic and magnetic field applied). As it was advised by the responsible engineer, Standard mode was chosen for this project, in which ETD and T1 detectors can be operated [50].

For image focusing, three parameters can be adjusted: free working distance (WD), acceleration voltage (898 V – 30 kV) and beam current (0.78 pA - 0,41 µA). In general terms, for both low acceleration voltages and current, image resolution increases. However, some information about the sample may be lost or noisy images could be created. Hence, a wise trade between these parameters must be chosen.

The EDS detector is outside the chamber and can be inserted when necessary. For processing the EDS signal, AzTec software is used in combination with the microscope. EDS measurements were taken with a magnification of no less than 500µm and an optimal WD of 10mm.

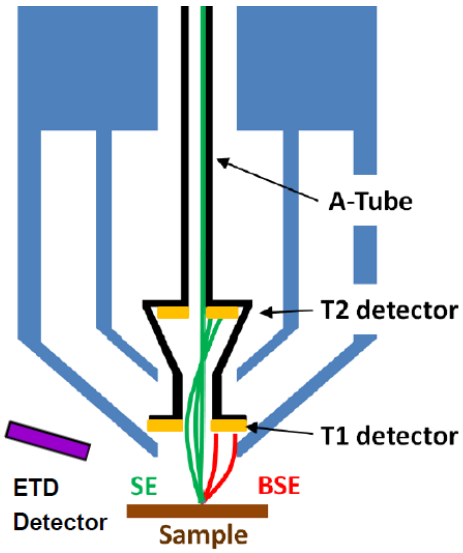

Figure 3.11 SEM Apreo outline [50].

To acquire data from SEM Apreo, the first step was to prepare the **cross-section pellet**, in order to attain a flat surface suitable for elemental mapping. For that purpose, QuickStick 135 mounting wax was placed on top of an iron holder, which was heated up to 120 ºC until the wax melted. Then, the pellet was soaked half into the wax and the iron holder was let to cool down until the pellet was sticked (Figure 3.12). Pellets were gently sanded by hand with European #2400 and #4000 polishing pads (8µm and 5µm grain size, respectively) until the cross section was achieved. Finally, the iron holder was heated up again to remove the pellet from the wax.

As a post-treatment, cross-section pellets were soaked in acetone for 5 minutes until the excess of wax was removed. Then, to clear away the particles which might have spread through the surface during the polishing step, the cross-section was sprayed again with acetone and cleaned with fine laboratory paper. It is of great importance to remove these particles because they can disturb SEM/EDS measurements when trying to prove the egg-shell structure. As a final step, the cross-section pellets were put in a high temperature furnace at 60 ºC for 3 hours to let the acetone left inside evaporate.

Figure 3.12 Iron holder and mounting wax. Pellet of about 1mm diameter rounded in red.

In SEM Apreo, the cross-section pellets were placed into a stage holder on the top of a carbon tape. The stage holder was loaded into the microscope chamber, which was previously vented (Figure 3.13). Then, the chamber was pumped again. The electron beam was turned on, moved to the region of interest, and the Z-position was linked to the actual free working distance (FWD) of the instrument. With these steps are done, image focusing and EDS analysis can start.

Figure 3.13 Cross-section pellets in stage holder (left) and loading to SEM Apreo (right).

3.4. Laboratory setup

This section includes a brief description of the **laboratory set-up**, which will be used to test the sorbents afterwards. However, it is not explained in detail, as it has not been an active part of this project due to different problems with instrument availability.

The set-up consists of three fundamental sections: gas supply with control system, reactor-furnace structure, and gas analysing instrumentation. The gas supply includes the main components of a model raw syngas: H_2, CO and CO_2 (later added) , H_2O, H_2S (1% in Ar), and H_2O. The composition can vary for testing different conditions and it is regulated by Bronkhorst mass flow controllers (MFCs). N_2 is used as inert gas for flushing the lines after each cycle, and air is used as the regeneration agent to recover the spent sorbent.

The tubular quartz fixed bed reactor where the sorbent is tested, is enclosed by a furnace, in which the temperature is regulated by a Eurotherm 2408 controller. After the sorption process, the product gas is analysed by a ThermoStarTM GSD 320 T1 C with a quadrupole mass spectrometer. The three-way valve prior to the reactor, directs the flow either to the reactor or to the bypass line, which is used to stabilize the gas signal in the mass spectrometer (MS). Besides, to prevent any damage to the MS, a condenser and a drying column of $CaCl_2$ is placed before the analysis takes place. Thermofisher 450i sulfur analyser is used to detect the concentration of H_2S and SO_2 [14].

In Figure 3.14 a simplified diagram of the laboratory set-up is shown. An updated and detailed laboratory setup together with the unit card can be found in Appendix A.

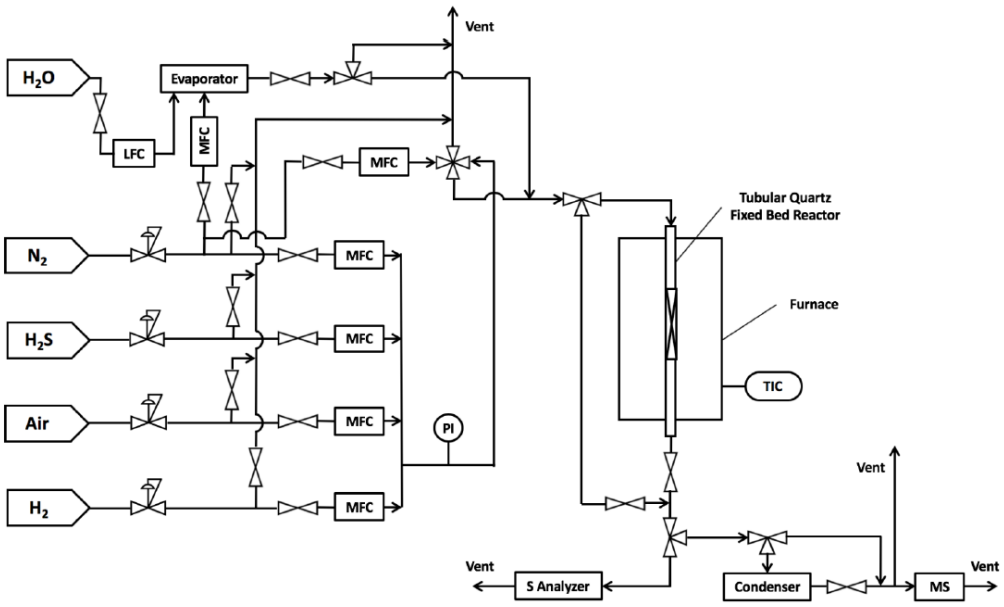

Figure 3.14 Simplified laboratory setup [14].

4. Results and discussion

4.1. Sorbent preparation

Time efficiency of the preparation methods and physical characteristics of the sorbents are two important parameters regarding an industrial application [11]. In this section, they are going to be discussed.

Some of the sorbents prepared by the EG-SQ method needed a total of five impregnations to achieve the desired loading. Two Mn and three Mo impregnations were needed for the synthesis of the sorbent 15Mn8Mo, noting that the promoter (Mo) is harder to impregnate than the based material (Mn). In contrast, for the same sorbent with EG-Co method, only two co-impregnations were needed. This suggest the mixed oxide $MnMoO_4$ formed during co-impregnation can easily attach to alumina pellets. Furthermore, the time employed is drastically reduced. In Table 4.1, a comparison of the time needed to perform one impregnation is shown. In Table 4.2, the total time for the preparation of one sorbent is calculated, and a measure of the efficiency [51] is presented as the output (one sorbent) divided by the time employed,

$$\text{Efficiency} = \frac{\text{Output (sorbents)}}{\text{Time employed (days)}} \quad (4.1)$$

which gives an idea of the '*sorbents per day'* that can be prepared. Despite more time is used for one impregnation in both EG-Co and GL-Co methods (21,7 and 25,8 h, respectively) than in EG-SQ (21,3 h), as the number of impregnations is reduced, the efficiency increases. In Table 4.3, the overall efficiency is compared. Four sorbents were synthesized for the EG approaches with 18 and 10 impregnations, respectively (Table 3.1). For the GL-Co method, the worst-case scenario of 8 impregnations (2 for each sorbent) has been chosen as a hypothesis, given that not all the sorbent compositions had been prepared. Even though, the overall efficiency remains the highest, confirming that GL-Co gives the best results in terms of time efficiency.

Table 4.1 Time needed for one impregnation depending on the approach.

Time (min)	EG-Soaking	Dissolving	Impregnation	Synthesis	Drying	Calcination	Post-treatment	Overall (min)	Overall (h)
EG-SQ (WI)	30	-	20	50	750	480	1230	1280	21,3
EG-Co (WI)	30	20	20	70	750	480	1230	1300	21,7
GL-Co (IWI)	-	20	60	80	990	480	1470	1550	25,8

Table 4.2 Synthesis efficiency for sorbent 15Mn8Mo depending on the approach.

15Mn8Mo	Output	Nº Imp.	Days/imp.	Total time (day)	Efficiency
EG-SQ (WI)	1	5	0,89	4,44	0,23
EG-Co (WI)	1	2	0,90	1,81	0,55
GL-Co (IWI)	1	1	1,08	1,08	0,93

Table 4.3 Overall efficiency depending on the approach.

Method	Output	Nº Imp.	Days/imp.	Total time (day)	Efficiency
EG-SQ (WI)	4	18	0,89	16,0	0,25
EG-Co (WI)	4	10	0,90	9,03	0,44
GL-Co (IWI)	4	8*	1,08	8,61	0,46

*worst-case scenario

For both EG-SQ and EG-Co, the physical properties of the final sorbents were of high standard. The colour was homogeneous and no imperfections where found. Besides, mechanical resistance was high. However, in the GL-Co sorbents, the colour was not homogeneous and **attrition** phenomenon was observed, likely due to abrasion or internal surface area loss, which entails damage of the active material and could affect the sorption capacity [52]. To establish further conclusions, sorption experiment results from the laboratory set-up are needed.

4.2. Sorbent characterization

4.2.1. X-Ray Fluorescence

XRF characterization was carried out in between the impregnations to know if the desired loading was achieved. If it was not sufficient, another impregnation was done afterwards. In Appendix B some XRF reports are shown, including an example of reproducible measurements. The target sorbents compositions for **EG approaches** are compiled in Table 4.4 and Table 4.5. Both oxide and atomic mass percentages are calculated by the XRF analyzer. Although, since it is not possible to add oxygen as a separated element in the software, there may be an overestimation of the atomic mass percentage of the metals.

The Mo atomic percentage, i.e. Mo(%), is mostly near the desired composition (2.5, 5, 8 and 10%). However, Mn(%) ranges from 15-19%. This oscillation can be best appreciated throughout consecutive impregnations.

Sorbents 15Mn8Mo and 15Mn10Mo are chosen to illustrate this phenomenon in both EG-SQ (Table 4.6 and Table 4.7) and EG-Co (Table 4.8 and Table 4.9) methods.

Table 4.4 Target sorbents compositions for EG-SQ method.

EG-SQ Method	Oxide (%)		Atomic (%)	
	MnO	MoO_3	Mn	Mo
15Mn	10,8	-	16,6	-
15Mn2.5Mo	10,3	1,5	15,8	2,2
15Mn5Mo	10,6	1,9	18,6	4,5
15Mn8Mo	8,7	2,9	19,2	8,4
15Mn10Mo	8,1	3,9	18,7	9,2

Table 4.5 Target sorbents compositions for EG-Co method.

EG-Co Method	Oxide (%)		Atomic (%)	
	MnO	MoO_3	Mn	Mo
15Mn2.5Mo	10,5	1,8	16,0	2,5
15Mn5Mo	7,0	1,8	17,7	4,7
15Mn8Mo	8,4	3,2	19,3	7,7
15Mn10Mo	9,0	6,3	19,0	13,0

In EG-SQ, as expected, Mn(%) increases in both 1st and 2nd impregnations. Mo(%) also has a clear trend in 3-5th impregnations. However, Mn(%) increases in the 3rd and 4th impregnations, even though no Mn is added, and lowers again in the 5th impregnation. This could be either due to uncertainty of the instrument or to a not fine sample preparation (not sufficiently small particle size when crushing the sample).

Table 4.6 Consecutive impregnation compositions for 15Mn8Mo sorbent (EG-SQ).

EG-SQ Method	Oxide (%)		Atomic (%)	
15Mn8Mo	MnO	MoO_3	Mn	Mo
Imp. 1- Mn	6,9	-	10,9	-
Imp. 2- Mn	9,7	-	15,0	-
Imp. 3- Mo	10,6	1,9	22,3	4,5
Imp. 4- Mo	11,8	2,3	23,6	7,2
Imp. 5- Mo	8,7	2,9	19,2	8,4

Table 4.7 Consecutive impregnation compositions for 15Mn10Mo sorbent (EG-SQ).

EG-SQ Method	Oxide (%)		Atomic (%)	
15Mn10Mo	MnO	MoO_3	Mn	Mo
Imp. 1- Mn	5,8	-	9,2	-
Imp. 2- Mn	8,3	-	13,0	-
Imp. 3- Mo	9,8	1,0	15,2	1,4
Imp. 4- Mo	9,7	2,5	20,6	5,7
Imp. 5- Mo	8,0	3,9	18,7	9,2

In EG-Co, both Mn and Mo(%) increase in 1st and 2nd co-impregnations as expected. Besides, the desired composition is attained with less impregnations than before. Whether the formation of the complex $MnMoO_4$ is the reason for this phenomenon, as suggested before, will be cleared up with XRD results (Section 4.2.2). Again, the same increase in Mn(%) is observed in the 3rd impregnation, for the 15Mn10Mo sorbent.

Table 4.8 Consecutive impregnation compositions for 15Mn8Mo sorbent (EG-Co).

EG-Co Method	Oxide (%)		Atomic (%)	
15Mn8Mo	MnO	MoO_3	Mn	Mo
Imp. 1- MnMo	8,0	1,4	12,3	2,0
Imp. 2- MnMo	8,4	3,2	19,3	7,7

Table 4.9 Consecutive impregnation compositions for 15Mn10Mo sorbent (EG-Co).

EG-Co Method	Oxide (%)		Atomic (%)	
15Mn10Mo	MnO	MoO_3	Mn	Mo
Imp. 1- MnMo	5,7	0,9	9,0	1,4
Imp. 2- MnMo	7,5	2,2	11,7	3,2
Imp. 3-Mo	9,0	6,3	19,0	13,0

For the **GL-Co approach** (Table 4.10), the desired Mn(%) is achieved with one impregnation, but the Mo(%) is lower than expected. Besides, an increase in both Mn and Mo(%) can be appreciated with an increment in the impregnation time. This is due to a deeper penetration of the precursors/glycerol solution into the porous media as impregnation time increases.

Table 4.10 Target sorbent compositions for GL-Co method.Table 4.10

GL-Co Method	Oxide (%)		Atomic (%)	
15Mn8Mo	**MnO**	**MoO_3**	**Mn**	**Mo**
Imp. 20 min	9,7	1,8	14,7	2,5
Imp. 40 min	11,6	1,7	23,9	4,0
Imp. 60 min	10,5	2,4	22,6	5,8

4.2.2. X-Ray Diffraction

The present chemical phases are identified using X-Ray diffraction. For the EG methods, XRD patterns are shown in Figure 4.1. Sorbent 15Mn is used as the reference for both graphs and the characteristic peaks are identified using different databases. Some examples of peak identification with DIFFRAC.EVA can be found in Appendix C.

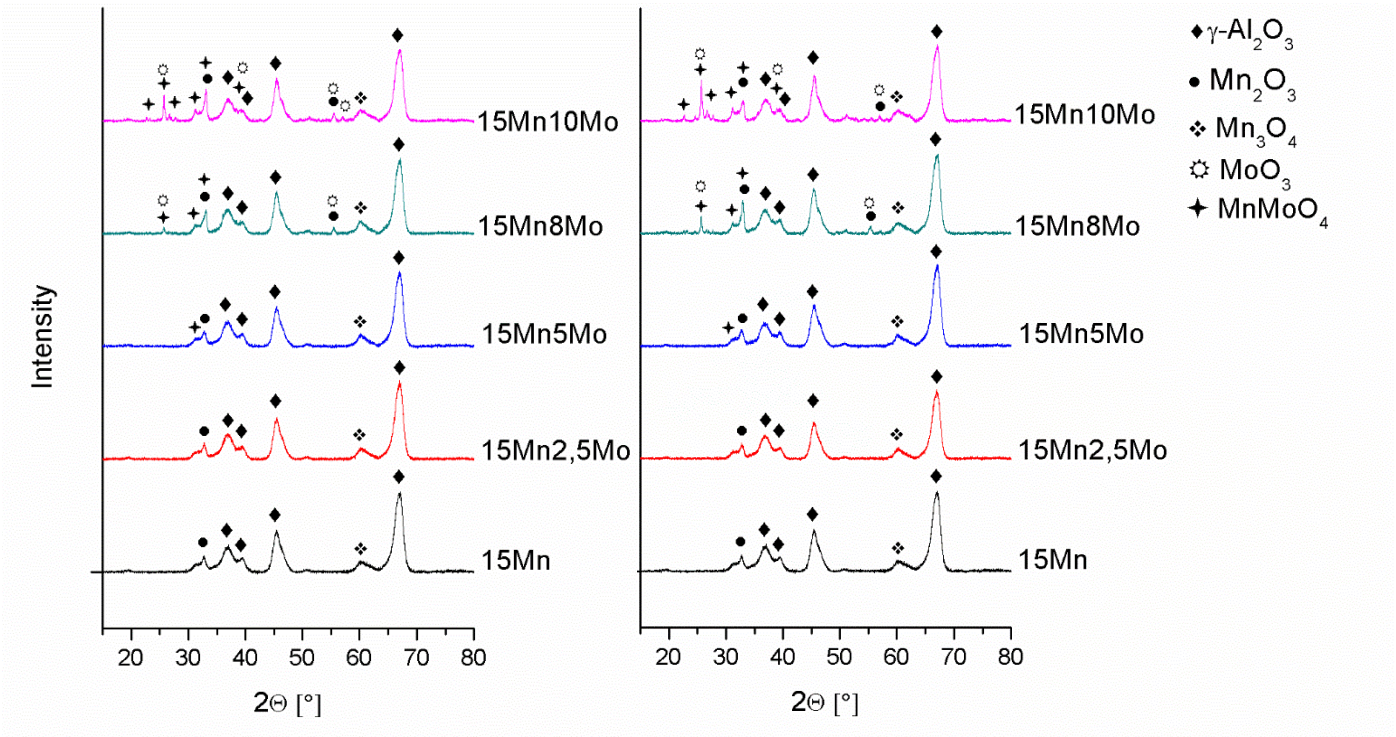

Figure 4.1 XRD patterns for EG-SQ (left) and EG-Co (right).

γ-Al_2O_3, Mn_2O_3 and Mn_3O_4 phases are present in all sorbent compositions. However, $MnMoO_4$ and MoO_3 phases are only visible at higher Mo-loadings, i.e. mainly 15Mn8Mo and 15Mn10Mo, overlapping with other previous peaks.

At an approximate 2θ angle of 46º and 67º, two intense peaks corresponding to **γ-Al_2O_3** appear. Besides, peaks at 37º and 40º also contribute to the γ-alumina phase. Its intensities are almost the same, regardless of the loading. The peak at 33º corresponds to the **Mn_2O_3** phase. It becomes more intense as Mo promotion increases, due to the overlapping with $MnMoO_4$ peaks at 31º and 33º. Other peaks at 55º and 57º appear in the highest loadings due to both Mn_2O_3 and MoO_3. The broad peak at 60º is a contribution of the **Mn_3O_4** phase. **$MnMoO_4$** phase emerges with Mo addition at 23º, 26º, 27º, 31º, 33º and 38º, clearly becoming sharper with increasing Mo-loading. **MoO_3** peaks, as advanced before, are mainly overlapped at 26º, 39º, 55º and 57º. These XRD patterns are congruent with the ones presented in the previous work [5]. XRD patterns of both EG methods are almost equivalent, specially at lower Mo-loadings. However, in 15Mn8Mo and 15Mn10Mo sorbents, there are some appreciable differences between the methods that are going to be discussed.

In Figure 4.2, XRD patterns for **15Mn8Mo** sorbent are shown for both EG approaches. It can be appreciated that $MnMoO_4$ peaks at 26º and 33º are sharper in the EG-Co sample. This effect confirms a higher formation of the mixed oxide when co-impregnation is performed. Hence, it can potentially imply an enhancement in the desulfurization efficiency, as suggested in the previous work [5]. The specific increase in the counts is shown to illustrate this effect. Other peaks counts are similar for both EG methods.

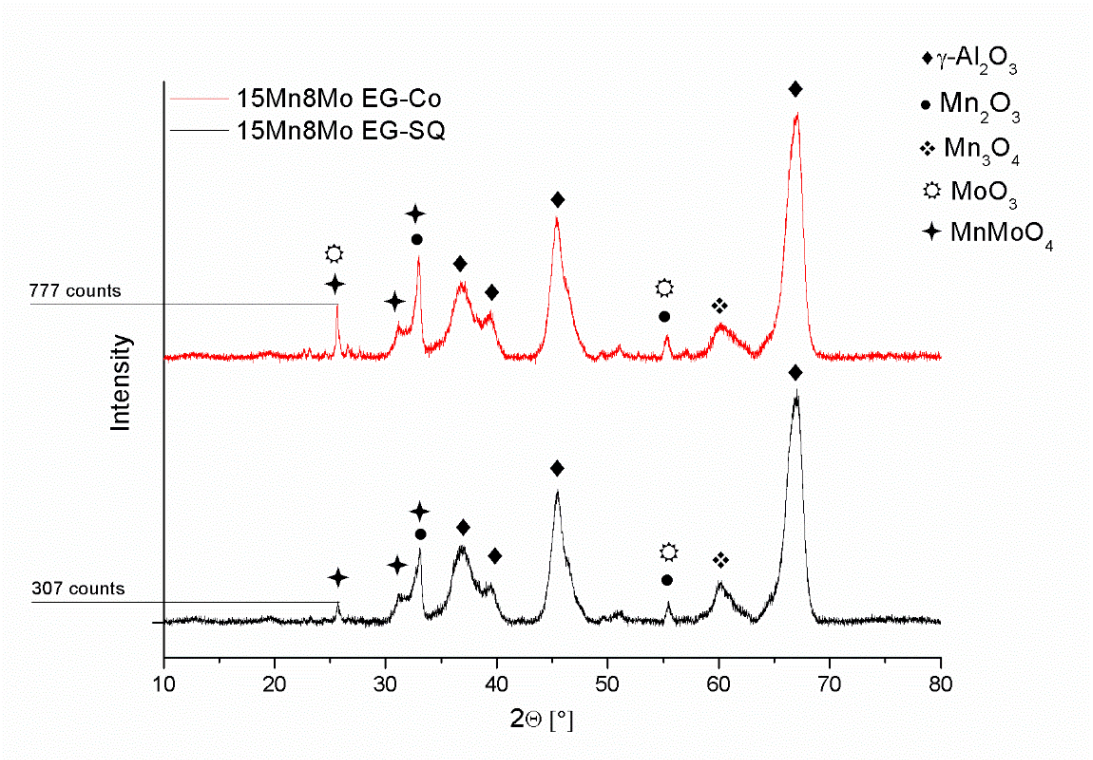

Figure 4.2 XRD patterns for 15Mn8Mo in EG-SQ and EG-Co methods.

In Figure 4.3, XRD patterns for **15Mn10Mo** sorbent are shown for both EG methods. The aforementioned effect can also be appreciated. Besides, the number of peaks and the counts for $MnMoO_4$ increase considerably around 2θ angle of 25º, as the promoter concentration is higher. Additionally, other peaks emerge in the 2θ angle range of 50-60º mainly due to a growing MoO_3 phase.

The same kind of peaks are assigned to the three samples from the **GL-Co approach** (Figure 4.4). A higher formation of $MnMoO_4$ mixed oxide is observed with only one impregnation, since clearer and higher intensity peaks are reported comparing to Figure 4.2. Furthermore, an increment in the impregnation time leads to a higher intensity of the strongest $MnMoO_4$ peak at 2θ angle of 26º, which is congruent with the concentration increase in XRF results. Altogether, agrees with the idea that the GL-Co method gives the largest $MnMoO_4$ formation with the less preparation time.

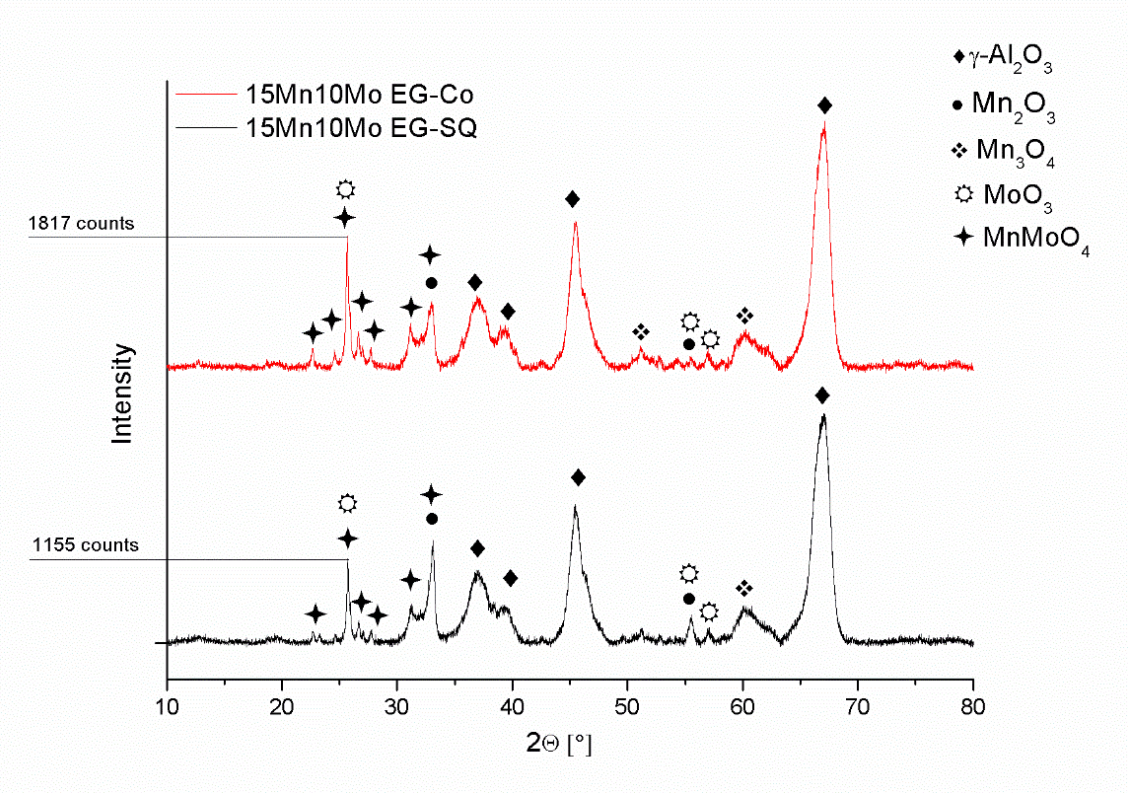

Figure 4.3 XRD patterns for 15Mn10Mo in EG-SQ and EG-Co methods.

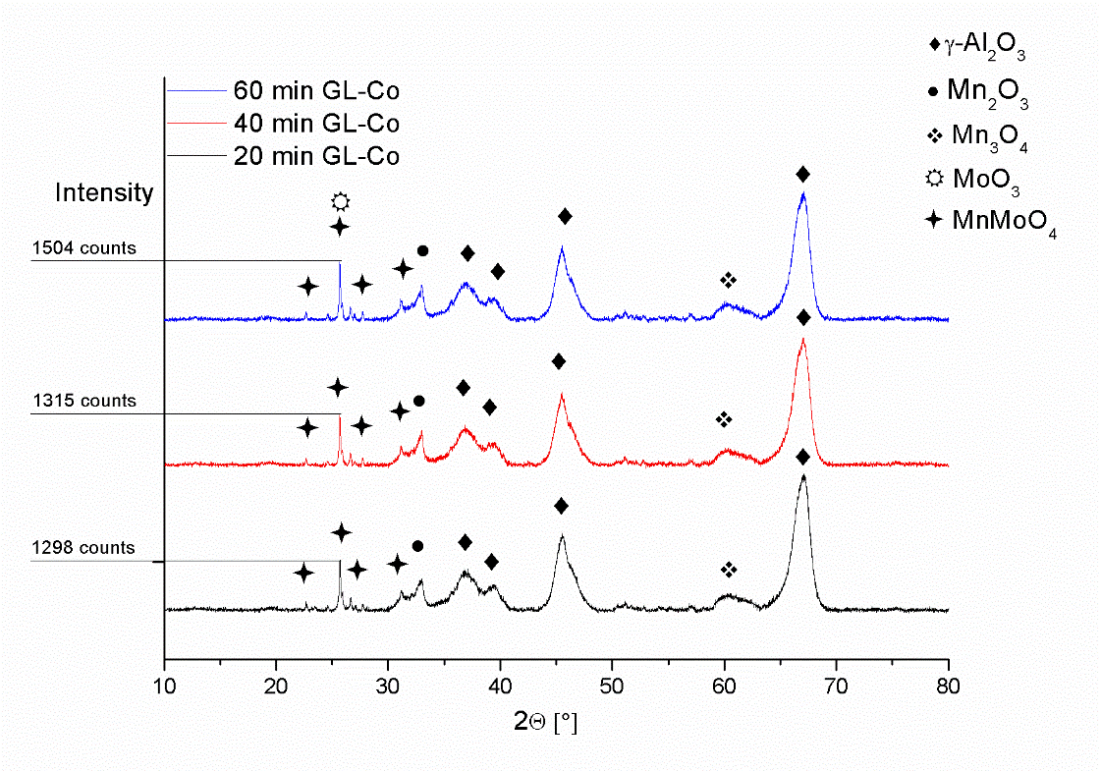

Figure 4.4 XRD patterns for 15Mn8Mo in GL-Co method.

4.2.3. N_2 Physisorption

Sorbent **textural properties** are evaluated conducting N_2 physisorption experiments. In this section, trends and changes regarding surface area (BET method), pore volume, median pore width and pore size distribution (BJH method) are discussed. In Appendix D, the summary part of a BET report can be consulted.

First, alumina beads were tested and compared with a one-time impregnated sorbent to verify if the isothermal type agrees with the one reported in literature (See section 2.6.3). Indeed, both curves correspond to isothermal type IV (Figure 4.5), i.e. mesoporous material with pore diameter between 2 and 50 nm. The amount of N_2 adsorbed by the one-time impregnated sorbent is less, because part of the alumina pores are filled up with metal oxide particles. This effect will be discussed in detail afterwards.

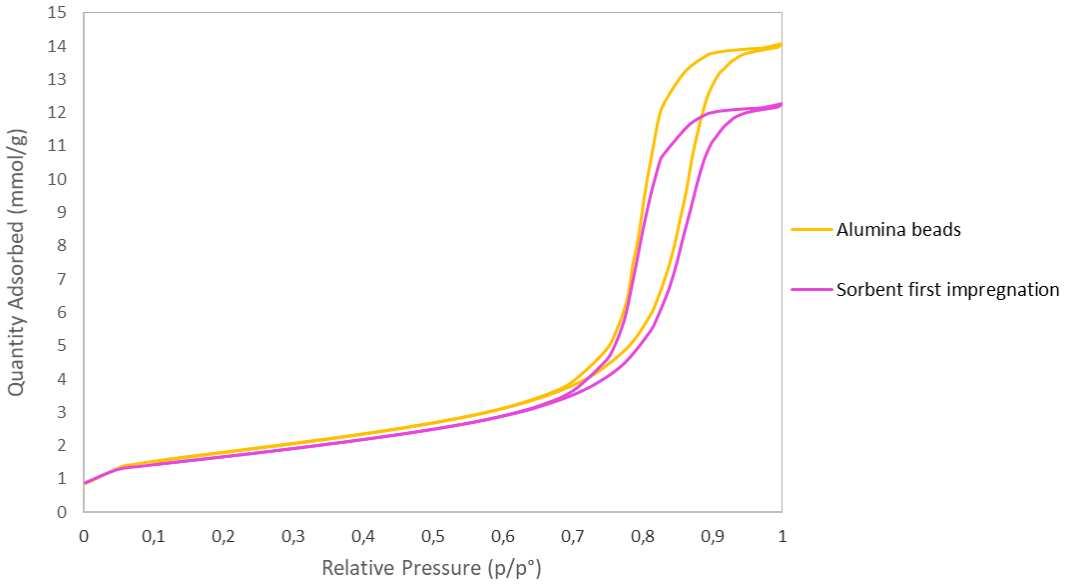

Figure 4.5 Alumina beads and sorbent first impregnation isotherms.

Target sorbents textural properties are compiled in Table 4.11, Table 4.12 and Table 4.13. In the **EG methods**, the trend in the surface area is to lower as Mo promotion increases, due to a greater number of impregnations and a higher concentration of metal oxide particles. Accordingly, pore volume decreases with Mo promotion, since less volume is available for N_2 adsorption. Median pore width generally becomes higher due to the change in pore size distribution, as small pores are filled up with the active phase. Pore size distribution throughout the impregnations, later discussed, will better illustrate the change in median pore width.

Sorbents 15Mn8Mo and 15Mn8Mo in EG-Co method have a higher surface area than in EG-SQ, as only two impregnations had been performed. However, sorbents 15Mn2.5Mo and 15Mn10Mo have similar surface area values in both EG methods, because three impregnations were needed for those compositions in EG-Co (Table 3.1).

In the **GL-Co method** high surface area values are attained. No significant change in surface area or median pore width is observed with impregnation time, although, pore volume slightly decreases due to a deeper glycerol penetration.

Table 4.11 Target sorbents textural properties for EG-SQ method.

EG-SQ Method	Surface area (m^2/g)	Pore volume (cm^3/g)	Median pore width (Å)
15Mn	128	0,397	145
15Mn2.5Mo	123	0,367	155
15Mn5Mo	119	0,358	155
15Mn8Mo	105	0,340	173
15Mn10Mo	101	0,335	175

Table 4.12 Target sorbents textural properties for EG-Co method.

EG-Co Method	Surface area (m^2/g)	Pore volume (cm^3/g)	Median pore width (Å)
15Mn2.5Mo	123	0,372	157
15Mn5Mo	135	0,395	148
15Mn8Mo	114	0,360	165
15Mn10Mo	97	0,329	174

Table 4.13 Target sorbent textural properties for GL-Co method.

GL-Co Method 15Mn8Mo	Surface area (m^2/g)	Pore volume (cm^3/g)	Median pore width (Å)
Imp. 20 min	120	0,379	148
Imp. 40 min	120	0,373	147
Imp. 60 min	121	0,367	150

Pore size distribution throughout consecutive impregnations is shown in Figure 4.6. Alumina beads show a bimodal pore size distribution with two main peaks. As impregnations are performed, the distribution becomes broader and small pores tend to disappear. The most suitable explanation for this phenomenon is the blockage of small mesopores for N_2 by metal oxide particles. Consequently, median pore width tends to show higher values, as mentioned before. These effects are congruent with other similar works [23].

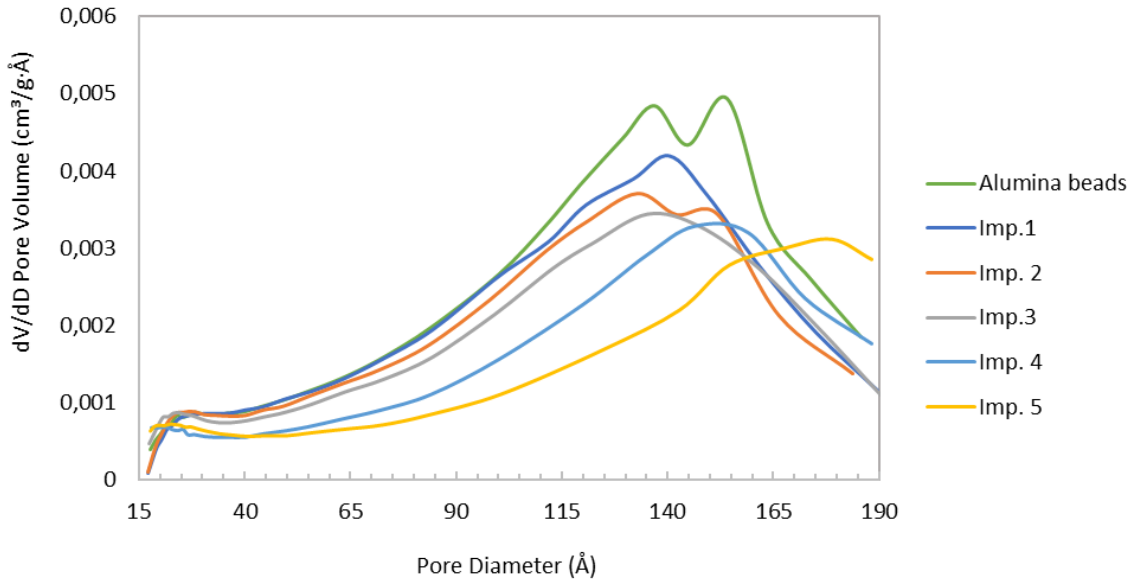

Figure 4.6 Pore size distribution for sorbent 15Mn10Mo (EG-SQ method).

The evolution of textural properties throughout consecutive impregnations is also interesting. 15Mn8Mo sorbent is taken as an example, for EG-SQ (Table 4.14 and Figure 4.7) and EG-Co (Table 4.15 and Figure 4.8) methods. Surface area, pore volume and median pore width follow the same trends as before. It is noted that one single Mn or Mo impregnation involves a smaller decrease in surface area than one MnMo co-impregnation. However, given the difference in number of impregnations, the final sorbent surface area is higher in the EG-Co method (114 m²/g comparing to 105 m²/g) which leads to the thought that this approach provides a higher standard in textural properties. In Appendix C, other compositions graphs can be consulted.

Table 4.14 Textural properties for 15Mn8Mo through consecutive impregnations (EQ-SQ).

EG-SQ Method 15Mn8Mo	Surface area (m²/g)	Pore volume (cm³/g)	Median pore width (Å)
Alumina beads	147	0,497	157
Imp. 1- Mn	135	0,405	152
Imp. 2- Mn	123	0,382	146
Imp. 3- Mo	119	0,358	155
Imp. 4- Mo	111	0,349	166
Imp. 5- Mo	105	0,340	173

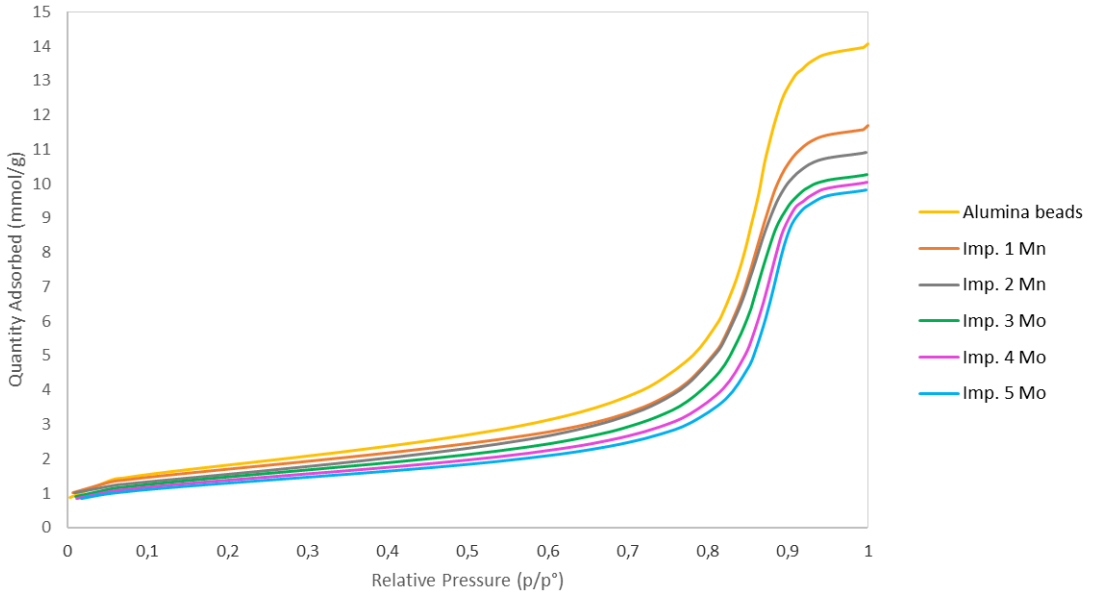

Figure 4.7 Adsorption isotherms for 15Mn8Mo through consecutive impregnations (EG-SQ).

Table 4.15 Textural properties for 15Mn8Mo through consecutive impregnations (EQ-Co).

EG-Co Method 15Mn8Mo	Surface area (m^2/g)	Pore volume (cm^3/g)	Median pore width (Å)
Alumina beads	147	0,497	157
Imp. 1- MnMo	131	0,391	146
Imp. 2- MnMo	114	0,360	165

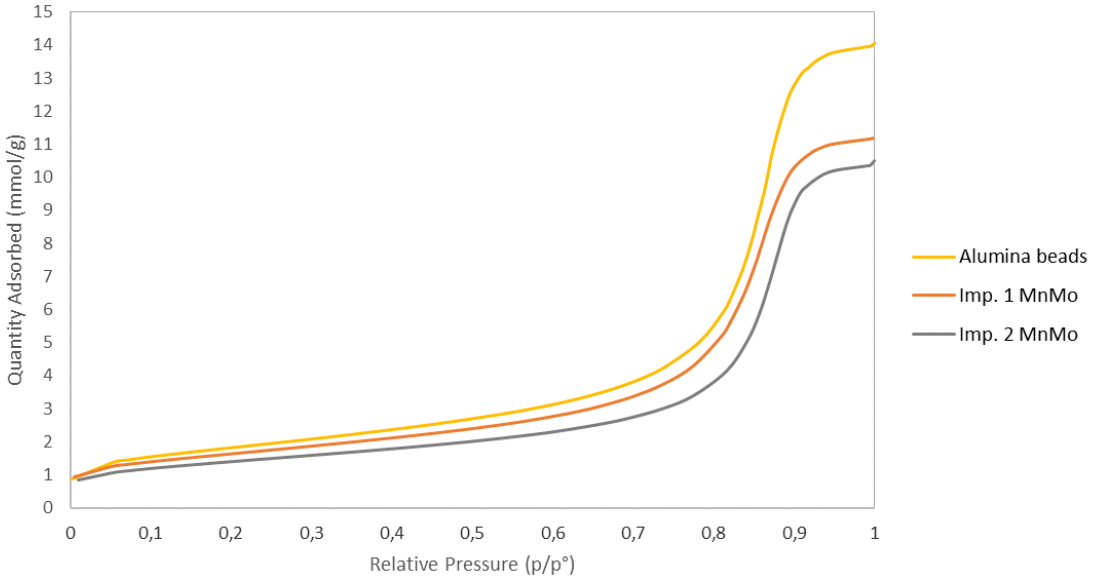

Figure 4.8 Adsorption isotherms for 15Mn8Mo through consecutive impregnations (EG-Co).

4.2.4. Scanning electron microscopy

Scanning electron microscopy is used to **verify the egg-shell structure** of the sorbents through **EDS analysis**. Line-profiling and mapping tools, available in AzTec software, are employed.

To perform a fine EDS analysis, the optimal detector, voltage, and beam current need to be chosen. As advanced in Section 2.6.4, the difference between ETD and T1 detectors is that they process SE and BSE, respectively. SE scape near the surface of the material, however, BSE can also scape from the inner volume, giving more precise information of the sample with contrast images [50]. The problem with BSE is the lower resolution and subsequent more difficult image focusing. In Figure 4.9 the difference between ETD and T1 detectors for our pellets is illustrated.

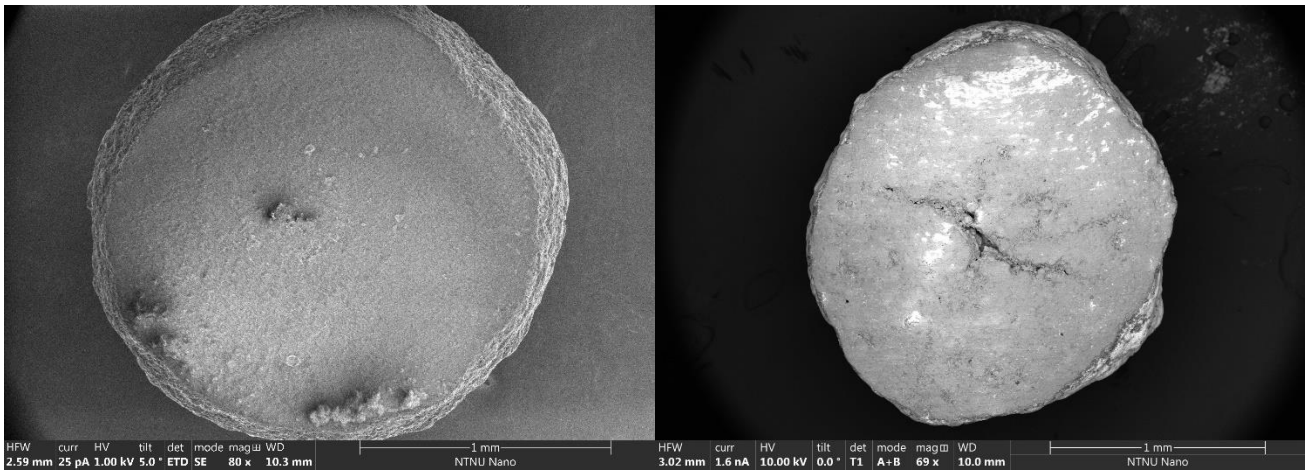

Figure 4.9 Cross-section pellet ETD detector image at 25pA and 1kV (left) and T1 detector image at 1,6nA and 10kV(right).

In general, at lower voltages and currents, higher resolution images are attained, but information can be lost while performing EDS analysis, due to a lack of signal for some of the elements. Thus, an optimal voltage needs to be chosen by consulting a periodic table for EDS analysis [53]. For Mn, when analyzing at 10 kV or higher, two electron transitions can be seen at energies of 0,637 and 5,894 keV. However, the latter cannot be seen working at 5 kV. For Mo, at 10kV the electron transition at 2,293 KeV can also be appreciated. Hence, a voltage of 10 kV is chosen, together with a sufficiently high intensity (around 1,6 nA). In Appendix E, a periodic table for EDS analysis can be consulted. Sorbent 15Mn8Mo is chosen for EDS analysis in both EG methods.

For **EG-SQ**, two line scans are performed (Figure 4.10). EDS analysis clearly shows a higher concentration of the active metals in the outer part of the pellet (Figure 4.11 and Figure 4.12) with a signal of more than 2000 counts, proving the existence of an egg-shell distribution. Molybdenum signal is higher, plausibly because the last three impregnations were performed with Mo. The **egg-shell thickness** is of approximately **200µm,** evenly distributed in both sides of the pellet (Figure 4.12).

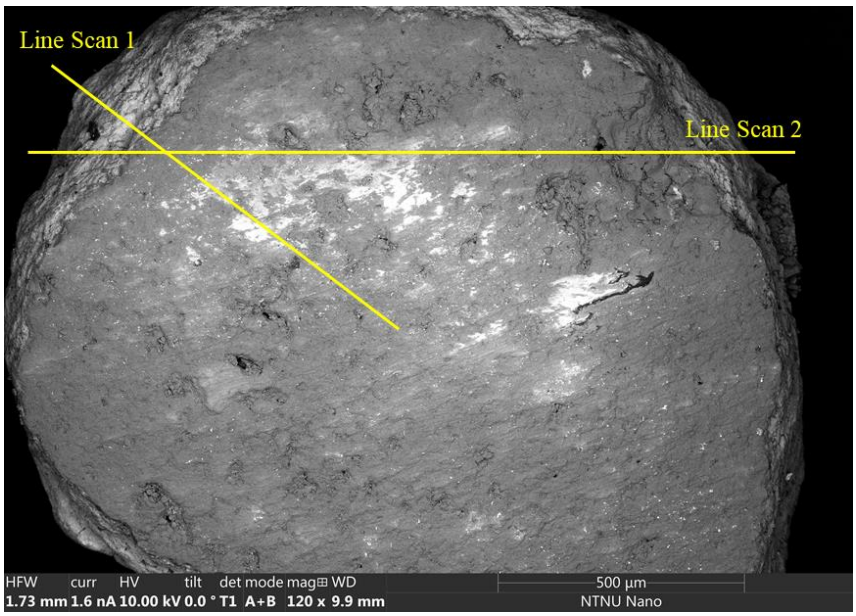

Figure 4.10 Sorbent 15Mn8Mo line scans (EG-SQ method).

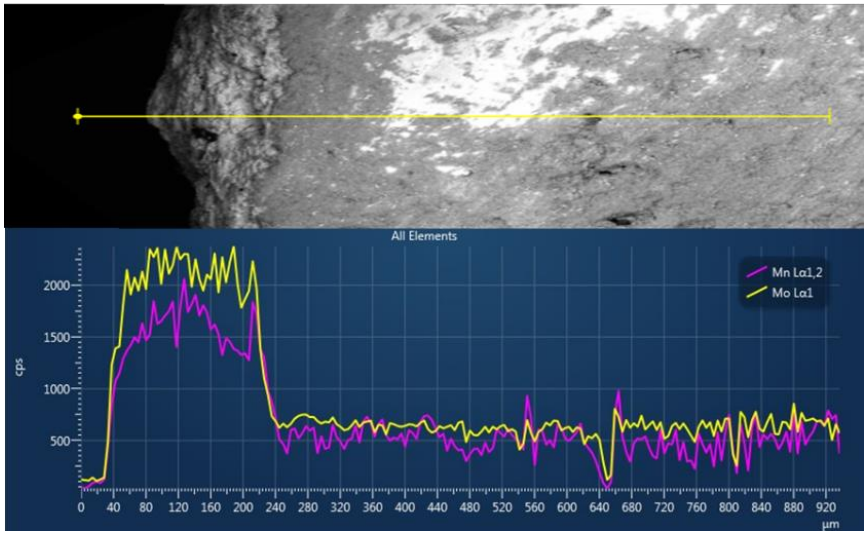

Figure 4.11 Sorbent 15Mn8Mo line scan 1 with EDS analysis for Mn and Mo (EG-SQ method).

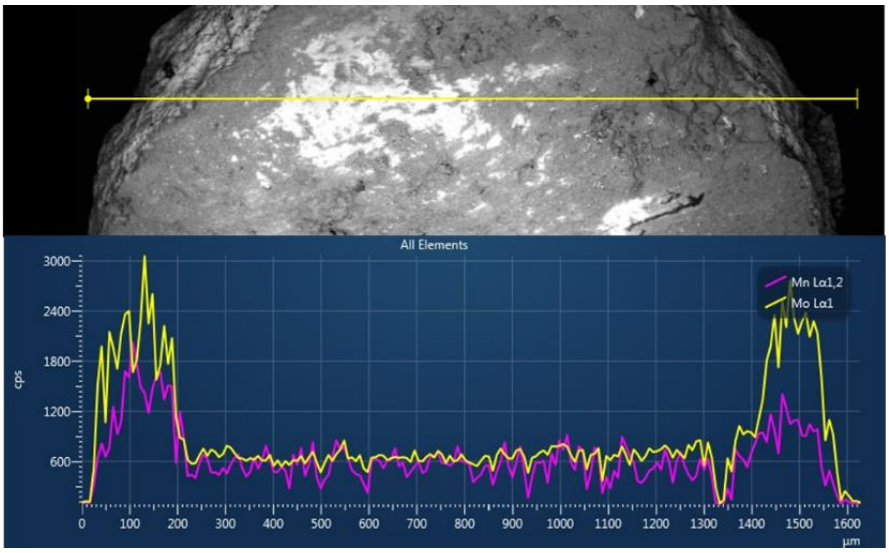

Figure 4.12 Sorbent 15Mn8Mo line scan 2 with EDS analysis for Mn and Mo (EG-SQ method).

Elemental mapping is reported below in Figure 4.13. The results show a dominance of the support elements (Al and O) and clearly display the egg-shell profile for both Mo and Mn, congruent with the line scans results.

In both line scans and mapping, a residual signal of Mn and Mo along the surface can be appreciated. The most feasible explanation is that, even after spraying and washing the cross-section pellet, little particles remain in the surface due to the polishing step. In Figure 4.14 this particles and polishing scratches can be identified. Its size is approximately 5µm, the grain size of the last polishing step (See Section 3.3.4). The noise along the line scans may also be due to a non-smooth surface.

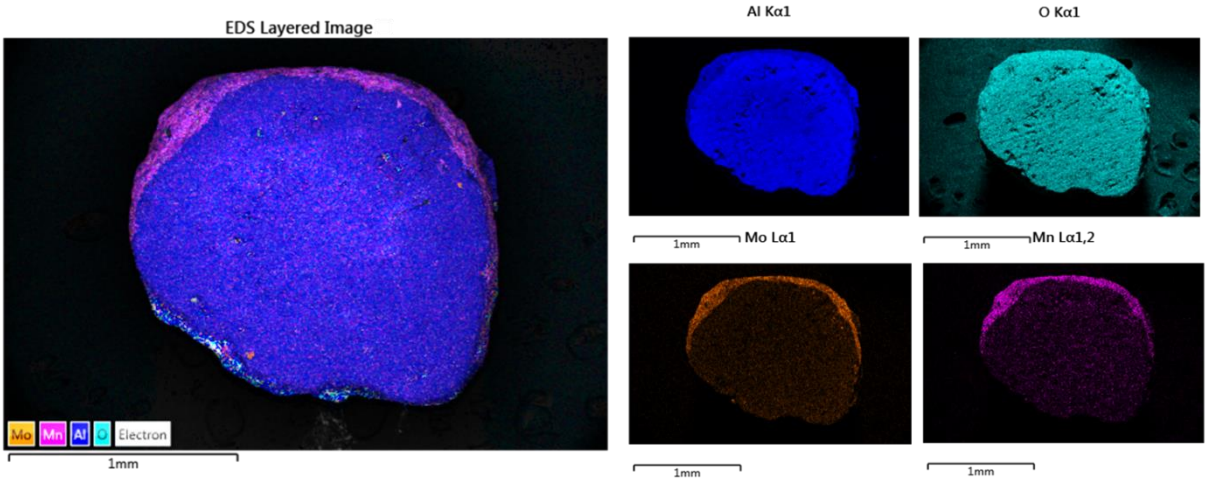

Figure 4.13 Sorbent 15Mn8Mo main elements mapping (EG-SQ).

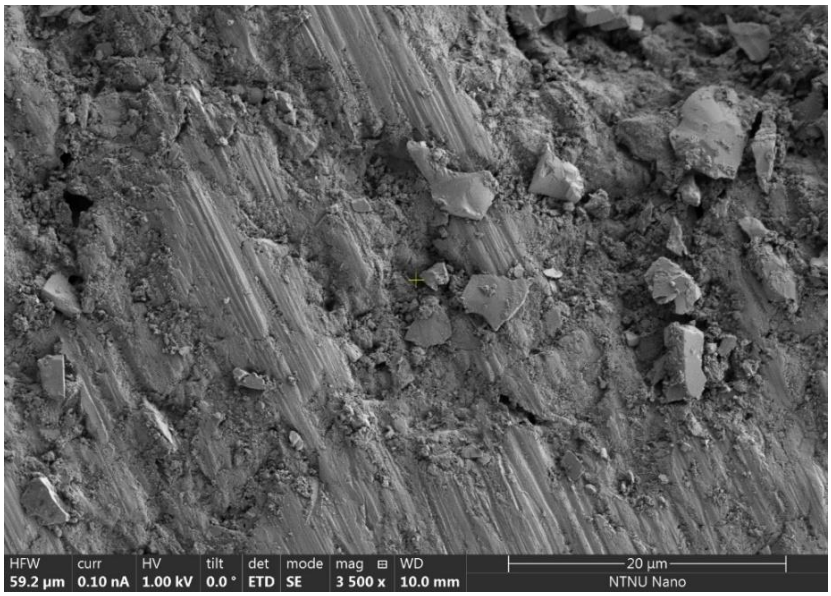

Figure 4.14 Surface of a cross-section pellet: SEM image at 20µm magnification.

For **EG-Co**, the same analysis is performed in order to compare both egg-shell thicknesses. As it can be seen in Figure 4.15, the **egg-shell thickness** is smaller than before, approximately around **100µm**, possibly due to a lower number of impregnations. Additionally, Mo signal is very intense in comparison with Mn. As a hypothesis, it may be due to the contribution of the mixed oxide $MnMoO_4$. Phase identification can also be done with EDS analysis. However, given the nature of the sample (large for SEM analysis), it could be a complex process and X-Ray diffraction is more appropriate for that purpose.

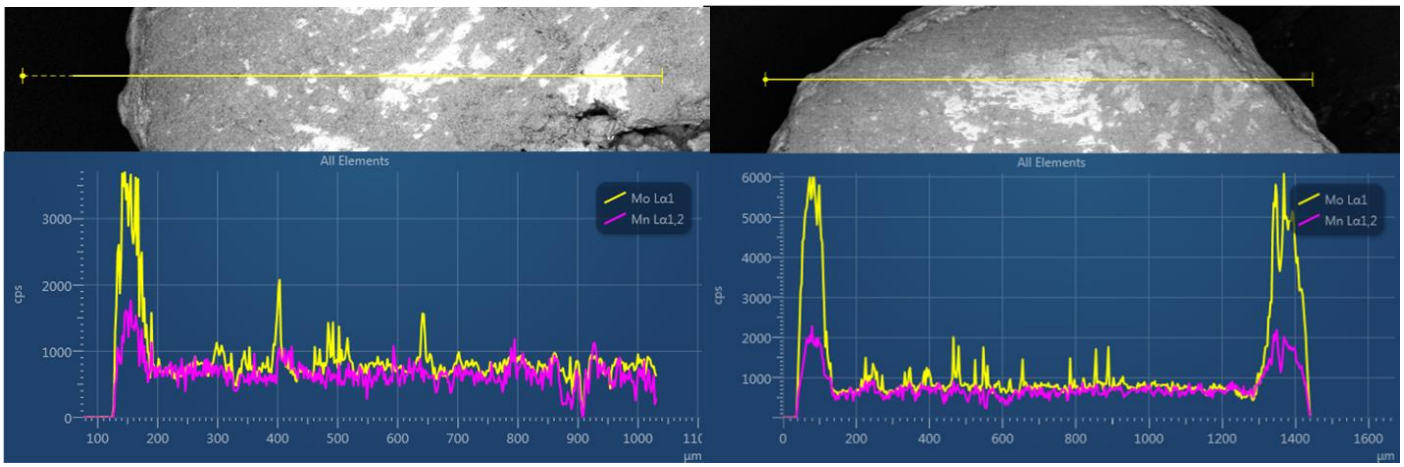

Figure 4.15 Sorbent 15Mn8Mo line scans with EDS analysis for Mn and Mo (EG-Co method).

Elemental mapping is reported in Figure 4.16. The results are very similar to the EG-SQ method. However, the egg-shell profile is thinner than before, equally congruent with the line scans results. The same residual signal of Mn and Mo along the surface can be appreciated, due to the aforementioned reasons.

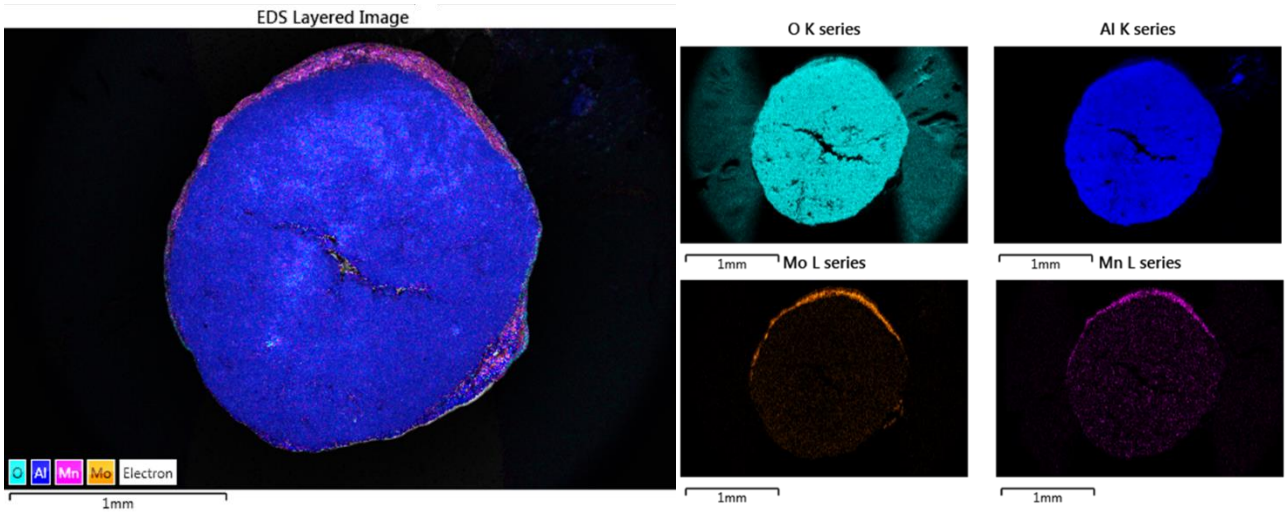

Figure 4.16 Sorbent 15Mn8Mo main elements mapping (EG-Co).

For **GL-Co**, the 40 minutes impregnation sample has been chosen for discussion. A naked-eye image of the cross-section pellet is reported in Figure 4.17. Its appearance is different from the homogeneous colour of the EG methods: the core has a white colour, and the outside is dark brown. The first guess is that the precursors/glycerol solution has penetrated, forming an egg-shell profile, and the white core is the support, congruent with other works in the topic [32]. EDS analysis will confirm the validity of this hypothesis.

Figure 4.17 Naked-eye cross-section pellet (GL-Co, 40 minutes imp.)

A line scan, showing an egg-shell profile, with a thickness of approximately 100µm is reported in Figure 4.18. Further penetration of Mn can be observed , while the Mo signal lowers faster. Mapping is also reported in Figure *4.19*, giving a clear egg-shell profile, consistent with the naked-eye figure hypothesis. Besides, the further penetration of Mn can also be observed, revealing a non-uniform egg-shell thickness. This effect could be due to the higher concentration of Mn in the precursor's solution leading to a faster diffusion throughout the pellet.

An approximate egg-shell thickness of 60µm and 140µm for 20 and 60-minutes impregnations was obtained, respectively (Appendix E). Thus, impregnation time is a key variable to control the egg-shell thickness in GL-Co method. However, the egg-shell profile for was not as clear as the ones reported before and needs to be improved. A general spectrum, line-scans with all the elements and more SEM images can also be found in Appendix E.

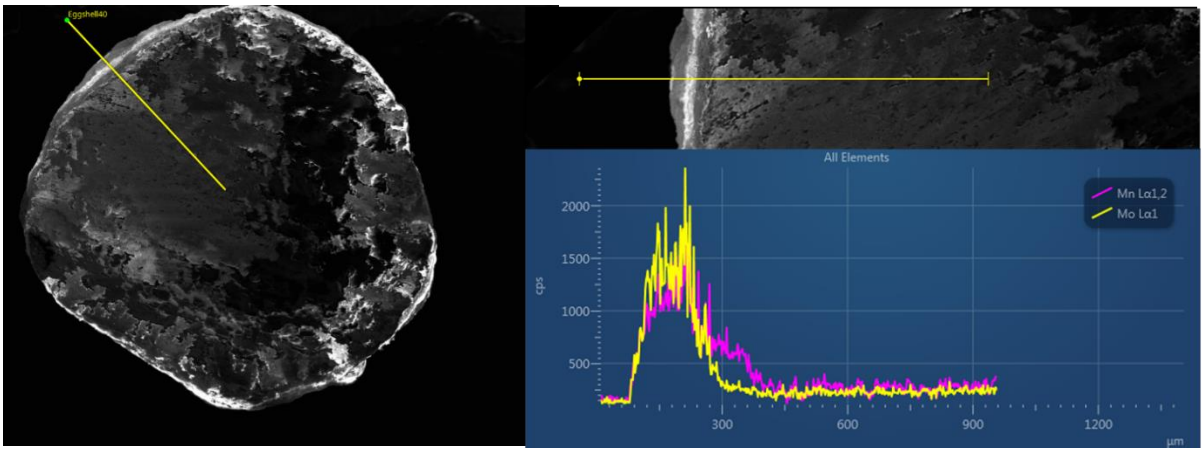

Figure 4.18 Line scan with EDS analysis for Mn and Mo (GL-Co, 40 minutes imp.)

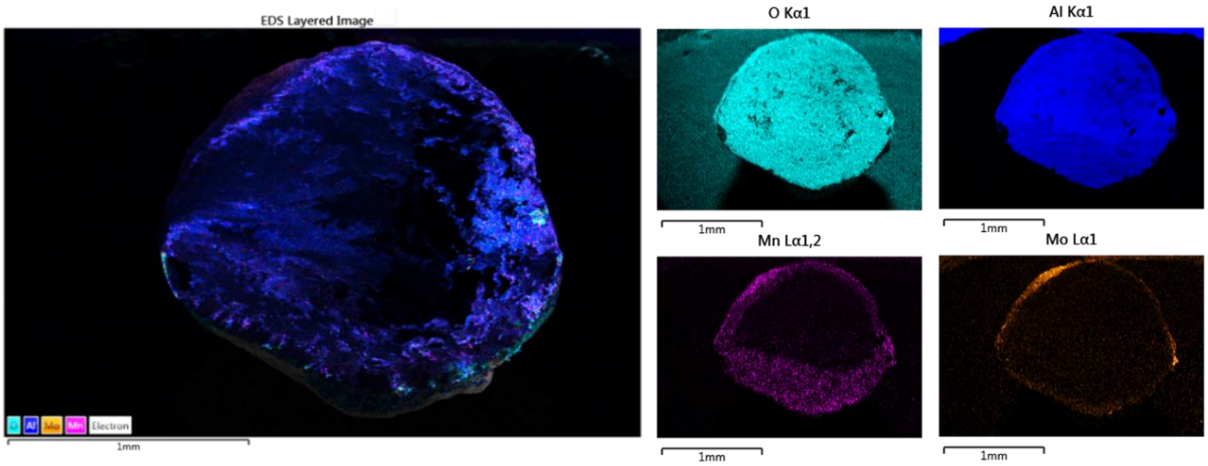

Figure 4.19 Main elements mapping (GL-Co, Glycerol 40 minutes imp.)

5. Conclusion

The preparation and characterization of Mn-based/γ-Al_2O_3, Mo-promoted solid sorbents for high temperature desulfurization of biomass-derived syngas was studied in this work, with focus on three synthesis approaches: EG-SQ, EG-Co and GL-Co. The main findings are presented in this section.

An evaluation and comparison of the methods was established based on the experience of sorbent preparation. **Time efficiency** results revealed that GL-Co method is the most convenient. However, the physical properties of these sorbents showed critical issues such as non-homogeneous appearance and powder loss (attrition), which need to be further improved. In both ethylene glycol methods, sorbents presented a high standard in physical properties, but time efficiency was lower, particularly in EG-SQ. Performance tests and subsequent desulfurization efficiency will give a better understanding of the most convenient method.

Characterization results gave insights into textural properties, metal loading, crystallographic phases, and egg-shell profile distribution. XRF analysis revealed that GL-Co can achieve the highest **metal loading** with one single impregnation, while EG-SQ requires of up to five impregnations and EG-Co between two and three. Additionally, some fluctuations in the Mn atomic percentage have been found, either due to instrument uncertainty or sample preparation. A more precise characterization technique like MP-AES could be employed to clarify this effect.

In general terms, sorbent **diffractograms** show a similar aspect for the three approaches, which implies that crystallographic structure is not deeply affected by the preparation method. However, a higher formation of the mixed oxide **$MnMoO_4$** was reported with co-impregnation methods. This result is promising, since it can entail an enhancement in the desulfurization efficiency, given that $MnMoO_4$ plays a role in the promotion mechanism, as suggested in the previous work [5].

Textural properties, analysed by N_2 physisorption, followed the expected trends regarding surface area and pore volume, which decreased in each of the impregnations. Besides, surface area remained high after several impregnations, implying the preparation method is satisfactory and does not cause any pore blockage or surface area sharp decrease.

The creation of an **egg-shell profile** has been verified using scanning electron microscopy coupled with energy dispersive spectroscopy (EDS), which was a call in the further work of previous studies in this project [54]. Both line scans and elemental mapping showed a clear distribution of the active metals on the outer part of the cross-section pellet.

Regarding the **egg-shell thickness**, it was found to be dependent on the preparation method, as well as the impregnation time for GL-Co approach. For the same sorbent composition, an egg-shell thickness of 200 μm was obtained for sequential impregnation and around 100 μm for co-impregnation. The implications of this finding on the sorbent's capacity will give further insights on how egg-shell thickness affects the overall sorption process.

6. Further studies

To establish a proper conclusion regarding the synthesis methods, both capacity and stability of the sorbents must be evaluated (See section 2.7). Hence, **performance tests** in the laboratory set-up need to be carried out afterwards. The role of the complex $MnMoO_4$ in co-impregnation sorbents and Mo promotion will then be discussed more in depth. Likewise, **spent sorbents characterization** and subsequent comparison with the fresh sorbents is of great importance, and it will give key findings regarding material properties.

An **improvement** in the **GL-Co** preparation method is necessary to avoid poor physical properties which could imply a loss of efficiency during performance tests. Using continuous stirring and a glycerol flow rate during impregnation could improve the synthesis procedure [32].

The final **sorbent acidity** in the **EG-Co** method, due to HNO_3 addition, could also affect the desulfurization efficiency. Thus, it needs to be further studied. Another possible approach which has already given good results with molybdenum salts, given its ability to inhibit precipitate formation, is the use of citric acid [55]. This approach could be considered for further investigations.

Regarding the characterization techniques, **MP-AES** (Microwave Plasma-Atomic Emission Spectroscopy) is recommended in the next work to precisely know the metal loading of the samples, given that XRF implies some uncertainty, and the preparation method available is not sufficiently fine. Although, γ-Al_2O_3 digestion is required for MP-AES analysis, which could be a challenging procedure.

With respect to the **cross-section preparation** for electron microscopy analysis, an improvement must be achieved. The noisy signals obtained in SEM due to the particle-scattering throughout the surface could be avoided using a laser cutter, which will give a finer profile and trustworthy results. Although, the cost of these technique should be also taken into consideration.

A clearer relation between impregnation time and **egg-shell thickness** should be established for the GL-Co method. As stated before, together with an upgrade in the preparation method. The main challenge is the creation of a uniform egg-shell thickness, which can be modelled with impregnation time, according to the sorption process requirements.

References

[1] Our World in Data, "Energy Consumption by Source, World," 2020. [Online]. Available: https://ourworldindata.org/energy. [Accessed June 2021].

[2] Our World in Data, "Global greenhouse gas emissions by sector," 2020. [Online]. Available: https://ourworldindata.org/emissions-by-sector. [Accessed 16 June 2021].

[3] United Nations, "Sustainable Development Goals, 7. Affordable and Clean energy," [Online]. Available: https://www.un.org/sustainabledevelopment/energy/. [Accessed 16 June 2021].

[4] IEA, "Global supply of low-carbon fuel by scenario, 2019-2040," 2020. [Online]. Available: https://www.iea.org/data-and-statistics/charts/. [Accessed 18 June 2021].

[5] J. Ma, K. R. Rout, M. Sauer, M. Mahmoodinia, and E. A. Blekkan, "Investigations of molybdenum-promoted manganese-based solid sorbents for H2S capture," *Biomass and Bioenergy,* vol. 143, no. 105843, 2020.

[6] Thomas B. Johansson et. al, "The Potentials of Renewable Energy," 2004.

[7] MENG, Xiangmei, Biomass gasification: the understanding of sulfur, tar, and char reaction in fluidized bed gasifiers, Ph.D. Thesis, TU Delft, 2012.

[8] F. Saladini, N. Patrizi, F. M. Pulselli, N. Marchettini, and S. Bastianoni, "Guidelines for emergy evaluation of first, second and third generation biofuels," *Renewable and Sustainable Energy Reviews,* vol. 66, pp. 221-227, 2016.

[9] A. Akhtar, V. Krepl, and T. Ivanova, "A Combined Overview of Combustion, Pyrolysis, and Gasification of Biomass," *Energy & Fuels,* vol. 32, pp. 7294-7318, 2018.

[10] N. C. Cruz, F. C. Silva, L. A.C.Tarelho, and S. M. Rodrigues, «Critical review of key variables affecting potential recycling applications of ash produced at large-scale biomass combustion plants,» *Resources, Conservation and Recycling,* vol. 150, nº 104427, 2019.

[11] P.J. Woolcock, and R. C. Brown, «A review of cleaning technologies for biomass-derived syngas,» *Biomass and Bioenergy,* vol. 52, pp. 54-84, 2013.

[12] M. Hillestad, M. Ostadi, G. d. A. Serrano, E. Rytter, B. Austbø, J. G. Pharoah, and O.S.Burheime, «Improving carbon efficiency and profitability of the biomass to liquid process with hydrogen from renewable power,» *Fuel,* vol. 234, pp. 1431-1451, 2018.

[13] J. Watson, Y. Zhang, B. Si, W-T. Chen, and R. de Souza, "Gasification of biowaste: A critical review and outlooks," *Renewable and Sustainable Energy Reviews,* vol. 83, pp. 1-17, 2018.

[14] J. Ma, Ph.D. Thesis, High-temperature desulfurization of biomass-derived synthesis gas using solid sorbents, Trondheim, NTNU, 2020.

[15] N. Abdoulmoumine, S. Adhikari, A. Kulkarni, and S. Chattanathan, "A review on biomass gasification syngas cleanup," *Applied Energy,* vol. 155, pp. 294-307, 2015.

[16] P. R. Westmoreland, and D. P. Harrison, "Evaluation of candidate solids for high-temperature desulfurization of low-Btu gases," *Environ. Sci. Technol.,* vol. 10, no. 7, pp. 659-661, 1976.

[17] H. Hu, and K. Xu, "Chapter 8 - Physicochemical technologies for HRPs and risk control," in *High-Risk Pollutants in Wastewater*, 2020, pp. 169-207.

[18] J. Agnew, E. Hampartsoumian, J. M. Jones, and W. Nimmo, «The effect of sintering on sulphur capture by limestone and dolomite,» *J.Enery Inst.,* vol. 72, nº 2, pp. 81-89, 2005.

[19] S. Yaşyerli, İ. Ar, G. Doğu, and T.Doğu, «Removal of hydrogen sulfide by clinoptilolite in a fixed bed adsorber,» *Chemical Engineering and Processing: Process Intensification,* vol. 41, nº 9, pp. 785-792, 2002.

[20] W. J.W. Bakker, F. Kapteijn, and J. A. Moulijn, «A high capacity manganese-based sorbent for regenerative high temperature desulfurization with direct sulfur production: Conceptual process application to coal gas cleaning,» *Chem. Eng J.*, vol. 96, pp. 223-235, 2003.

[21] R. Li, M. D. Krcha, M. J. Janik, A. D. Roy, and K. M. Dooley, «Ce–Mn Oxides for High-Temperature Gasifier Effluent Desulfurization,» *Energy Fuels,* vol. 26, pp. 6765-6776, 2012.

[22] H. Xia, B. Liu, Q. Li, Z. Huang, and A. S-C. Cheung, «High capacity Mn-Fe-Mo/FSM-16 sorbents in hot coal gas desulfurization and mechanism of elemental sulfur formation,» *Appl. Catal. B Environ.*, vol. 200, pp. 552-565, 2017.

[23] Q. Liu, Z. Zhang, B. Liu, and H. Xia, «Rare earth oxide doping and synthesis of spinel ZnMn2O4/KIT-1 with double gyroidal mesopores for desulfurization nature of hot coal gas,» *Applied Catalysis B: Environmental,* vol. 237, pp. 855-865, 2018.

[24] Q. Liu, B. Liu, Q. Liu, Q. Zhang, R. Xu, X. Wu, and H. Xia, «Walnut wood-derived hierarchically 3D self-assembly of (a%Ce–Mn)yAl_2−yO_x and rapid diffusion character of straight micron channel during hot coal gas desulfurization,» *Chemical Engineering Journal,* vol. 393, nº 124761, 2020.

[25] J. T. Richardson, Principles of catalyst development, New York: Plenum Press, 1989.

[26] K. P. de Jong, "Impregnation and Drying," in *Synthesis of solid catalysts*, Weinheim, Wiley-VCH, 2009, pp. 59-82.

[27] R. Sadegh-Vaziri, and M. U. Babler, "Removal of Hydrogen Sulfide with Metal Oxides in Packed Bed Reactors—A Review from a Modeling Perspective with Practical Implications," *Applied Sciences,* vol. 9, no. 24, 2019.

[28] V. Russo, L. Mastroianni, R. Tesser, T. Salmi, and Martino Di Serio, "Intraparticle Modeling of Non Uniform Active Phase Distribution Catalyst," *Chem.Engineering,* vol. 4, no. 2, 2020.

[29] A.Gavriilidis, and A. Varma, “Optimal catalyst activity profiles in pellets: 9. Study of ethylene epoxidation,” *AIChE Journal,* vol. 38, no. 2, pp. 291-296, 1992.

[30] S. K. Mazidi, M. T. Sadeghi, and M. A. Marvast, «Optimization of Fischer-Tropsch Process in a Fixed-Bed Reactor Using Non-uniform Catalysts,» *Chem. Eng. Technol.,* vol. 36, pp. 62-72, 2012.

[31] H. Zarrin, M. T. Sadeghi, and M. A. Marvast, “Modeling and sensitivity analysis of a catalyst pellet with non-uniform activity distribution in Fisher-Tropsch synthesis,” *nt. J. Chem. React. Eng.,* vol. 7, no. A52, 2009.

[32] H. Silva, M. G. Nielsen, E. M. Fiordaliso, C. D. Damsgaard, C. Gundlach, T. Kasama, I.b. Chorkendorff, and D. Chakraborty, “Synthesis and characterization of Fe–Ni/γ-Al_2O_3 egg-shell catalyst for H_2 generation by ammonia decomposition,” *Applied Catalysis A: General,* vol. 505, pp. 548-556, 2015.

[33] B. Liu, Y. Chai, Y. Liu, Y. Wang, Y. Liu, and C. Liu, “A simple method for preparation of presulfided egg-shell CoMoS/γ-Al_2O_3catalysts for hydrodesulfurization of dibenzothiophene,” *Fuel,* vol. 95, pp. 457-463, 2012.

[34] M-S. Janga, E. Hyun Cho, K. Y. Koo, W. L. Yoon, and C. H. Ko, “Facile preparation of egg-shell-type pellet catalysts usingimmiscibility between hydrophobic solvent and hydrophilic solution: Enhancement of catalytic activity due to position control of metallicnickel inside alumina pellet,” *Applied Catalysis A: General,* vol. 530, pp. 211-216, 2017.

[35] Y. Q. Zhuang, M. Claeys, E. van Steen, «Novel synthesis route for egg-shell, egg-white and egg-yolk type of cobalt on silica catalysts,» *Applied Catalysis A: General,* vol. 301, pp. 138-142, 2006.

[36] “PubChem. Compound summary: Glycerol,” National Library of Medicine, [Online]. Available: https://pubchem.ncbi.nlm.nih.gov/compound/Glycerol. [Accessed 19 June 2021].

[37] B. Liu, Y. Chai, Y. Wang, T. Zhang, Y. Liu, and C. Liu, «A simple technique for preparation of presulfided eggshell MoS_2/Al_2O_3 catalysts and kinetics approach for highly selective hydrodesulfurization of FCC gasoline,» *Applied Catalysis A: General,* vol. 388, pp. 248-255, 2010.

[38] E. Marguí, and R. V. Griekiem, X-Ray Fluorescence Spectrometry and Related Techniques : An Introduction, 2013.

[39] R. Jenkins, X-Ray Fluorescence Spectrometry, Second Edition, 2001.

[40] J. N. I. Chorkendorff, Concepts of Modern Catalysis and Kinetics, 2007.

[41] P. M. V. Raja, and A. R. Barron, “Chemistry LibreTexts,” March 2021. [Online]. Available: https://chem.libretexts.org/. [Accessed 24 May 2021].

[42] J. Niemantsverdriet, Spectroscopy in Catalysis, An Introduction, 2000.

[43] K.S.W. Sing, “Reporting physisorption data for gas/solid systems,” *Pure & Appl. Chem,* vol. 54, no. 11, pp. 2201-2218, 1982.

[44] J. S. L.M. Skinner, “The Kelvin Equation - A review,” *Aerosol Science,* vol. 3, pp. 199-210, 1972.

[45] M. Karlík, “Lattice imaging in transmission electron microscopy,” *Materials Structure,* vol. 8, no. 1, 2001.

[46] J. I. Goldstein, D. E. Newbury, J. R.Michael, N. W.M. Ritchie, J.H. J. Scott, and D. C. Joy, Scanning Electron Microscopy and X-ray Microanalysis, Springer, 2018.

[47] Rigaku, *Rigaku SUpermini200 Analyser, User Manual,* 2018.

[48] K. H. Wells, “Routine Powder Diffraction ("Da Vinci 1"),” 24 February 2020. [Online]. Available: https://www.ntnu.no/wiki/pages. [Accessed 3 June 2021].

[49] NTNU NanoLab, “Working in a cleanroom environment,” in *The Cleanroom booklet*, 2 ed., 2018, pp. 5-10.

[50] NTNU NanoLab, *SEM Apreo Introduction Course,* 2021.

[51] R. C. Sickles and V. Zelenyuk, Measurement of Productivityand Efficiency, Cambridge University Press, 2019.

[52] K. P. de Jong, «Shaping of Solid Catalysts,» in *Synthesis of solid catalysts*, 2009, pp. 173-198.

[53] JEOL Posters, “Periodic table for EDS Analysis,” [Online]. Available: https://www.jeolusa.com/. [Accessed 10 May 2021].

[54] R. O. Sánchez-Ramos, «Bachelor's Thesis, Pelletized shaped Mn-based solid-sorbents for chemical looping desulfurization,» 2020.

[55] D. J. Rensel, S. Rouvimov, M. E. Gin, and J. C. Hicks, “Highly selective bimetallic FeMoP catalyst for C–O bond cleavage of aryl ethers,” *Journal of Catalysis,* vol. 305, pp. 256-263, 2013.

Appendices

Appendix A

Laboratory set-up

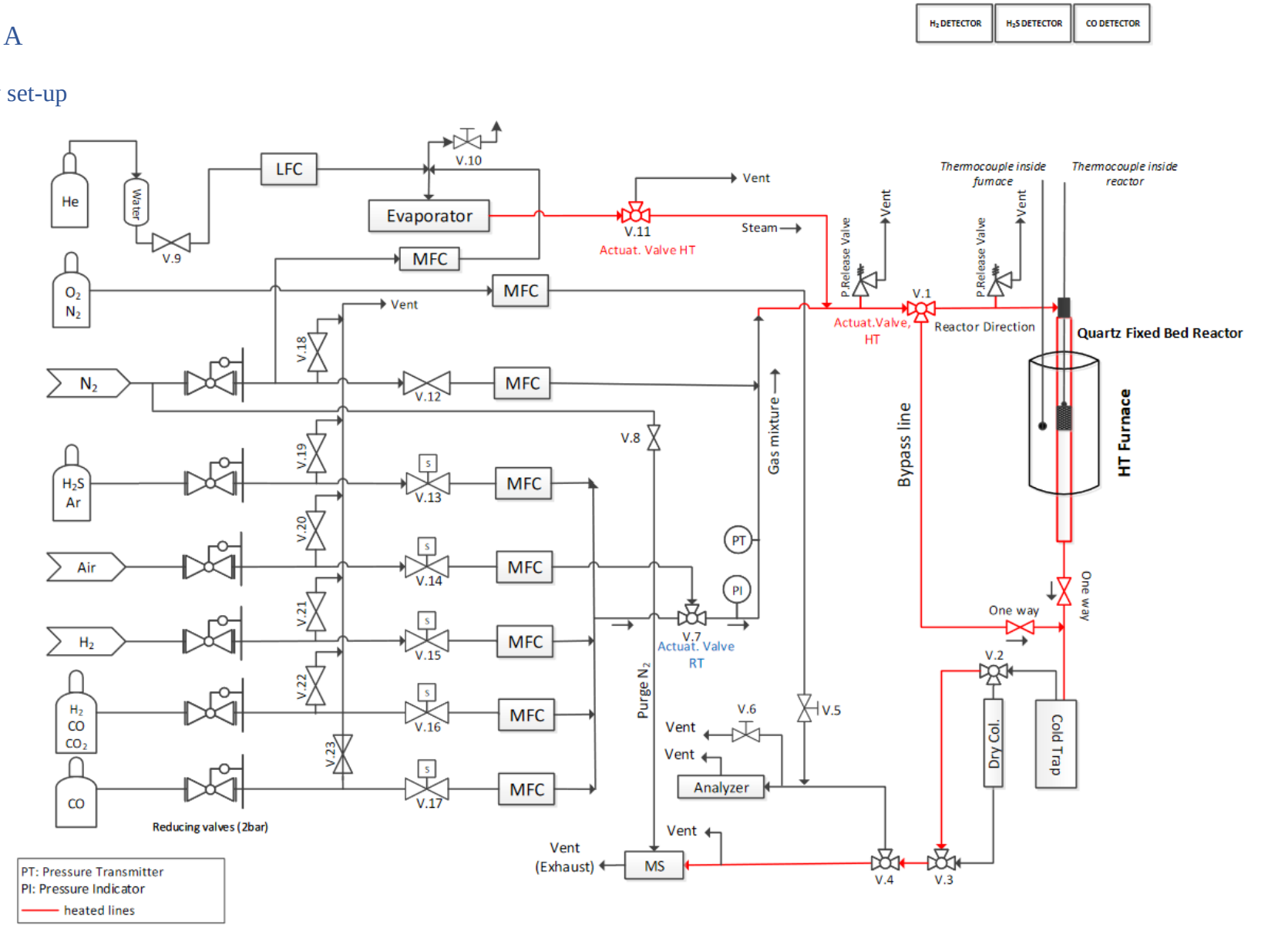

UNIT CARD

SINTEF

NTNU Faculty of Natural Sciences
Department of Chemical Engineering

UNIT	
Rig 1.2 Gas cleaning by sorption at high Temperature	
CHEMICALS AND GASES	**QUANTITY**
0,1 and 1 vol% H_2S in Ar, He *H_2, N_2, Air*	*10L bottle* *From gas distribution lines*
SAFETY HAZARDS	
High Temperature furnace, toxic gases (H_2S), flammable gas, (H2, H2s), mixing H2 and O2, pressure build-up in the reactor	
MANDATORY PROTECTIVE EQUIPMENT	
Gloves, goggles, lab coat, gas detectors for H2 and Hs2, H2S protection mask when changing H2S bottle.	
RESTRICTIONS IN WORKING HOURS	**MAXIMUM TIME FOR UNATTENDED OPERATION**
no	*12h*
EMERGENCY SHUTDOWN PROCEDURE	
Close gas cylinders, shut-off valves from gas distribution lines, stop temperature controller, press emergency button (red knob)	
OTHER SAFETY MEASURES/INFORMATION	
Read MSDS of the chemicals	
UNIT RESPONSIBLE	**OPERATOR**
Edd Blekkan, Supervisor – 735 94 157 **Mehdi Mahmoodinia**, Co-Supervisor - 40385665	**Isabel Maria Pascual Garcia** Master student
VALIDITY DATE from to	***10.02.2021 – 09.02.2022***

Appendix B

X-Ray Fluorescence

- First impregnation XRF analysis for EG-SQ method and reproducibility

File name	CLD46-0 Mn (1)						OXIDE
Sample name	CLD46-0.1						
Date analyzed	07/04/2021 13:43						
Sample type	Oxide Powder						
Component type	Oxide						
Matching library							
Sample film corr.	P.P.Film						
Impurity corr.							
Component	Result	Unit	Det. limit	El. line	Intensity	w/o normal	Analyzing depth(mm)
Al2O3	93,4844	mass%	0,22588	Al-KA	8,5609	101,1092	0,0136
SiO2	0,2953	mass%	0,085	Si-KA	0,0255	0,3193	0,0182
SO3	0,0636	mass%	0,05705	S -KA	0,0141	0,0688	0,0358
K2O	0,2664	mass%	0,05906	K -KA	0,1296	0,2882	0,1138
MnO	5,8411	mass%	0,03529	Mn-KA	4,8634	6,3175	0,6208
Fe2O3	0,0493	mass%	0,02517	Fe-KA	0,0737	0,0533	0,7968
H3BO3	14,0529					14,0529	

File name	CLD46-0 Mn (1)						ATOM
Sample name	CLD46-0.1						
Date analyzed	07/04/2021 13:43						
Sample type	Oxide Powder						
Component type	Metal						
Matching library							
Sample film corr.	P.P.Film						
Impurity corr.							
Component	Result	Unit	Det. limit	El. line	Intensity	w/o normal	Analyzing depth(mm)
Al	89,9237	mass%	0,11831	Al-KA	8,5609	52,9571	0,0139
Si	0,2705	mass%	0,0424	Si-KA	0,0255	0,1593	0,0173
S	0,0503	mass%	0,02455	S -KA	0,0141	0,0296	0,0336
K	0,439	mass%	0,05299	K -KA	0,1296	0,2586	0,1061
Mn	9,2568	mass%	0,03046	Mn-KA	4,8634	5,4514	0,5649
Fe	0,0597	mass%	0,02058	Fe-KA	0,0737	0,0352	0,7238
H3BO3	14,0529					14,0529	

File name	CLD46-0 Mn (2)						OXIDE
Sample name	CLD46-0.2						
Date analyzed	07/04/2021 14:13						
Sample type	Oxide Powder						
Component type	Oxide						
Matching library							
Sample film corr.	P.P.Film						
Impurity corr.							
Component	Result	Unit	Det. limit	El. line	Intensity	w/o normal	Analyzing depth(mm)
Al2O3	93,6842	mass%	0,24315	Al-KA	10,2562	117,0536	0,0135
SiO2	0,089	mass%	0,06633	Si-KA	0,0092	0,1112	0,0181
SO3	0,0247	mass%	0,05469	S -KA	0,0065	0,0309	0,0356
K2O	0,2121	mass%	0,05684	K -KA	0,1303	0,265	0,1132
CaO	0,045	mass%	0,04139	Ca-KA	0,0297	0,0562	0,1541
TiO2	0,2002	mass%	0,05495	Ti-KA	0,0376	0,2501	0,2784
MnO	5,7448	mass%	0,03144	Mn-KA	5,6847	7,1779	0,6162
H3BO3	13,5463					13,5463	

File name	CLD46-0 Mn (2)						ATOM
Sample name	CLD46-0.2						
Date analyzed	07/04/2021 14:13						
Sample type	Oxide Powder						
Component type	Metal						
Matching library							
Sample film corr.	P.P.Film						
Impurity corr.							
Component	Result	Unit	Det. limit	El. line	Intensity	w/o normal	Analyzing depth(mm)
Al	90,1023	mass%	0,1273	Al-KA	10,2562	61,285	0,0139
Si	0,0817	mass%	0,03316	Si-KA	0,0092	0,0556	0,0171
S	0,0196	mass%	0,02359	S -KA	0,0065	0,0133	0,0334
K	0,3503	mass%	0,05111	K -KA	0,1303	0,2383	0,1053
Ca	0,0642	mass%	0,03213	Ca-KA	0,0297	0,0437	0,1428
Ti	0,2418	mass%	0,03613	Ti-KA	0,0376	0,1645	0,2549
Mn	9,1402	mass%	0,02723	Mn-KA	5,6847	6,2169	0,5588
H3BO3	13,5463					13,5463	

- First impregnation XRF analysis for EG-Co method

File name	CLD53-0						OXIDE
Sample name	CLD53-0						
Date analyzed	14/06/2021 17:36						
Sample type	Oxide Powder						
Component type	Oxide						
Matching library							
Sample film corr.	P.P.Film						
Impurity corr.							
Component	Result	Unit	Det. limit	El. line	Intensity	w/o normal	Analyzing depth(mm)
Al2O3	92,7484	mass%	0,23594	Al-KA	10,058	118,3739	0,0136
SiO2	0,165	mass%	0,06365	Si-KA	0,0169	0,2105	0,0182
K2O	0,2393	mass%	0,05937	K -KA	0,1221	0,3054	0,1134
TiO2	0,221	mass%	0,04854	Ti-KA	0,0412	0,2821	0,2789
MnO	5,6855	mass%	0,0388	Mn-KA	5,5826	7,2564	0,6173
MoO3	0,9407	mass%	0,01148	Mo-KA	19,452	1,2007	11,9202
H3BO3	13,994					13,994	
File name	CLD53-0						ATOM
Sample name	CLD53-0						
Date analyzed	14/06/2021 17:36						
Sample type	Oxide Powder						
Component type	Metal						
Matching library							
Sample film corr.	P.P.Film						
Impurity corr.							
Component	Result	Unit	Det. limit	El. line	Intensity	w/o normal	Analyzing depth(mm)
Al	88,8454	mass%	0,12364	Al-KA	10,058	62,0324	0,0139
Si	0,1504	mass%	0,03174	Si-KA	0,0169	0,105	0,0172
K	0,3935	mass%	0,05341	K -KA	0,1221	0,2747	0,1054
Ti	0,2658	mass%	0,03193	Ti-KA	0,0412	0,1856	0,2551
Mn	8,9997	mass%	0,0336	Mn-KA	5,5826	6,2836	0,5591
Mo	1,3454	mass%	0,00898	Mo-KA	19,452	0,9393	10,2756
H3BO3	13,994					13,994	

- Sorbent 15Mn8Mo XRF analysis for EG-SQ method

File name	CLD47-4						OXIDE
Sample name	CLD47-4						
Date analyzed	07/05/2021 12:59						
Sample type	Oxide Powder						
Component type	Oxide						
Matching library							
Sample film corr.	P.P.Film						
Impurity corr.							
Component	Result	Unit	Det. limit	El. line	Intensity	w/o normal	Analyzing depth(mm)
Al2O3	88,0621	mass%	0,2231	Al-KA	7,8404	91,4712	0,0135
SiO2	0,151	mass%	0,0746	Si-KA	0,0127	0,1568	0,0182
K2O	0,2654	mass%	0,05813	K -KA	0,1126	0,2757	0,1126
TiO2	0,1546	mass%	0,05374	Ti-KA	0,0236	0,1606	0,2761
MnO	8,6812	mass%	0,03339	Mn-KA	6,9328	9,0173	0,6095
MoO3	2,9225	mass%	0,01151	Mo-KA	42,0798	2,724	11,2462
H3BO3	13,8162					13,8162	
File name	CLD47-4						ATOM
Sample name	CLD47-4						
Date analyzed	07/05/2021 12:59						
Sample type	Oxide Powder						
Component type	Metal						
Matching library							
Sample film corr.	P.P.Film						
Impurity corr.							
Component	Result	Unit	Det. limit	El. line	Intensity	w/o normal	Analyzing depth(mm)
Al	73,5433	mass%	0,11831	Al-KA	7,8404	26,9825	0,0136
Si	0,2106	mass%	0,03678	Si-KA	0,0127	0,0772	0,0174
K	0,6746	mass%	0,05238	K -KA	0,1126	0,2475	0,1035
Ti	0,2883	mass%	0,03546	Ti-KA	0,0236	0,1058	0,2481
Mn	19,178	mass%	0,02961	Mn-KA	6,9328	7,0362	0,5385
Mo	8,4053	mass%	0,01029	Mo-KA	42,0798	2,24	8,5234
H3BO3	13,8162					13,8162	

- Sorbent 15Mn8Mo XRF analysis for EG-Co method

File name	CLD52-1						OXIDE
Sample name	CLD52-1bb						
Date analyzed	13/06/2021 18:30						
Sample type	Oxide Powder						
Component type	Oxide						
Matching library							
Sample film corr.	P.P.Film						
Impurity corr.							
Component	Result	Unit	Det. limit	El. line	Intensity	w/o normal	Analyzing depth(mm)
Al2O3	87,7977	mass%	0,21702	Al-KA	6,8722	78,7459	0,0135
P2O5	0,008	mass%	0,07381	P -KA	0,0176	0,0072	0,0258
K2O	0,2829	mass%	0,05519	K -KA	0,1233	0,2537	0,112
TiO2	0,17	mass%	0,05282	Ti-KA	0,0227	0,1525	0,2744
MnO	8,4411	mass%	0,02906	Mn-KA	5,8984	7,5709	0,6056
MoO3	3,2219	mass%	0,01141	Mo-KA	44,9943	2,8897	11,1292
H3BO3	13,548					13,548	

File name	CLD52-1						ATOM
Sample name	CLD52-1bb						
Date analyzed	13/06/2021 18:30						
Sample type	Oxide Powder						
Component type	Metal						
Matching library							
Sample film corr.	P.P.Film						
Impurity corr.							
Component	Result	Unit	Det. limit	El. line	Intensity	w/o normal	Analyzing depth(mm)
Al	71,9221	mass%	0,11525	Al-KA	6,8722	21,9322	0,0135
P	0	mass%	0,13148	P -KA	0,0176	0	0,0245
K	0,7503	mass%	0,04998	K -KA	0,1233	0,2288	0,1024
Ti	0,3315	mass%	0,03508	Ti-KA	0,0227	0,1011	0,2449
Mn	19,2838	mass%	0,02595	Mn-KA	5,8984	5,8805	0,5306
Mo	7,7123	mass%	0,01043	Mo-KA	44,9943	2,3518	8,271
H3BO3	13,548					13,548	

Appendix C

X-Ray Diffraction

- Peak identification with DIFRAC.EVA for γ-Al_2O_3 and Mn-related phases.

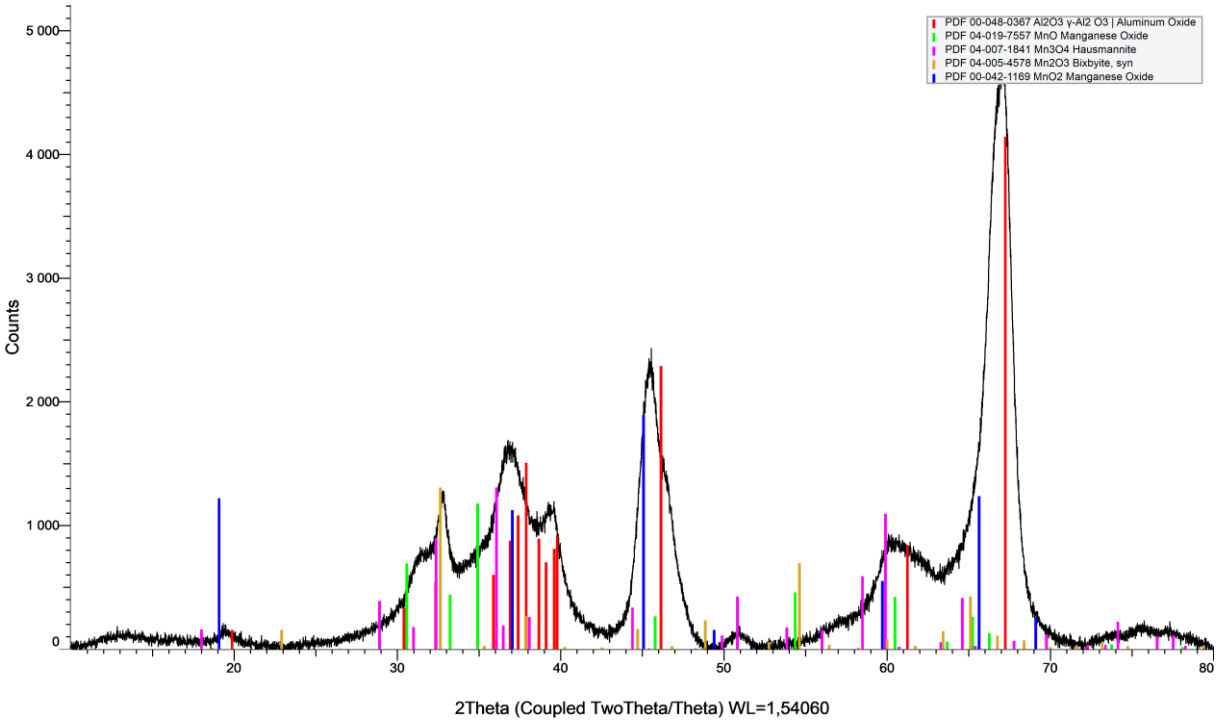

- Peak identification with DIFRAC.EVA for Mo-related phases.

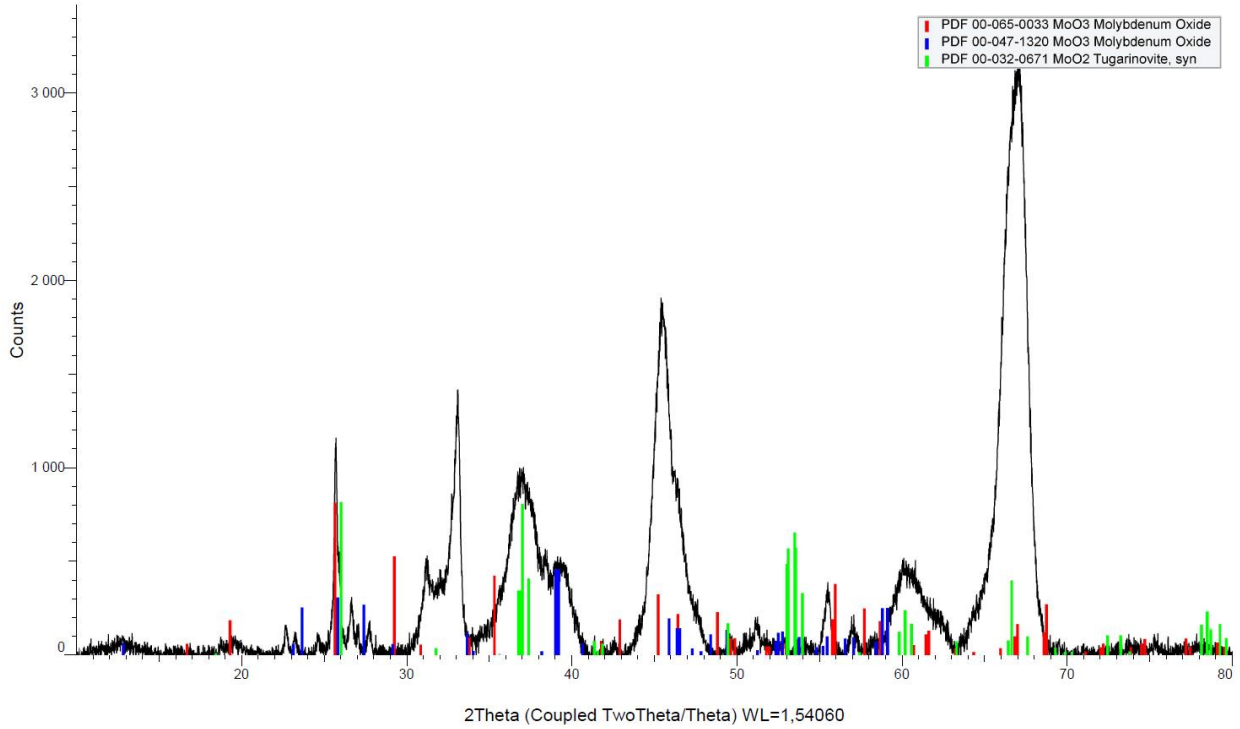

- Peak identification with DIFRAC.EVA for $MnMoO_4$.

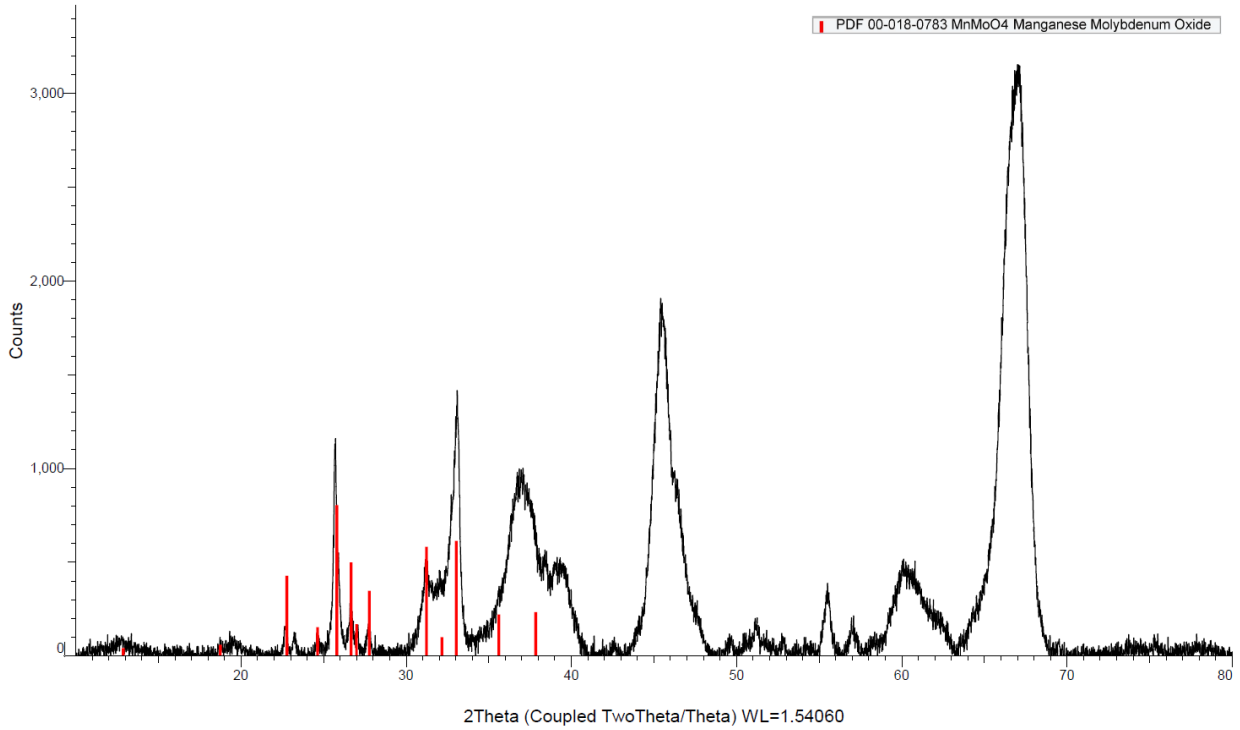

Appendix D

N_2 Physisorption

- Summary Report

Full Report Set

MicroActive 5.01 | TriStar II 3020 Version 3.02 Serial # 731 Unit 1 Port 1 | Page 1 of 33

Sample: CLD45-0.1
Operator: Isabel
Submitter:
File: C:\TriStar II 3020\data\Master stude...\CLD45-0.1c.SMP

Started:	3/16/2021 10:38:23 AM	Analysis adsorptive:	N2
Completed:	3/16/2021 11:46:28 PM	Analysis bath temp.:	77,350 K
Report time:	3/17/2021 10:38:49 AM	Thermal correction:	No
Sample mass:	0,2600 g	Ambient free space:	11,0409 cm³ Measured
Analysis free space:	31,5559 cm³	Equilibration interval:	10 s
Low pressure dose:	None	Sample density:	1,000 g/cm³
Automatic degas:	No		

Summary Report

Surface Area

Single point surface area at p/p° = 0,109463716:	126,5435 m²/g
BET Surface Area:	133,1330 m²/g
Langmuir Surface Area:	347,1303 m²/g
t-Plot Micropore Area:	10,3756 m²/g
t-Plot external surface area:	122,7574 m²/g
BJH Adsorption cumulative surface area of pores between 17,000 Å and 3 000,000 Å diameter:	157,2958 m²/g
BJH Desorption cumulative surface area of pores between 17,000 Å and 3 000,000 Å diameter:	180,0171 m²/g
D-H Adsorption cumulative surface area of pores between 17,000 Å and 3 000,000 Å diameter:	138,2183 m²/g
D-H Desorption cumulative surface area of pores between 17,000 Å and 3 000,000 Å diameter:	168,9714 m²/g

Pore Volume

Single point adsorption total pore volume of pores less than 11,415 Å diameter at p/p° = 0,010000000:	0,033998 cm³/g
Single point desorption total pore volume of pores less than 206,503 Å diameter at p/p° = 0,900000000:	0,416225 cm³/g
t-Plot micropore volume:	0,004474 cm³/g
BJH Adsorption cumulative volume of pores between 17,000 Å and 3 000,000 Å diameter:	0,385798 cm³/g
BJH Desorption cumulative volume of pores between 17,000 Å and 3 000,000 Å diameter:	0,416266 cm³/g
D-H Adsorption cumulative volume of pores between 17,000 Å and 3 000,000 Å diameter:	0,380382 cm³/g

Pore Volume

between 17,000 Å and 3 000,000 Å diameter: 0,427620 cm³/g

Pore Size

Adsorption average pore diameter (4V/A by BET): 10,215 Å

Desorption average pore diameter (4V/A by BET): 125,055 Å

BJH Adsorption average pore diameter (4V/A): 98,108 Å

BJH Desorption average pore diameter (4V/A): 92,495 Å

D-H Adsorption average pore diameter (4V/A): 110,081 Å

D-H Desorption average pore diameter (4V/A): 101,229 Å

Freundlich

Qm·C: 0,01648 ± 0,00295 mmol/g

m: 1,5257 ± 0,1600

Temkin

q·alpha/Qm: 0,219655 ± 0,032843 kJ/mol·(mmol/g)

A: 0,1937 ± 0,1798 kPa

Nanoparticle Size:

Average Particle Size 450,677 Å

Horvath-Kawazoe

Maximum pore volume at p/p° = 0,898724376: 0,383472 cm³/g

Median pore width: 153,037 Å

Dubinin-Astakhov

Micropore surface area: 247,6229 m²/g

Limiting micropore volume: 0,205428 cm³/g

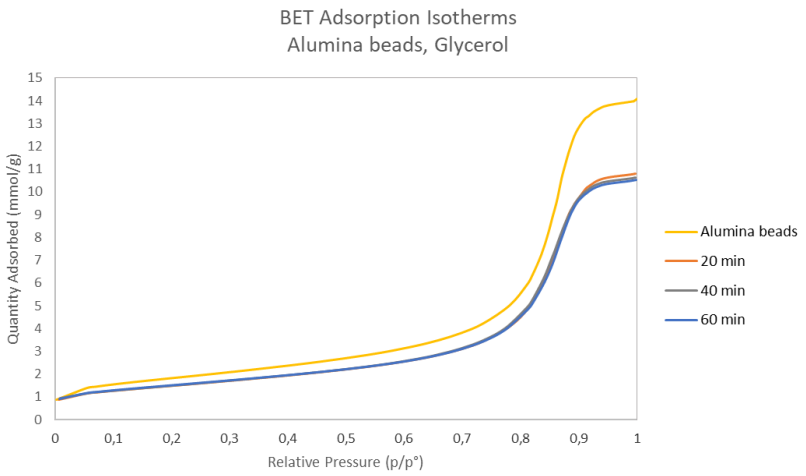

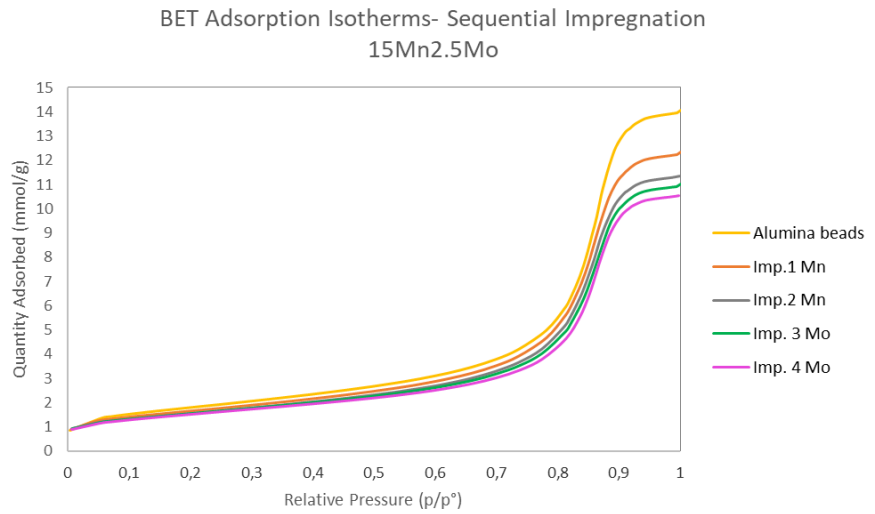
BET Adsorption Isotherms- Sequential Impregnation
15Mn2.5Mo
Quantity Adsorbed (mmol/g)
Relative Pressure (p/p°)
Alumina beads
Imp.1 Mn
Imp.2 Mn
Imp. 3 Mo
Imp. 4 Mo

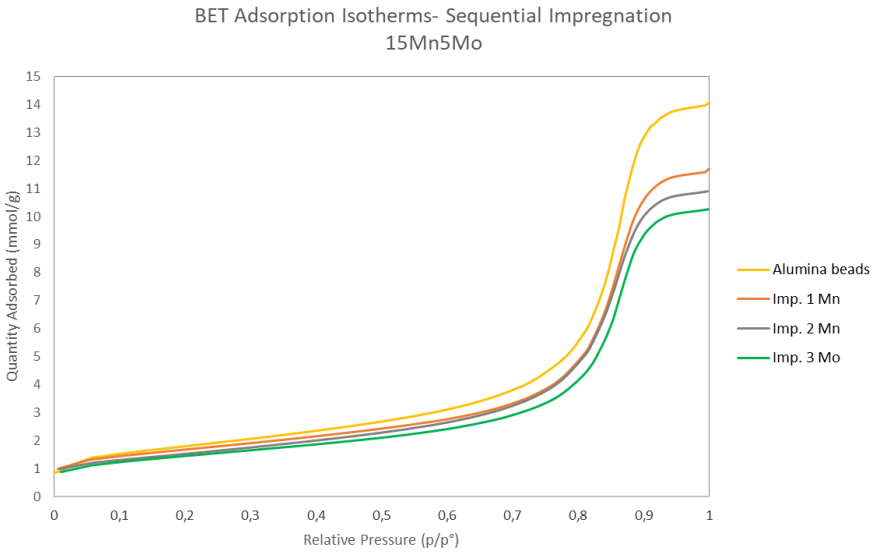
BET Adsorption Isotherms- Sequential Impregnation
15Mn5Mo
Quantity Adsorbed (mmol/g)
Relative Pressure (p/p°)
Alumina beads
Imp. 1 Mn
Imp. 2 Mn
Imp. 3 Mo

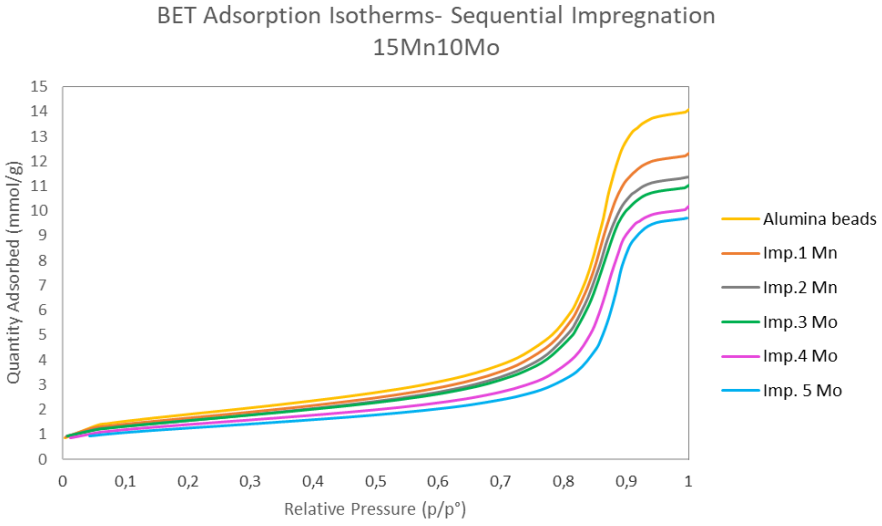
BET Adsorption Isotherms- Sequential Impregnation
15Mn10Mo
Quantity Adsorbed (mmol/g)
Relative Pressure (p/p°)
Alumina beads
Imp.1 Mn
Imp.2 Mn
Imp.3 Mo
Imp.4 Mo
Imp. 5 Mo

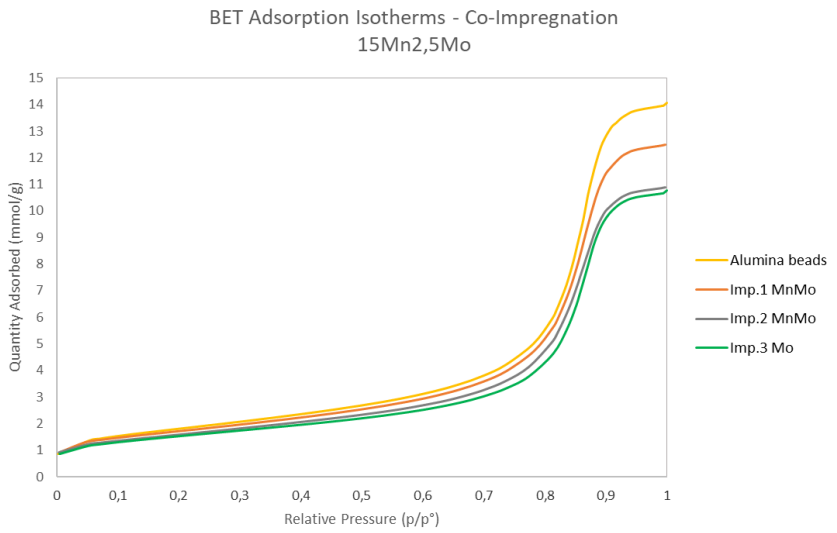
BET Adsorption Isotherms - Co-Impregnation
15Mn2,5Mo
Quantity Adsorbed (mmol/g)
Relative Pressure (p/p°)
Alumina beads
Imp.1 MnMo
Imp.2 MnMo
Imp.3 Mo

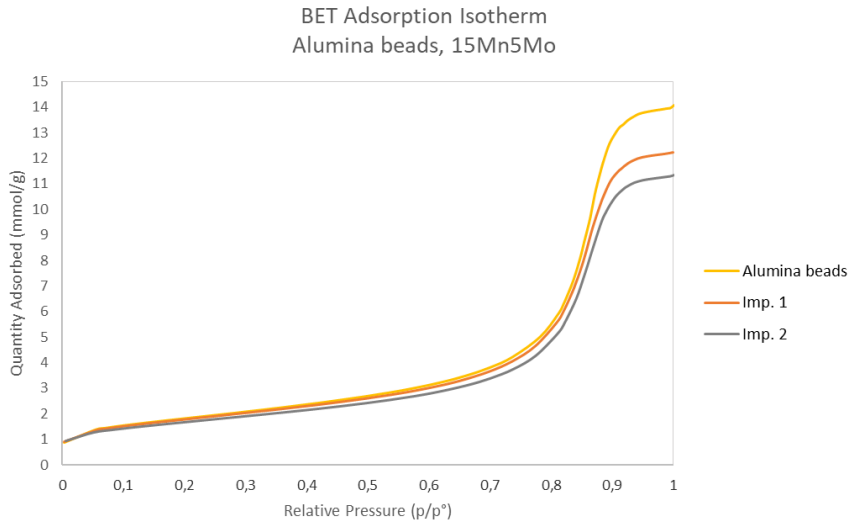
BET Adsorption Isotherm
Alumina beads, 15Mn5Mo
Quantity Adsorbed (mmol/g)
Relative Pressure (p/p°)
Alumina beads
Imp. 1
Imp. 2

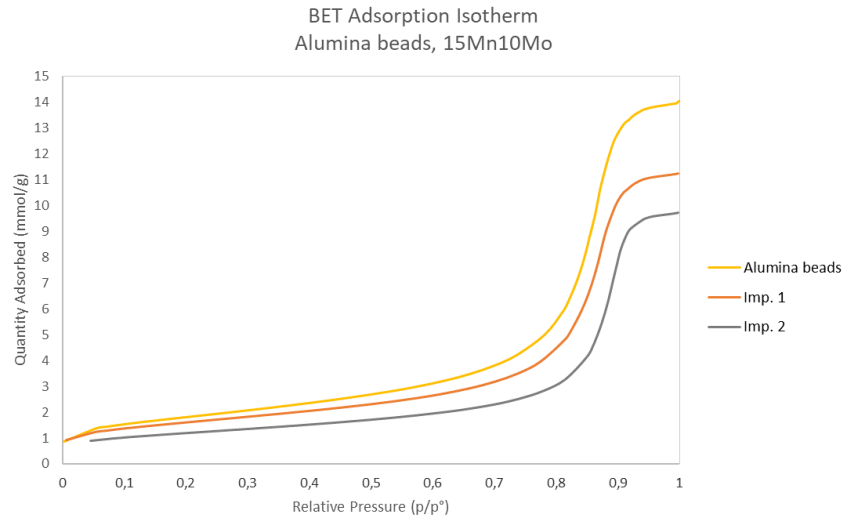
BET Adsorption Isotherm
Alumina beads, 15Mn10Mo
Quantity Adsorbed (mmol/g)
Relative Pressure (p/p°)
Alumina beads
Imp. 1
Imp. 2

Appendix E Scanning electron microscopy

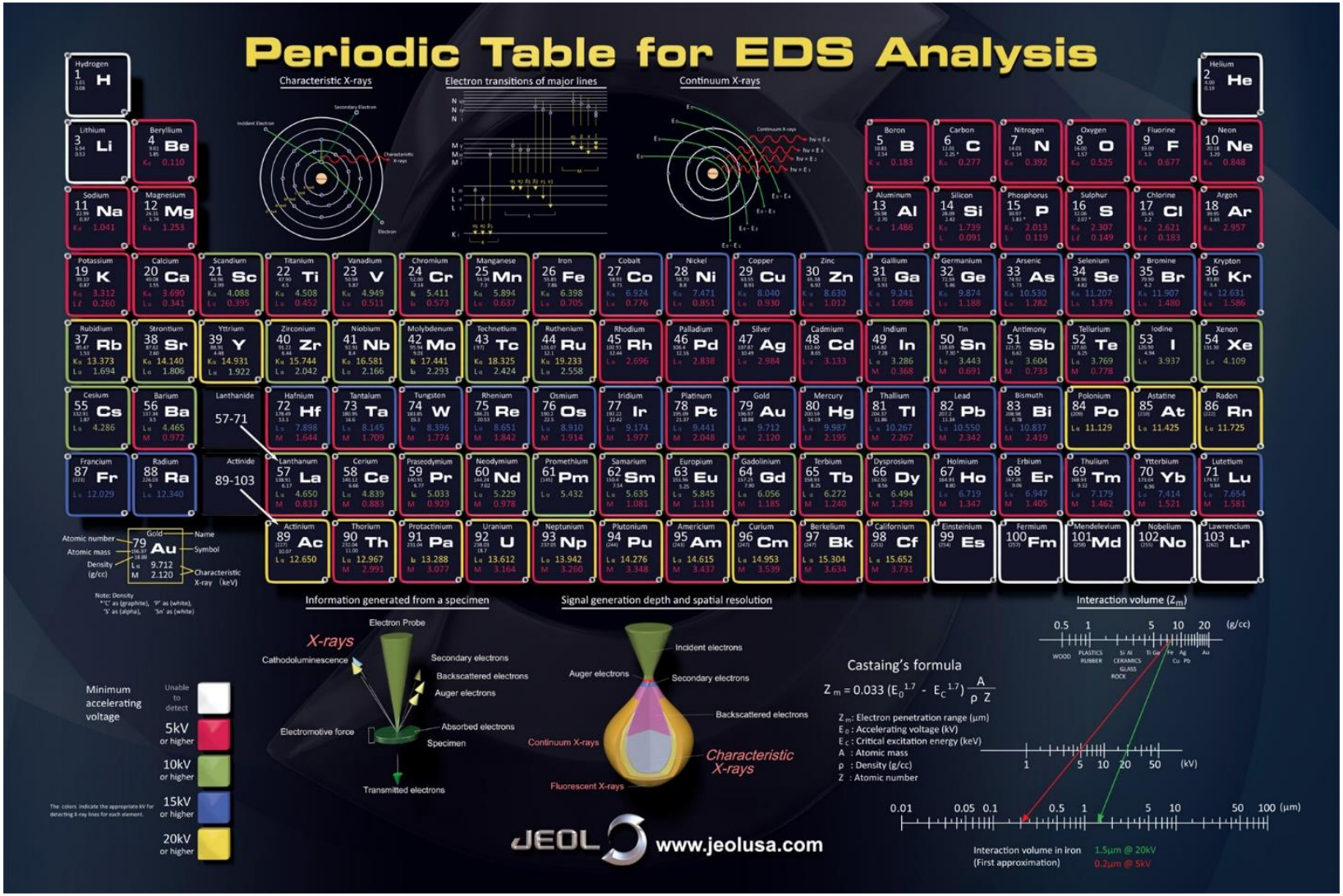

- General SEM spectrum for all elements

  (C appears because of the carbon tape in which the pellet is placed)

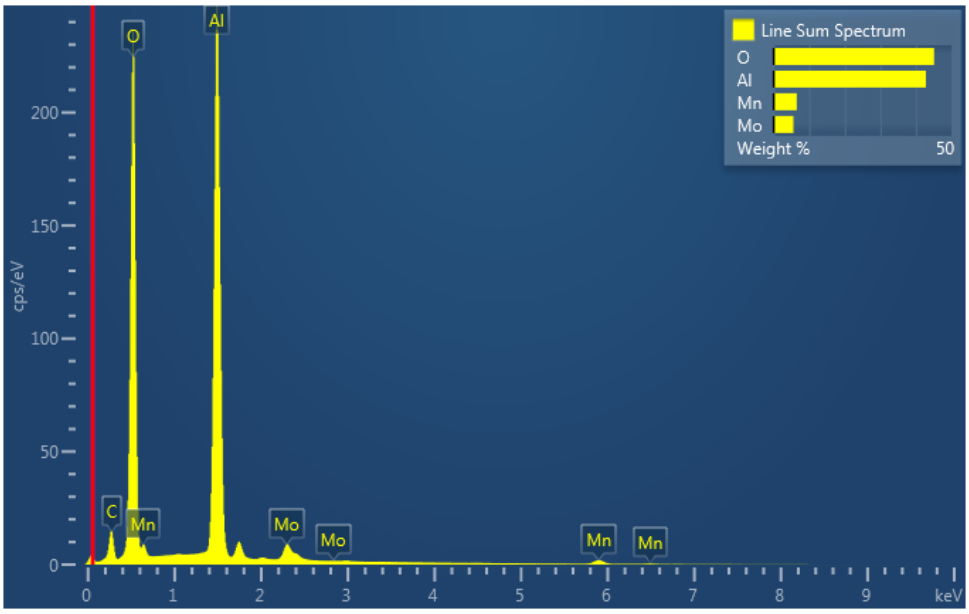

- Examples of line scans for all elements (Mo, Mn, Al, O)

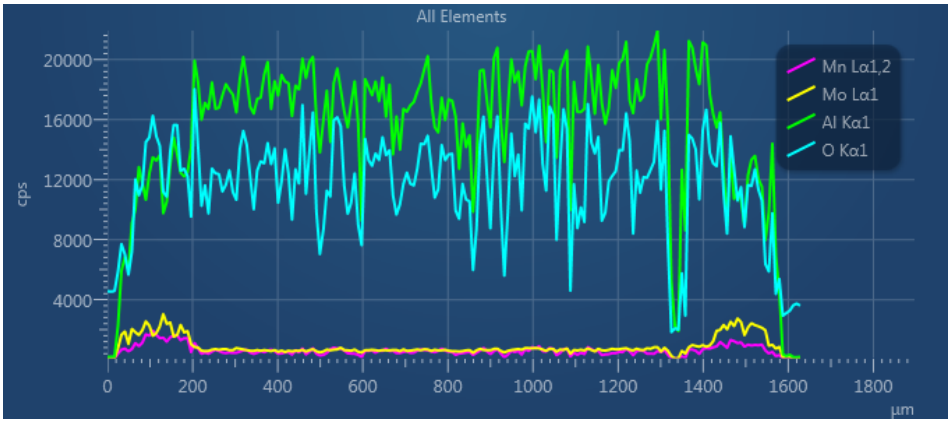

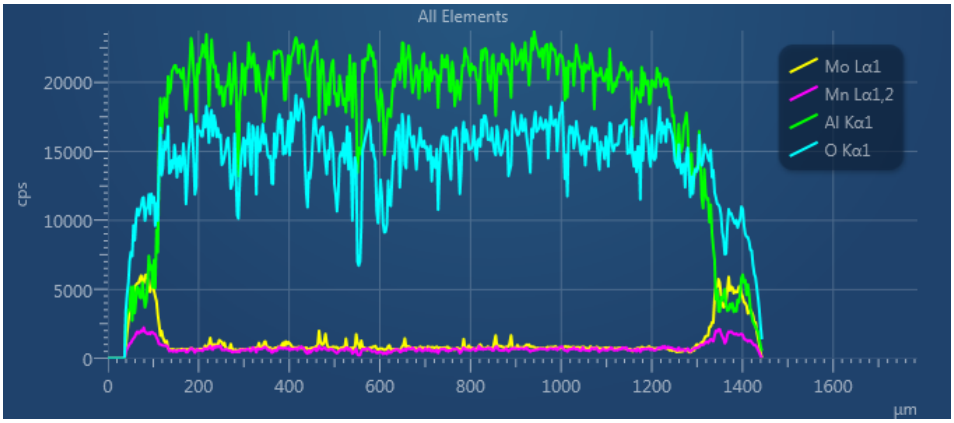

- Line scan for glycerol 20 minutes impregnation

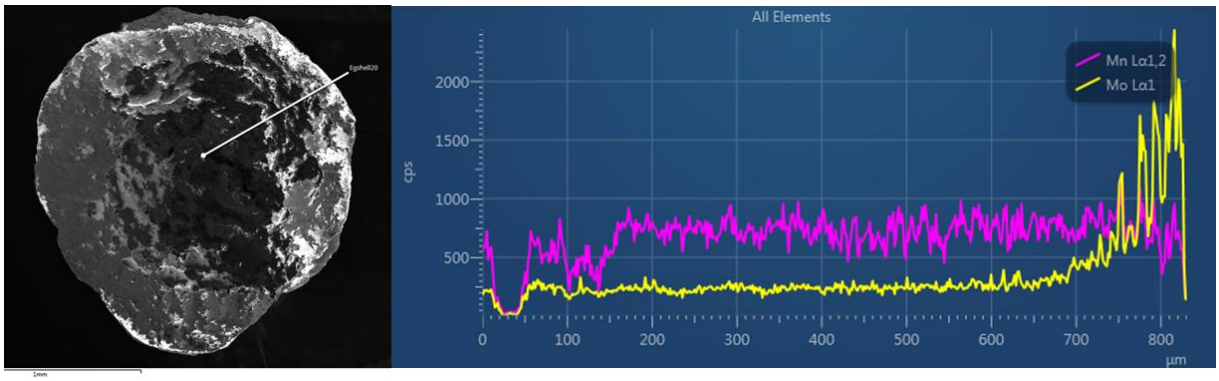

- Line scan for glycerol 60 minutes impregnation

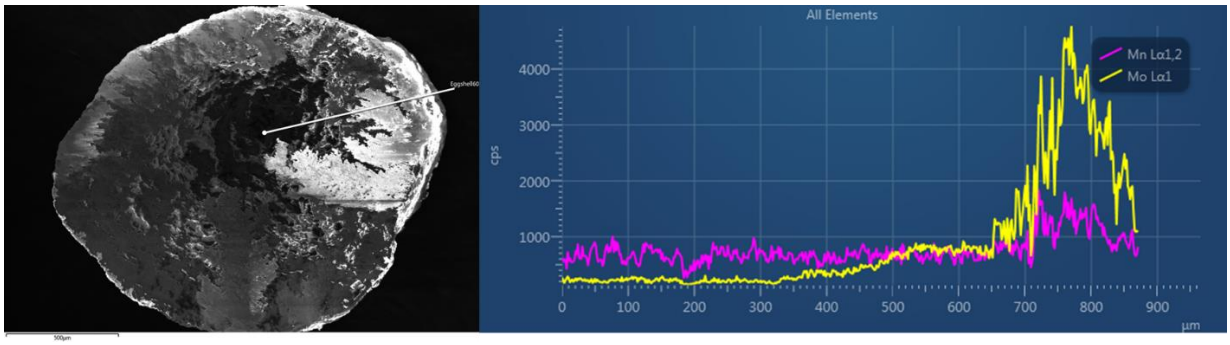

- 5µm magnification SEM image

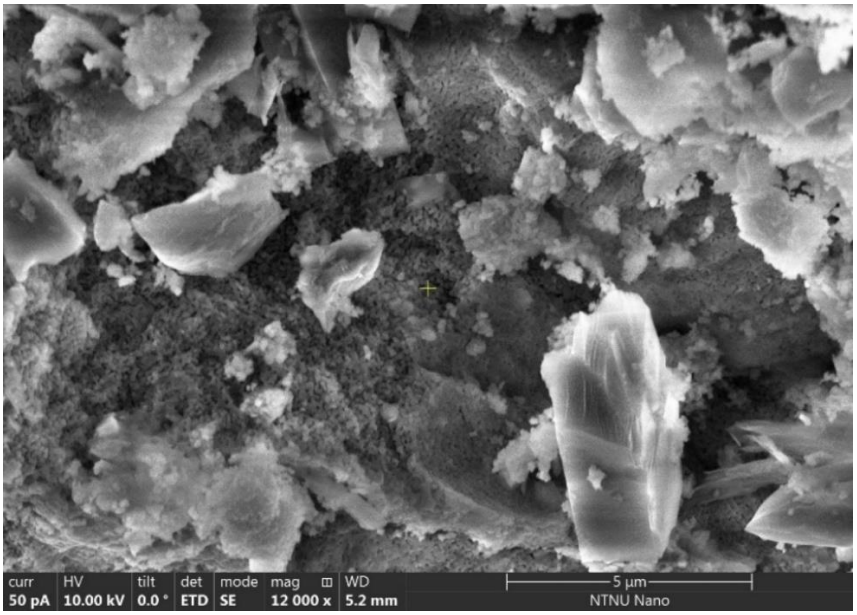

- 1mm magnification SEM image

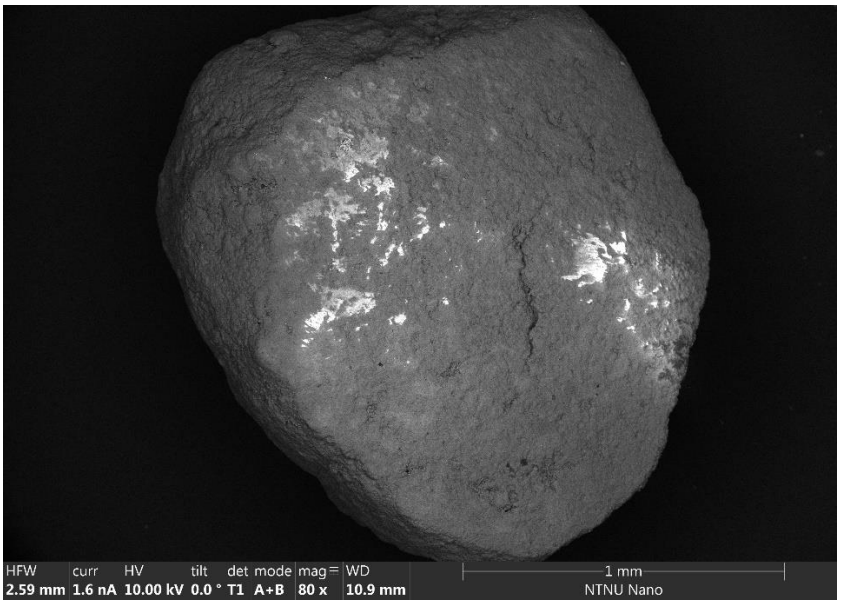

Appendix F

Risk Assessment

ID	41232	**Status**	**Date**
Risk Area	Risikovurdering: Helse, miljø og sikkerhet (HMS)	Created	03.02.2021
Created by	Isabel Maria Pascual Garcia	Assessment started	09.02.2021
Responsible	Isabel Maria Pascual Garcia	Measures decided	09.02.2021
		Closed	

Risk Assessment:

CAT, Master student, 2021, Isabel María Pascual García

Valid from-to date:
2/1/2021 - 7/1/2021

Location:
IKP- Institutt for kjemisk prosessteknologi

Goal / purpose

This risk assessment contains all activities that I will be performing in different laboratories during my Master's Thesis (spring semester 2021). The purpose is to risk assess my work in the lab, as detailed as possible. It involves synthesis of the catalysts/sorbents, characterization techniques, and usage of the Chemical Looping Desulphurization (CLD) setup located in the Chemistry Hall D (Unit 1.2) (find flowsheet of the Set-up and Unit card attached)

Pelletized solid sorbents with different concentrations (2,5- 15-wt%) manganese-based and Mo-promoted, supported on "γ-Al2O3", are going to be synthesized in the lab using three different approaches.

Sorbents/heterogeneous catalysts are also going to be characterized in order to investigate the material parameters such as crystal structure, morphology, surface area, etc. Characterization techniques are listed in the following section.

This risk assessment has been updated after specific trainings and changes in the project.

Covid-19 measures will be also taken into account.

Background

SYNTHESIS PROCEDURE
Method: Incipient Wetness Impregnation (IWI) and Wetness Impregnation (WI)
Materials:
- De-ionized water
- γ-Al2O3: Gamma-alumina (support material)
- Mn(NO3)2□4H2O: manganese nitrate tetrahydrate (manganese precursor)
- (NH4)6Mo7O24□4H2O: ammonium molybdate tetrahydrate (molybdenum precursor)
-Ethylene glycol (99,5% purity)
-Nitric acid (65% putity)
-Glycerol (99% purity)

Gamma-alumina is pre-calcined at 500 °C for 10 hours using a calcination setup with flowing air and a heating rate of 10 K/min. Gamma-alumina is soaked into ethylene glycol for 30 minutes at 30°C using an ultrasonic bath. Precursors are dissolved in the deionized water (WI) and the solution is added to the support under continuously stirring (20 min). Afterwards, the sorbent is then dried at 100 °C for 12 h (5K/min.) in a drying oven and calcined at 700 °C for 5 h using calcination set-up under air with a heating rate of 10K/min.
Nitric acid is used to dissolve a stable precipitate formed when co-impregnation is applied. Nitric acid addition should be gently and as small as possible. For another method (IWI), precursors are dissolved in glycerol and gamma alumina is soaked in the solution for different impregnation times. The post treatment also consists in drying and calcination using the same conditions as before.

Cleaning and disposal: The solution is disposed in an organic waste bottle. If there is a solid chemical left it will be placed into the red box for waste chemical.

CHARACTERIZATION TECHNIQUES
- BET (standard procedure in the lab)
- XRF (standard procedure in the lab)
- XRD (standard procedure in the lab)-Materials department specific training
- SEM (standard procedure in the lab). NanoLab cleanroom course and specific training.

PROCESS DESCRIPTION
The CLD process takes place under atmospheric pressure and a temperature range of 400-650 ºC. Although, pressure may biuld-up in the reactor and or in the lines. The pressure gauge has to be checked when starting the experiment and during the process (find attached performance test procedure). Pressure release valve (PSV) can also be considered as an extra safety measure in case of automation in the setup. During performance test, one has to be present in the lab and check the ongoing experiments. Be aware that a power cut-off may damage the mass spectrometer and/or analyser. Setup 1.2 is connected to; Ventilation, Furnace, Gas distribution system for H2, N2, and O2/Air, and pressurized gas bottles for 0.1 and 1% H2S in Ar), He gas bottle, CO and CO2 bottles, quadrupole mass spectrometer, and an analyser.
Three different steps happen in the process:
- Pre-reduction: Oxidation of MnO2 to MnO with Mn2O3 and Mn3O4 as intermediates. MnO provides the active sites for the desulfurization process.
- Sulfidation: The metal oxides (Mn) are converted to metal sulfides by exchanging oxygen with sulfur.
- Regeneration: The sulfidated sorbent then will be regenerated again under oxidising atmosphere (O2/Air).

REACTOR
The reactor is a tubular quartz fixed bed reactor enclosed by a furnace. Temperature is regulated by a Eurotherm 2408 temperature controller. Different gas flow compositions applied depending on the purpose of experiments and reaction types, and gas flow for H2, H2S, N2, CO, CO2, steam and O2/air may varies between 20-500 mL/min.

Description and limitations

SAFETY MEASURES FOR SYNTHESIS
Referred to in the SDS attached (precursors, glycerol, ethylene glycol and nitric acid). Be aware of the use of coat, goggles and gloves always.

SAFETY MEASURES IN THE SET UP (referred to in Rodrigo Ortiz's risk assessment)
The set-up consists on a system of different streams with different components in each stream (N2, H2, O2, H2S, H2O, CO, CO2) and a reactor (find flowsheet attached). The safety measures to take into account are:
- Leak-check: both with H2 and H2S portable detectors, and also with combustible gas detector.
- Make sure furnace is properly closed.
- In case of leakage, close the valves to all lines, fix the leakage, and check again.
- Make sure thermocouples are properly connected to Eurotherm and there is a proper reading from them.
- Pressure-drop need to be checked using the P-gauge.
- In case of P-drop, introduce the gas mixture to vent, close valve to all lines and find the source for blockage.
- Flashing with N2: should be properly done so the H2 and O2 level during sorption and regeneration drop to below 4e-10A, to avoid H2/O2 mixing and explosion.
- Never open the O2 and H2 valves to the gas mixture line at the same time.
- When working with pellets, not powder, there is no possibility to inhale dust.
-The pressure gauge is checked with highest gas flow, and in case of P-drop this will be evaluated.

Prerequesites, assumptions and simplifications

PROTECTIVE EQUIPMENT
-Gloves (mandatory)
-Goggles (mandatory)
-Lab coat (mandatory)
-Mask (if necessary)
All of them must be used when working in all the labs: synthesis, characterization and performance test.

SAFETY MEASURES RELATED TO COVID-19:
- Disinfect with ethanol before and after using all surfaces, materials, door knob, PC screen, keyboard, mouse, desk and label printing machine.
- Use the mask when necessary
- Keep a 2 meter distance from colleagues
- Wash hands very often
- Avoid touching the face

Attachments

Set-up1.2-modifed-final_version.pdf
Ammonium Molybdate.pdf
MANGANESE-II--NITRATE-TE-250GR-.pdf
hydrogen-gas-h2-safety-data-sheet-sds-p4604.pdf
H2S-SDS.pdf
carbon-monoxide-sds-e-4576.pdf
1.2_Mehdi_Unit_card.pdf
CO2-SDS.pdf
Nitric acid_msds.pdf
Ethylene glycol_msds.pdf
Glycerol_msds.pdf

References

[Ingen registreringer]

Summary, result and final evaluation

The summary presents an overview of hazards and incidents, in addtition to risk result for each consequence area.

Hazard: **H2 gas explosion**

Incident: **H2 gas explosion**

Consequence area:			
	Helse	Risk before measures:	Risiko after measures:
	Ytre miljø	Risk before measures:	Risiko after measures:
	Materielle verdier	Risk before measures:	Risiko after measures:
	Omdømme	Risk before measures:	Risiko after measures:

Measure	Responsible	Registered	Deadline	Status
HSE procedures	Isabel Maria Pascual Garcia	09.02.2021		New

Hazard: **H2S leakage**

Incident: **H2S toxic gas leakage**

Consequence area:			
	Helse	Risk before measures:	Risiko after measures:
	Ytre miljø	Risk before measures:	Risiko after measures:
	Materielle verdier	Risk before measures:	Risiko after measures:
	Omdømme	Risk before measures:	Risiko after measures:

Measure	Responsible	Registered	Deadline	Status
HSE procedures	Isabel Maria Pascual Garcia	09.02.2021		New
H2S protection mask	Isabel Maria Pascual Garcia	09.02.2021		New

Hazard: **High temperature in reactor**

Incident: **High temperature in reactor damages to operator**

Consequence area:			
	Helse	Risk before measures:	Risiko after measures:
	Ytre miljø	Risk before measures:	Risiko after measures:
	Materielle verdier	Risk before measures:	Risiko after measures:
	Omdømme	Risk before measures:	Risiko after measures:

Measure	Responsible	Registered	Deadline	Status
HSE procedures	Isabel Maria Pascual Garcia	09.02.2021		New

Hazard: **Catalyst manipulation**

Incident: **Skin exposure or chemical inhalation**

Consequence area:	Helse	Risk before measures:		Risiko after measures:	
	Ytre miljø	Risk before measures:		Risiko after measures:	

Hazard: **Pressure build up in reactor**

Incident: **Pressure buid up in reactor**

Consequence area:	Helse	Risk before measures:		Risiko after measures:	
	Ytre miljø	Risk before measures:		Risiko after measures:	
	Materielle verdier	Risk before measures:		Risiko after measures:	

Hazard: **Working in the lab under Covid19-situation**

Incident: **Handle something without gloves unconsciously**

Consequence area:	Helse	Risk before measures:		Risiko after measures:	
	Ytre miljø	Risk before measures:		Risiko after measures:	
	Materielle verdier	Risk before measures:		Risiko after measures:	
	Omdømme	Risk before measures:		Risiko after measures:	

Measure	Responsible	Registered	Deadline	Status
Covid19-Protocol	Isabel Maria Pascual Garcia	09.02.2021		New

Hazard: **CO leakage**

Incident: **CO leakage**

Consequence area:	Helse	Risk before measures:		Risiko after measures:	
	Ytre miljø	Risk before measures:		Risiko after measures:	
	Materielle verdier	Risk before measures:		Risiko after measures:	
	Omdømme	Risk before measures:		Risiko after measures:	

Measure	Responsible	Registered	Deadline	Status
HSE procedures	Isabel Maria Pascual Garcia	09.02.2021		New

Final evaluation

Organizational units and people involved

A risk assessment may apply to one or more organizational units, and involve several people. These are lsited below.

Organizational units which this risk assessment applies to

- Institutt for kjemisk prosessteknologi

Participants

Mehdi Mahmoodinia
Edd Anders Blekkan
Estelle Marie M. Vanhaecke
Karin Wiggen Dragsten
Anne Hoff

Readers

Gunn Torill Wikdahl
Mikael Hammer
Ketil Torset Helland
Eva Rise

Others involved/stakeholders

[Ingen registreringer]

The following accept criteria have been decided for the risk area Risikovurdering: Helse, miljø og sikkerhet (HMS):

Helse	Materielle verdier	Omdømme	Ytre miljø
			

Overview of existing relevant measures which have been taken into account

The table below presents existing measures which have been take into account when assessing the likelihood and consequence of relevant incidents.

Hazard	Incident	Measures taken into account
H2 gas explosion	H2 gas explosion	Ventilation
	H2 gas explosion	Gas-detectors
	H2 gas explosion	All users get proper training before using this unit
	H2 gas explosion	Personal protective equipment
H2S leakage	H2S toxic gas leakage	Ventilation
	H2S toxic gas leakage	Gas-detectors
	H2S toxic gas leakage	All users get proper training before using this unit
	H2S toxic gas leakage	Personal protective equipment
High temperature in reactor	High temperature in reactor damages to operator	Ventilation
	High temperature in reactor damages to operator	All users get proper training before using this unit
	High temperature in reactor damages to operator	Personal protective equipment
	High temperature in reactor damages to operator	HSE protocol
Catalyst manipulation	Skin exposure or chemical inhalation	All users get proper training before using this unit
	Skin exposure or chemical inhalation	Personal protective equipment
	Skin exposure or chemical inhalation	HSE protocol
Pressure build up in reactor	Pressure buid up in reactor	Ventilation
	Pressure buid up in reactor	Gas-detectors
	Pressure buid up in reactor	All users get proper training before using this unit
Working in the lab under Covid19-situation	Handle something without gloves unconsciously	All users get proper training before using this unit
	Handle something without gloves unconsciously	Personal protective equipment
CO leakage	CO leakage	Ventilation
	CO leakage	Gas-detectors
	CO leakage	All users get proper training before using this unit
	CO leakage	Personal protective equipment
	CO leakage	Leak testing
	CO leakage	HSE protocol

Existing relevant measures with descriptions:

Ventilation

The unit is connected to the ventilation system. The door must be closed when the unit is in use.

Gas-detectors

The set-up is placed inside a cabinet with ventilation and CO, CH4, H2S and H2 gas-detectors, as well as portable H2S gas detector. The detectors will trigger in case of leakage.
A portable H2 detector is also available in the unit which must be used for leak test before running the experiments.

All users get proper training before using this unit

[Ingen registreringer]

Personal protective equipment

The hall contains glasses, other safety measures and a first-aid kit.There are also gloves, lab coats and more protective equipment available upon request.

Installation and change of gas cylinders

Only performed by authorized personnel.

Leak testing

The reactor and gas line connections must be tested for leaks before heating the reactor.

HSE protocol

- The labs in hall D (1st and 2nd floor) have updated room card,
- The installed instruments have a copy of the risk assessment, an operating instructions and apparatus card with information regarding safety and information in case of emergency stop.
- Emergency phone numbers are provided in case of any incident.

Risk analysis with evaluation of likelihood and consequence

This part of the report presents detailed documentation of hazards, incidents and causes which have been evaluated. A summary of hazards and associated incidents is listed at the beginning.

The following hazards and incidents has been evaluated in this risk assessment:

- **H2 gas explosion**
  - H2 gas explosion
- **H2S leakage**
  - H2S toxic gas leakage
- **High temperature in reactor**
  - High temperature in reactor damages to operator
- **Catalyst manipulation**
  - Skin exposure or chemical inhalation
- **Pressure build up in reactor**
  - Pressure buid up in reactor
- **Working in the lab under Covid19-situation**
  - Handle something without gloves unconsciously
- **CO leakage**
  - CO leakage

Detailed view of hazards and incidents:

Hazard: H2 gas explosion

Incident: H2 gas explosion

Likelihood of the incident (common to all consequence areas): **Unlikely (1)**

Kommentar:

The H2 leakage are checked twice every stage of the experiment through a mass spectrometer and with a manual detector. Moreover, there are detectors inside the cabin. Each cycle, the H2 leakage is checked 5 times and with three different devices.

Consequence area: Helse

Risk:

Assessed consequence: **Large (3)**

Comment: Although a H2 explosion is really dangerous, during the experiments the responsible person is outside the cabin measuring everything through the MS to make sure nothing worse happens.

Consequence area: Ytre miljø

Risk:

Assessed consequence: **Medium (2)**

Comment: [Ingen registreringer]

Consequence area: Materielle verdier

Risk:

Assessed consequence: **Medium (2)**

Comment: [Ingen registreringer]

Consequence area: Omdømme

Risk:

Assessed consequence: **Medium (2)**

Comment: [Ingen registreringer]

Hazard: H2S leakage

Incident: H2S toxic gas leakage

Likelihood of the incident (common to all consequence areas): **Less likely (2)**

Kommentar:

Leakage test are checked twice before staring experiments.
- Gas detectors are installed in the cabinet
- Portable gas detectors are placed very close to oven and setup and have very low detection limits (ppm)

Consequence area: Helse

Risk:

Assessed consequence: **Very large (4)**

Comment: [Ingen registreringer]

Consequence area: Ytre miljø

Risk:

Assessed consequence: **Large (3)**

Comment: [Ingen registreringer]

Consequence area: Materielle verdier

Risk:

Assessed consequence: **Small (1)**

Comment: [Ingen registreringer]

Consequence area: Omdømme

Risk:

Assessed consequence: **Small (1)**

Comment: [Ingen registreringer]

Hazard: High temperature in reactor

Incident: High temperature in reactor damages to operator

Likelihood of the incident (common to all consequence areas): **Less likely (2)**

Kommentar:

The oven temperature is controlled by Eurotherm controller with a maximum set point, and it is controlled during experiments.
If the thermocouples are not well connected or do not work correctly, the reactor can get high temperatures without knowing it. However, if one of those problems happen, the temperature controller will show nothing or a very high number.

Consequence area: Helse

Risk:

Assessed consequence: **Large (3)**

Comment: [Ingen registreringer]

Consequence area: Ytre miljø

Risk:

Assessed consequence: **Small (1)**

Comment: [Ingen registreringer]

Consequence area: Materielle verdier

Risk:

Assessed consequence: **Small (1)**

Comment: [Ingen registreringer]

Consequence area: Omdømme

Risk:

Assessed consequence: **Small (1)**

Comment: [Ingen registreringer]

Hazard: Catalyst manipulation

Incident: Skin exposure or chemical inhalation

Likelihood of the incident (common to all consequence areas): **Less likely (2)**

Kommentar:

Gloves are mandatory when working with chemicals.
In case of skin exposure, take all the contaminated clothes off. Rinse skin with water/shower. Wash contaminated clothing before reuse (according to MSDS).
Inhalation: when working with large particles there is less chance for inhalation, but in case of inhalation of sorbent dust, act according MSDS. (attached)

Consequence area: Helse

Risk:

Assessed consequence: **Medium (2)**

Comment: - Amonium Molybdate is irritant (skin and eye irritation) and harmful if inhaled.

- Manganese (II) Nitrate Tetrahydrate is an oxidizer, harmful if swallowed and causes severe skin burns and eye damage. It may also intesify fire.

Consequence area: Ytre miljø

Risk:

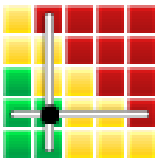

Assessed consequence: **Medium (2)**

Comment: - Amonium Molybdate: LC50 fish: 60mg/L. Persistence is unlikely. Readily degradable in the environment.
- Manganese (II) Nitrate Tetrahydrate: Harmful to aquatic organisms, may cause long-term adverse effects in the aquatic environment. Soluble in water. Persistence is unlikely.

Hazard: Pressure build up in reactor

Incident: Pressure buid up in reactor

Likelihood of the incident (common to all consequence areas): **Unlikely (1)**

Kommentar:

The pressure is checked everytime a valve is switched or a flow is changed.

Consequence area: Helse

Risk:

Assessed consequence: **Medium (2)**

Comment: If the pressure increases too much, it may cause a gas leak. This leakage will be previously detected in the MS as a deep change in the Ion Current and if the gas concentration still increases the detectors will start working. Therefore, all the valves will closed and the operation stopped. The only moment when the pressure may build up the operator will be out of the cabin checking the corresponding risk.

Consequence area: Ytre miljø

Risk:

Assessed consequence: **Medium (2)**

Comment: [Ingen registreringer]

Consequence area: Materielle verdier

Risk:

Assessed consequence: **Small (1)**

Comment: [Ingen registreringer]

Hazard: Working in the lab under Covid19-situation

Incident: Handle something without gloves unconsciously

It can be the case some of us handle something without gloves. First, it should be important to be aware that the use of gloves is indispensable. If the problem of using something without gloves comes, disinfect inmediatly.

Likelihood of the incident (common to all consequence areas): **Less likely (2)**

Kommentar:

Disinfect all the objects and surfaces touched. Make sure everything is clean before and after working.

Consequence area: Helse

Risk:

Assessed consequence: **Very large (4)**

Comment: Covid-19 infection

Consequence area: Ytre miljø

Risk:

Assessed consequence: **Very large (4)**

Comment: [Ingen registreringer]

Consequence area: Materielle verdier

Risk:

Assessed consequence: **Very large (4)**

Comment: [Ingen registreringer]

Consequence area: Omdømme

Risk:

Assessed consequence: **Medium (2)**

Comment: [Ingen registreringer]

Hazard: CO leakage

Incident: CO leakage

Likelihood of the incident (common to all consequence areas): **Unlikely (1)**

Kommentar:

Leakage test are checked twice before staring experiments.
- Gas detectors are installed in the cabinet
- Portable gas detectors are placed very close to oven and setup and have very low detection limits (ppm)

Consequence area: Helse

Risk:

Assessed consequence: **Very large (4)**

Comment: CO is toxic at the level of ppm, so it is crucial to have gas detectors and follow the alarm instructions. For blue alarm (low) check what is happening and for red alarm (high) evacuate the building immediately.

Consequence area: Ytre miljø

Risk:

Assessed consequence: **Large (3)**

Comment: [Ingen registreringer]

Consequence area: Materielle verdier

Risk:

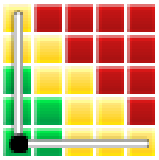

Assessed consequence: **Small (1)**

Comment: [Ingen registreringer]

Consequence area: Omdømme

Risk:

Assessed consequence: **Medium (2)**

Comment: [Ingen registreringer]

Overview of risk mitiating measures which have been decided:

Below is an overview of risk mitigating measures, which are intended to contribute towards minimizing the likelihood and/or consequence of incidents:

- HSE procedures
- H2S protection mask
- Covid19-Protocol

Overview of risk mitigating measures which have been decided, with description:

HSE procedures

Take into account al the HSE protocol and put in into practice when the incident takes place

Measure decided by: Isabel Maria Pascual Garcia

Responsible for execution: Isabel Maria Pascual Garcia

Deadline for execution:

H2S protection mask

Put the mask on in case of H2S handling leak

Measure decided by: Isabel Maria Pascual Garcia

Responsible for execution: Isabel Maria Pascual Garcia

Deadline for execution:

Covid19-Protocol

Take into account al the Covid-19 protocol and put in into practice when the incident takes place

Measure decided by: Isabel Maria Pascual Garcia

Responsible for execution: Isabel Maria Pascual Garcia

Deadline for execution:

Detailed view of assessed risk for each hazard/incident before and after mitigating measures

Hazard: H2 gas explosion

Incident: H2 gas explosion

Likelihood assessment (common to all consequence areas)

Initial likelihood: Unlikely (1)

Reason: The H2 leakage are checked twice every stage of the experiment through a mass spectrometer and with a manual detector. Moreover, there are detectors inside the cabin. Each cycle, the H2 leakage is checked 5 times
and with three different devices.

Likelihood after measures: Unlikely (1)

Reason:

Consequence assessments:

Consequence area: Helse ***Risk:***

Initial consequence: Large (3)

Reason: Although a H2 explosion is really dangerous, during the experiments the
responsible person is outside the cabin measuring everything through the MS to make sure nothing worse happens.

Consequence after measures: Medium (2)

Reason:

Consequence area: Ytre miljø ***Risk:***

Initial consequence: Medium (2)

Reason:

Consequence after measures: Medium (2)

Reason:

Consequence area: **Materielle verdier** ***Risk:***

Initial consequence: Medium (2)

Reason:

Consequence after measures: Medium (2)

Reason:

Consequence area: **Omdømme** ***Risk:***

Initial consequence: Medium (2)

Reason:

Consequence after measures: Medium (2)

Reason:

Hazard: **H2S leakage**

Incident: **H2S toxic gas leakage**

Likelihood assessment (common to all consequence areas)

Initial likelihood: Less likely (2)

Reason: Leakage test are checked twice before staring experiments.
- Gas detectors are installed in the cabinet
- Portable gas detectors are placed very close to oven and setup and have very low detection limits (ppm)

Likelihood after measures: Less likely (2)

Reason:

Consequence assessments:

Consequence area: **Helse** ***Risk:***

Initial consequence: Very large (4)

Reason:

Consequence after measures: Medium (2)

Reason:

Consequence area: **Ytre miljø** ***Risk:***

Initial consequence: Large (3)

Reason:

Consequence after measures: Medium (2)

Reason:

Consequence area: **Materielle verdier** ***Risk:***

Initial consequence: Small (1)

Reason:

Consequence after measures: Small (1)

Reason:

Consequence area: **Omdømme** ***Risk:***

Initial consequence: Small (1)

Reason:

Consequence after measures: Small (1)

Reason:

Hazard: High temperature in reactor

Incident: High temperature in reactor damages to operator

Likelihood assessment (common to all consequence areas)

Initial likelihood: Less likely (2)

Reason: The oven temperature is controlled by Eurotherm controller with a maximum set point, and it is controlled during experiments.
If the thermocouples are not well connected or do not work correctly, the reactor can get high temperatures without knowing it. However, if one of those problems happen, the temperature controller will show nothing or a very high number.

Likelihood after measures: Less likely (2)

Reason:

Consequence assessments:

Consequence area: Helse ***Risk:***

Initial consequence: Large (3)

Reason:

Consequence after measures: Medium (2)

Reason:

Consequence area: Ytre miljø ***Risk:***

Initial consequence: Small (1)

Reason:

Consequence after measures: Small (1)

Reason:

Consequence area: Materielle verdier ***Risk:***

Initial consequence: Small (1)

Reason:

Consequence after measures: Small (1)

Reason:

Consequence area: Omdømme ***Risk:***

Initial consequence: Small (1)

Reason:

Consequence after measures: Small (1)

Reason:

Hazard: Working in the lab under Covid19-situation

Incident: Handle something without gloves unconsciously

Likelihood assessment (common to all consequence areas)

Initial likelihood: Less likely (2)

Reason: Disinfect all the objects and surfaces touched. Make sure everything is clean before and after working.

Likelihood after measures: Less likely (2)

Reason:

Consequence assessments:

Consequence area: Helse ***Risk:***

Initial consequence: Very large (4)

Reason: Covid-19 infection

Consequence after measures: Medium (2)

Reason:

Consequence area: Ytre miljø ***Risk:***

Initial consequence: Very large (4)

Reason:

Consequence after measures: Medium (2)

Reason:

Consequence area: Materielle verdier ***Risk:***

Initial consequence: Very large (4)

Reason:

Consequence after measures: Medium (2)

Reason:

Consequence area: Omdømme ***Risk:***

Initial consequence: Medium (2)

Reason:

Consequence after measures: Medium (2)

Reason:

Hazard: CO leakage

Incident: CO leakage

Likelihood assessment (common to all consequence areas)

Initial likelihood: Unlikely (1)

Reason: Leakage test are checked twice before staring experiments.
- Gas detectors are installed in the cabinet
- Portable gas detectors are placed very close to oven and setup and have very low detection limits (ppm)

Likelihood after measures: Unlikely (1)

Reason:

Consequence assessments:

Consequence area: Helse ***Risk:***

Initial consequence: Very large (4)

Reason: CO is toxic at the level of ppm, so it is crucial to have gas detectors and follow the alarm instructions. For blue alarm (low) check what is happening and for red alarm (high) evacuate the building immediately.

Consequence after measures: Medium (2)

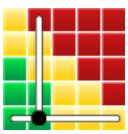

Reason:

Consequence area: **Ytre miljø** ***Risk:***

Initial consequence: Large (3)

Reason:

Consequence after measures: Medium (2)

Reason:

Consequence area: **Materielle verdier** ***Risk:***

Initial consequence: Small (1)

Reason:

Consequence after measures: Small (1)

Reason:

Consequence area: **Omdømme** ***Risk:***

Initial consequence: Medium (2)

Reason:

Consequence after measures: Small (1)

Reason:

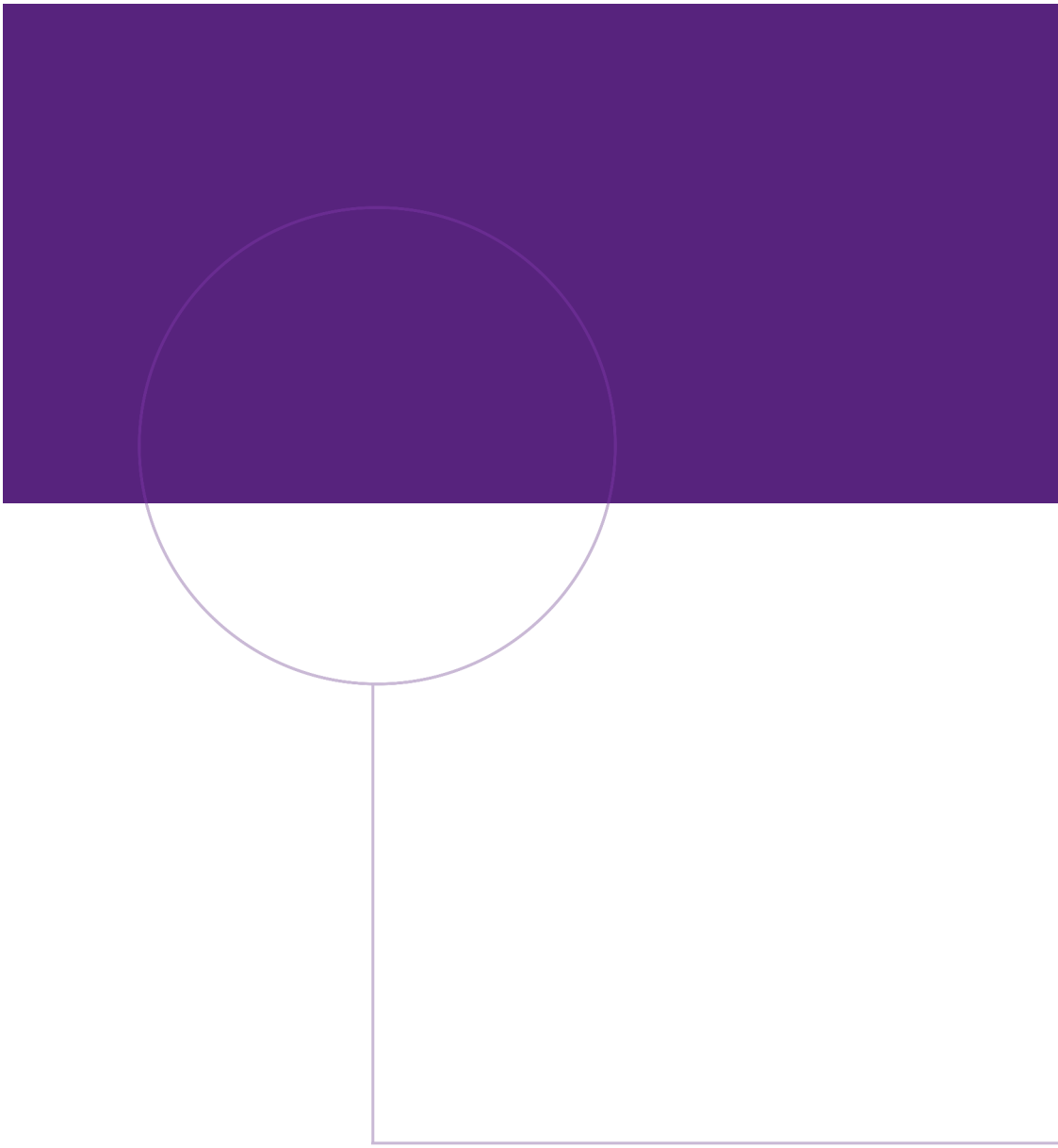

NTNU

Norwegian University of
Science and Technology